Analysis of the Hindfoot and Tibia Segment-Based Axes in the Oxford Foot Model - Anatomy and Accuracy

Adward Min Hyun Paik

St Edmund Hall

A thesis submitted to the University of Oxford in partial fulfillment of the requirements for the degree of Master of Science by Research

Department of Engineering Science

Hilary Term 2015

Analysis of the Hindfoot and Tibia Segment-Based Axes in the Oxford Foot Model - Anatomy and Accuracy

Adward Min Hyun Paik
St Edmund Hall

A thesis submitted to the University of Oxford in partial fulfillment of the requirements for the degree of Master of Science by Research

Hilary Term 2015

Abstract

The Oxford Foot Model (OFM) is a multi-segment foot model, which consists of three rigid segments (tibia, hindfoot and forefoot). The segments are defined by surface markers placed on bony landmarks on the foot and leg. The accuracy of the OFM angle calculations depends on how the markers and segment axes relate to the underlying anatomy. Several previous studies have reported particularly large variability in the hindfoot-tibia rotation and this finding has made gait data interpretation and, consequently, treatment recommendation more uncertain. The aim of this research project was to investigate the agreement between marker-based and anatomy-based hindfoot and tibia segment axes in the Oxford Foot Model. Twenty-one adult females participated in the study (42 feet). The calcaneus and talus first principal axes, as well as 3D coordinates of markers and of the points corresponding to the ideal marker locations, were extracted from CT images. Gait analysis was used to measure lower-limb joint kinematics during level walking trials. The results showed that there is a significant discrepancy between the OFM hindfoot (A-P) axis and the calcaneus first principal axis in the transverse plane. This relationship suggested a clinical implication that the A-P axis definition in relation to the underlying anatomy is likely to be less accurate in a deformed foot like clubfoot. Moreover, the insignificant root mean squared difference between the hindfoot-tibia kinematics, estimated by a rigid-body transformation method and that computed from the standard stereophotogrammetric procedure implied that the hindfoot and tibia rigidity assumption was valid in estimating the motion of the underling anatomy from the marker-based segment axes definition. Furthermore, a discrepancy between the OFM hindfoot and tibia axes and the corrected OFM hindfoot and tibia axes in the transverse plane was evident, and this led to differences in the transverse plane joint angles during walking. Therefore it can be inferred that these two reasons instigate the large variability in transverse plane hindfoot-tibia kinematics, as reported by past literatures. This information has potential to optimise the hindfoot and tibia segment definitions in accurately describing the motion of the underlying anatomy and thus improve interpretation of gait data and subsequently treatment recommendations for patients with foot deformity.

Contents

List of Figures

List of Tables

1 Introduction

This chapter explains the motivation behind and the aim of the current thesis. A summary of each chapter of the thesis has been outlined in the last section.

1.1 Purpose and Aims

The measurement of kinematics via stereophotogrammetry is a well-established part of clinical decision-making for patients with known gait disabilities. Conventional lower body models, which comprise a rigid pelvis, femur and lower leg segments, do not provide adequate information about foot kinematics during in vivo motion analysis of the foot. Hence this has been a problem for treatment specific to feet. In order to address this issue, many multi-segment foot models have been developed. These models have been thoroughly tested for repeatability and clinical significance to justify their clinical use. Multi-segment foot models have their own set of small segments, defined by strategically placed markers, and systematic procedures for detailed and repeatable attainment of foot kinematic results. Carson et al. [14] first proposed the Oxford Foot Model (OFM) and Stebbins et al. [78] later modified it for wider application. The OFM consists of three rigid segments (tibia, hindfoot and forefoot). Surface markers placed on specified bony landmarks on the foot and leg define the segments. A motion capture system is used to record the three-dimensional (3D) coordinates of these markers, that have been affixed to a moving test subject, at a given frame rate. The marker coordinates can be used to calculate the segmental axis orientations and hence the inter-segmental angles for each frame and this is the basis

of foot kinematic data collection.

However, there are limitations associated with estimating the orientation of bone from reconstructed skin-marker trajectories. Apart from the inevitable instrumental errors from motion capture systems, there are errors that originate from deformable tissues between the stereophotogrammetric system and the underlying bony segment. This is regarded as the primary limitation to interpreting human motion analysis [3].

Anatomical landmarks can be either external or bony and therefore accurate identification and reconstruction of the anatomical landmarks can be a difficult task. This affects the estimation of the orientation of anatomical segment axes (or anatomical frames) which are defined by marker-based segment axes and consequently affects the computation and interpretation of joint kinematics. The accuracy of the OFM angle calculations depends on how the markers and segment axes relate to the underlying anatomy. In addition, skin motion and soft tissue artifacts can contribute to the relative movement between the markers and the corresponding bony anatomy. Inertial effects of the soft tissue deformation in areas close to the joints [12] and skin motion artefact owing to joint positions can weaken the rigid body assumption of the model segments and affect the estimation and interpretation of joint kinematics. The OFM hindfoot segment is an area where relatively thick layers of fat and soft tissue exist between the surface of skin and the underlying bony anatomy. This issue does not just relate to the Oxford Foot Model, since many multi-segment foot models [45, 49] use hindfoot definitions similar to that of the Oxford Foot Model. Hence, accurately measuring the movement of the underlying bone would not only benefit the Oxford Foot Model but also other similar models and therefore provides justification for this

study. While measuring the skin motion artefact would provide useful information in computing the errors it contributes to the dynamic angles, it was not a part of the scope of this study.

Moreover, the OFM tibia segment definition relies on the Knee Joint Centre and Ankle Joint Centre, both of which are calculated points. As particularly high variability has been observed in the hindfoot-tibia rotation (transverse rotation) [20], the Oxford Foot Model tibia and hindfoot segments were identified as key research areas. Therefore the aim of the current thesis was:

- To investigate the agreement between marker-based and anatomy-based hindfoot and tibia segment axes in the Oxford Foot Model.

The objectives of the current thesis were:

1. To investigate how well the marker-based and the anatomy-based hindfoot and tibia segment axes align.

2. To investigate the effect of any misalignment between the marker-based and the anatomy-based hindfoot and tibia segment axes on joint angles during motion.

3. To investigate how appropriate the rigidity assumption is in estimating the hindfoot and tibia anatomy-based segment definitions from the corresponding marker-based definition.

4. To investigate how marker misplacement affects the calculated kinematics of the hindfoot and tibia.

This thesis presents an investigation of the aim and the objectives using healthy adults. A summary of each chapter of the thesis is outlined in the following section.

1.2 Thesis Overview

Chapter 2 provides an essential introduction to the clinical and technical background required to comprehend this thesis. It starts by presenting the clinical terminology that is used throughout the thesis. The next section describes the skeletal and muscular anatomy of the foot and their corresponding biomechanics. This is followed by a section on various foot pathologies, how they affect gait and what the available common treatment methods are. The next section goes on to demonstrate how joint kinematics is calculated. Technical details of various lower-limb models that are available for use in both research and clinical settings are outlined. The details of the Oxford Foot Model, the lower-limb model used in this research, are also included in this section. Since this thesis is dedicated to the analysis of the Oxford Foot Model, its clinical utility has been summarised. The final section of this chapter addresses limitations associated with the default definition of the Oxford Foot Model and where in the hindfoot and tibia the problems related to accuracy might occur.

Chapter 3 describes the experimental data collection and protocols that were employed in the current thesis. Study design and subject recruitment are outlined. A description of the experimental data collection section is divided into subject recruitment, clinical examination, gait analysis and medical imaging. Ankle and foot kinematic data collected was processed using the protocol described in the kinematic data processing section. This section also summarises the protocol used to segment and reconstruct CT images. Lastly the rigid body transformations used to obtain dynamic inter-segmental angles are explained.

Chapter 4 provides a comprehensive analysis of static comparison of marker-based

hindfoot and tibia segment axes orientations with their anatomical definitions. The first and, partly, the fourth objectives of the thesis were investigated in this chapter.

Chapter 5 extends the work of the previous chapter and outlines the comparison of dynamic joint angles calculated from the marker-based hindfoot and tibia segment axes and anatomical definitions. The second, third and the fourth objectives of the thesis were investigated in this chapter.

Chapter 6 summarises the overall conclusions drawn from this investigation and outlines recommendations for future work.

2 Background And Literature Review

2.1 Clinical Terminology

2.1.1 Introduction

Clinical terms used to describe anatomical planes and directions as well as human body structures and motions are outlined in this section.

2.1.2 Anatomical Planes and Directions

The body is referenced in three anatomical planes (Figure 2.1). The transverse plane is the plane normal to the long axis of the body and the directions away from this plane are described as superior and inferior (Figure 2.2). The superior direction refers to the direction towards the head whereas the inferior direction refers to the direction towards the feet. The sagittal plane is a vertical plane, which divides the body into left and right halves, and the directions away from this plane are described as medial and lateral. The medial direction refers to the direction towards the mid-plane that divides the body into left and right halves, whereas the lateral direction refers to the direction away from the plane. The coronal (frontal) plane is the plane perpendicular to the transverse and sagittal planes and the directions away from this plane are described as anterior and posterior. The anterior direction refers to the direction towards the front of the body whereas the posterior direction refers to the direction towards the back of the body.

Also the terms proximal and distal are used to define nearer to and further away from a point of reference.

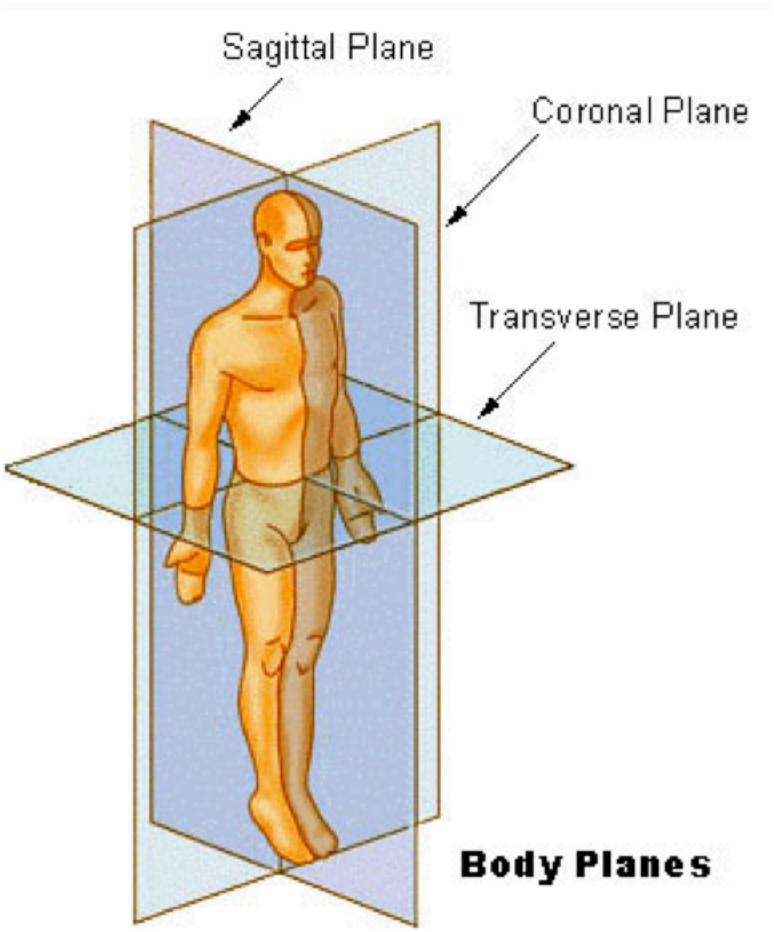

Figure 2.1: Anatomical Planes [99]

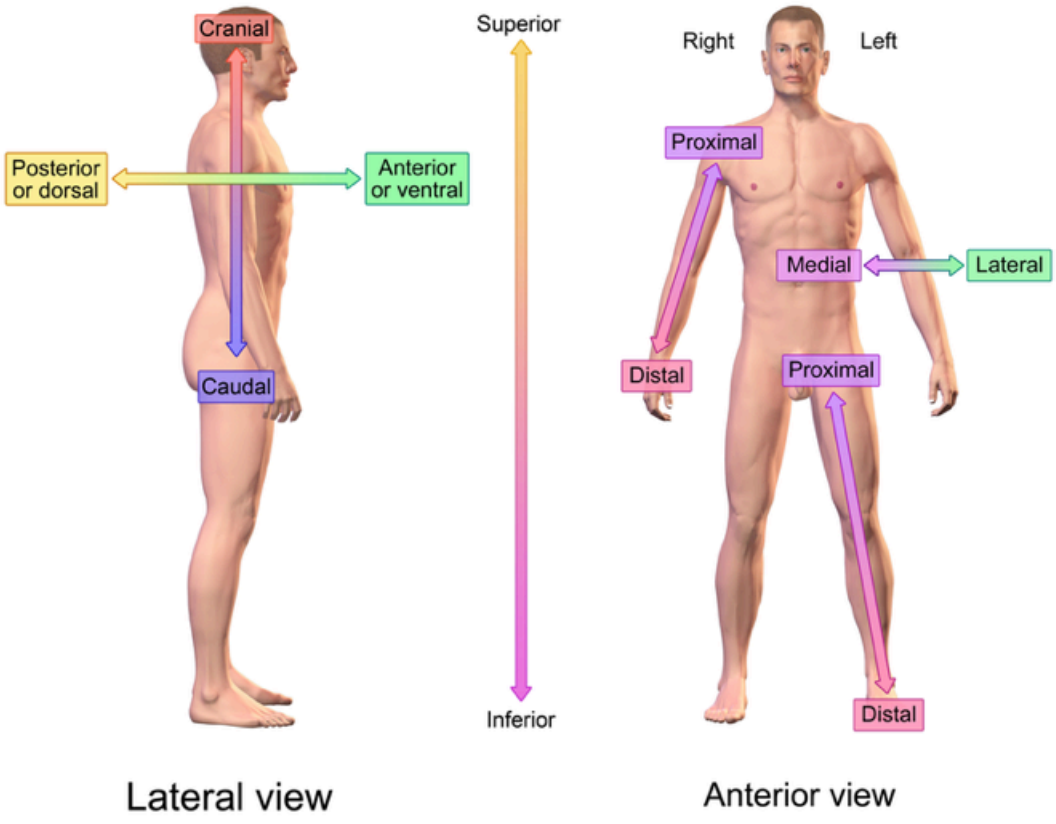

Figure 2.2: Anatomical Directions [99]

2.1.3 The Description of Human Motion

Flexion is used to describe the motion in the sagittal plane at a joint that brings the distal segment closer to the proximal segment, whereas extension is used to describe the motion opposite to flexion [62]. At the ankle joint, the terms dorsiflexion and plantarflexion are used to define flexion and extension, respectively. Abduction is used to describe motion of a body part that pulls it away from the midline of the body, whereas adduction is used to describe the motion opposite to abduction. Internal rotation is used to describe the rotational motion of a body part that rotates towards the midline of the body about its longitudinal axis, whereas external rotation is used to describe the motion opposite to internal rotation. Figure 2.3 is an illustration of the terms used to describe human motion.

Moreover, inversion is used to describe the rotational motion of a foot that rotates about the long axis of foot towards its mid-sagittal plane, whereas eversion is used to describe the motion opposite to inversion.

2.2 Anatomy and Biomechanics of the Foot

2.2.1 Introduction

The foot is a complex structure, consisting of 107 ligaments, 19 muscles, 28 bones and 33 joints [1]. It has four different functions [58]:

1. It provides a stable base of support to minimise muscular effort.

2. It accommodates rotation of more proximal limb segments during the weight-bearing phase of the gait cycle.

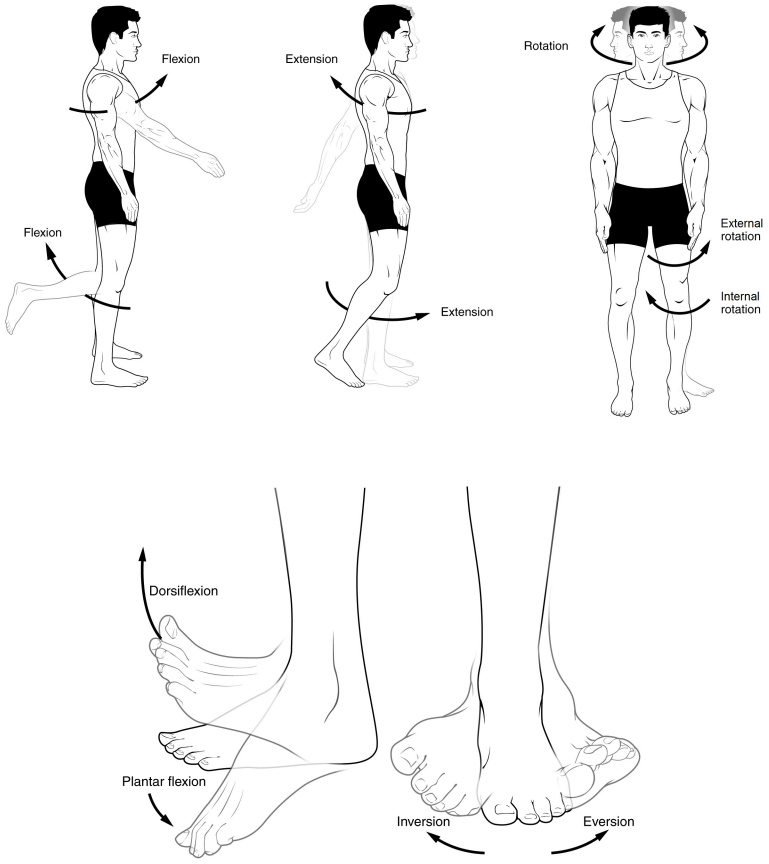

Figure 2.3: Description of Human Motion. Modified from [100]

3. Flexibility of the structures within the foot allows shock absorption and accommodation of the terrain.

4. Rigidity of structures within the foot allows leverage during push-off.

In order to execute all four functions, the foot needs to be able to make a transition from a flexible structure to a rigid and supportive structure and vice versa at various phases of the gait cycle. During initial contact, the foot is flexible to aid impact shock absorption. Then during the push-off phase, the foot joints lock together to act as a rigid lever, for propulsion [30].

2.2.2 Basic Anatomy and Biomechanics of the Foot

The skeletal anatomy of the foot is shown in Figure 2.4. The foot is separated from the shank by the ankle (tibiotalar) joint. In clinical terms, the hindfoot comprises the calcaneus and talus. The joint between the talus and the calcaneus is called the subtalar (talocalcaneal) joint. The midfoot consists of the navicular, cuboid and the three cuneiforms. The hindfoot and the midfoot are separated by the midtarsal (transverse tarsal) joint (combination of the talonavicular and calcaneocuboid joints). The forefoot is composed of the five metatarsals and the phalanges comprise the five proximal, middle and distal phalanges. The hallux refers to the big toe. The joints between the midfoot and the forefoot are called the tarsometatarsal joints, whereas joints between the forefoot and the phalanges are called the metatarso-phalangeal joints.

The muscular anatomy of the foot and the shank is shown in Figure 2.5. The ankle complex consists of 11 muscles which function as dorsiflexors and plantar flexors. The

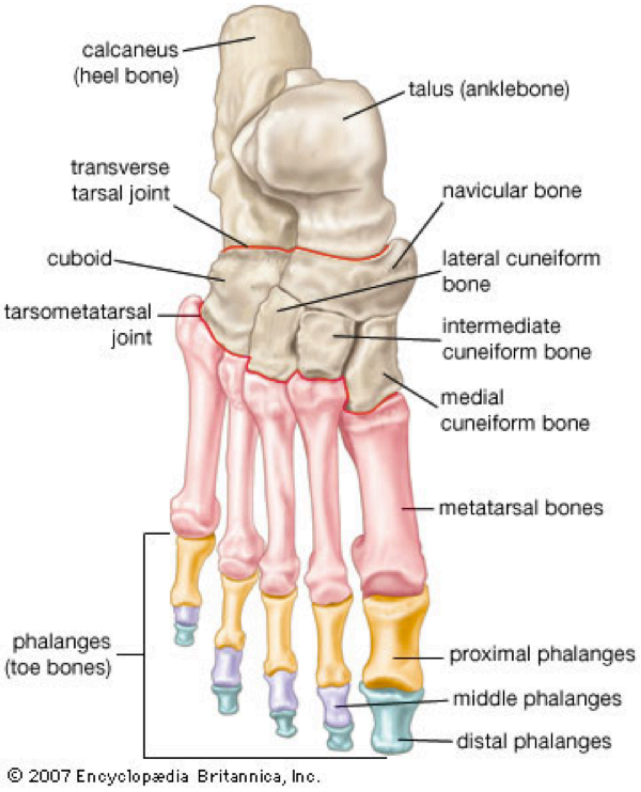

Figure 2.4: Foot Bony Anatomy [96]

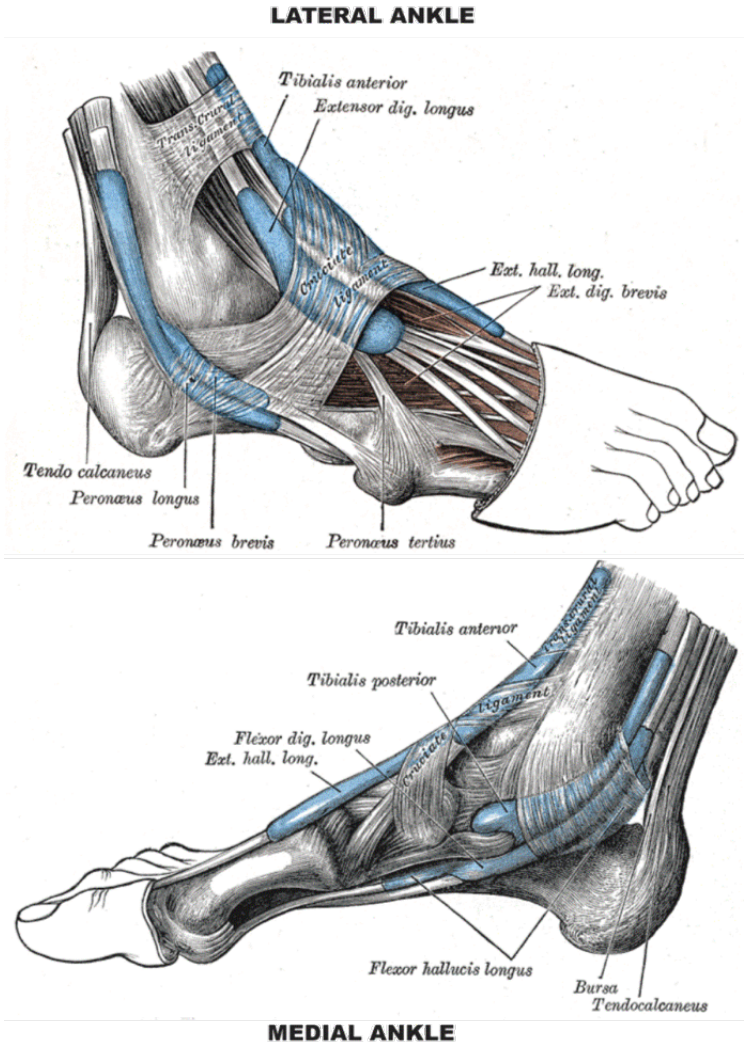

Figure 2.5: Foot Ligaments and Tendons [95]

dorsiflexors are the tibialis anterior (TA), extensor digitorum longus (EDL), extensor hallucis longus (EHL), and peroneus tertius, whereas the plantar flexors are the triceps surae (soleus and gastrocnemius) and the perimalleolar muscles. The perimalleolar muscles consist of the tibialis posterior (TP), peroneus longus, flexor hallucis longus (FHL), flexor digitorum longus (FDL) and peroneus brevis. The triceps surae are the primary ankle plantar flexors, providing 93% of the plantar flexor torque [35].

The aforementioned ankle muscles can also control subtalar joint inversion and eversion. The invertor muscles are all the muscles that are located medially with respect to the subtalar joint. They are the TA, EHL, TP, FDL and FHL. On the other hand, the evertor muscles are all the muscles that are located laterally with respect to the subtalar joint and they are the EDL, peroneus tertius, peroneus longus and peroneus brevis.

Extensor hallucis brevis (EHB) and extensor digitorum brevis (EDB) are located on the upper side of the foot. The EHB is just medial to the EDB and it helps to extend the big toe whereas the EDB helps to extend the digits 2, 3 and 4.

The plantar fascia of the foot is located underneath the arch and is tensed by metatarso-phalangeal joint dorsiflexion.

2.2.3 Gait Cycle

The gait cycle (GC) is a reference used to measure and analyse gait patterns. Each gait cycle begins with initial contact and ends with next initial contact of the ipsilateral foot [31] (Figure 2.6) It constitutes two periods: stance and swing. Stance refers to the period during which the foot is in contact with the ground. It accounts for

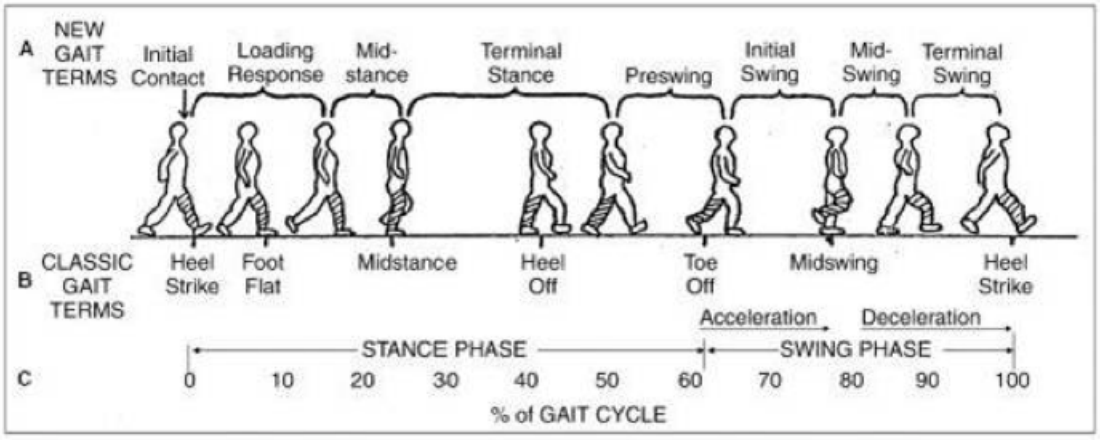

Figure 2.6: Normal Gait Cycle and Phases [99]

approximately 60% of the gait cycle and can be subdivided into three intervals: the initial double stance, single limb support and terminal double limb support. Swing refers to the period during which the foot is off the ground and accounts for the other 40% of the gait cycle.

Normal foot motion patterns during gait can be categorised into eight phases [62]: Initial contact (0% to 2% GC), loading response (2% to 12% GC), mid stance (12% to 31% GC), terminal stance (31% to 50% GC), pre-swing (50% to 62% GC), initial swing (62% to 75% GC), mid swing (75% to 87% GC) and terminal swing (87% to 100% GC).

Soon after initial contact, the ground reaction force can exceed body weight by up to 20% [58]. The ankle gradually plantarflexes from slight dorsiflexion to approximately 20° of plantarflexion [59]. During the loading response phase, the lower leg internally rotates which results in the body weight being progressively transferred to the supporting limb for weight-bearing stability [91]. Early research [36] indicated

that the hindfoot inverts during this phase but more recent researchers using three-dimensional gait analysis [53, 60, 69] have shown that the hindfoot, in fact, everts. Reinschmidt et al. [69] have also found that the hindfoot tends to abduct for the first 20% of the gait cycle. It is understood that this hindfoot nature at initial contact aids shock absorption [58].

From the mid stance to the terminal stance phase, the foot makes a transition from a flexible structure to a rigid and supportive structure to generate propulsive power. During this time, the hindfoot inverts [53, 59, 69, 91] in order to provide limb and trunk stability and facilitate progression of the body over and beyond the supporting foot. During terminal stance, the heel begins to rise and thus the hindfoot plantarflexes [58]. A pioneering work by Inman [38], which involved a roentgenographic analysis of motion, highlighted that the movement of the foot during mid to terminal stance can be categorised into four stages:

1. Gradual calcaneal inversion increases support for the talus and locks the midtarsal joint, as a result. The axes of the talonavicular and the calcaneo-cuboid joints are parallel prior to the start of the hindfoot inversion but become progressively misaligned with the inversion.

2. The hindfoot plantarflexion during terminal stance compresses the talus into the navicular, which further locks the midtarsal joint.

3. Intrinsic foot muscles contract to provide support for the longitudinal arch.

4. The first metatarsophalangeal joint dorsiflexes to tighten the plantar fascia and increase the longitudinal arch height. This phenomenon is known as the "wind-

lass mechanism". This mechanism prepares the foot to provide a rigid lever for propulsive power generation. During this phase, the ground reaction force may exceed the body weight by 20%.

During initial swing, the hindfoot dorsiflexes to allow for foot clearance of the floor and as the gait cycle reaches terminal swing, it plantarflexes again to prepare the foot for initial contact.

2.3 Effect of Foot Pathology on Gait

Foot pathologies are usually related to congenital bony deformity, acquired muscle weakness, pain and impaired control [62]. Changes in foot structure compromise the role of the foot during gait.

Bony deformity prohibits shock absorption and limits the range of motion and therefore alters the functions of the foot. In addition, poor joint alignment restricts the ability to generate propulsive power. This increases the loading on the adjacent muscles and therefore results in the muscles working inefficiently.

Muscle weakness often abnormally activates adjacent muscles to reduce demand on the weak muscle. This, in turn, puts abnormal loading on the compensatory muscles during stance and can lead to further foot deformity.

Pain is often overlooked in identifying gait dysfunction. Like muscle weakness, pain triggers compensatory foot mechanics and therefore increases the forces on the joint tissues and ligaments. Consequently, it increases the likelihood of developing further disability.

Impaired control arises from disruption of interchange of information between the

sensory and motor systems. Neurologic disease or trauma alters selective muscle control and thus the muscle precision, coordination, speed and versatility are inevitably affected as a result.

2.3.1 Common Types of Foot Pathology

Common types of foot pathology include clubfoot and flatfoot [62].

Congenital clubfoot is a condition where the deformed foot is adducted, inverted and in equinus and cavus at birth [47, 63, 65]. If untreated, the deformity can substantially disrupt stance stability, forward progression and foot clearance and can increase energy expenditure.

Flatfoot or pes planus is a condition where the medial longitudinal arch of the foot is absent or significantly reduced. There are various types and causes. Flatfoot is often painless and is more apparent in children than adults as most children overcome flatfooted-ness as the muscles, bones and tendons become stronger with age. Congenital flatfoot can be divided into two types: flexible and rigid flatfoot. Flexible flatfoot is a condition whereby the soft tissues (tendons and ligaments) of the arch stretch, tear or in the worst case, become inflamed. It is called flexible because the longitudinal arch is restored in the non-weight-bearing posture. In most cases, there are no symptoms but some may experience pain or fatigue in the foot, back, hip or knee, ankle over-pronation and shin splints. Rigid flatfoot refers to the condition where the plantar surface of the foot remains flat at all times due to bony impairment, like tarsal coalition. About a quarter of those affected experience foot pain. Flatfoot can be adult-acquired and is often caused by overuse of the posterior tibialis tendon,

weakening its ability to support the longitudinal arch. This condition is called posterior tibialis tendon dysfunction (PTTD) and its symptoms are pain, swelling and flattening of the longitudinal arch.

Rheumatoid arthritis is a disease in which some cells of the immune system malfunction and attach to the synovial membranes that cover the capsules of synovial joints that connect bones [68]. Initially, the synovial membrane and excess synovial fluid thickens and subsequently the tissues swell. The swollen tissues intrude into joint spaces and consequently lead to pain when they are compressed with motion [68]. Patients reduce motion to lessen pain and therefore reduce activity [25] and weaken the muscles [27]. Pain underneath the fibula is common. As the disease progresses, the bones shift out of their normal positions and thus results in a shift in the alignment of the foot. This may induce flatfoot deformity and cause pain and discomfort along the posterior tibial tendon, the main tendon that supports the arch. With it, the ligaments that support the midfoot weakens and cause collapse of the arch.

Cerebral palsy is a neurological disease, that affects muscle control and movement. These affected muscles are either flaccid or spastic and this may affect the foot kinematics. Although CP is a neurological disease, prolonged altered muscle activity inevitably changes the bony structure. Bony deformity may develop during growth as imbalanced muscle forces apply persistent loading on the immature bones. Bony deformity compromises shock absorption and the range of motion and therefore alters the function of the foot. In addition, poor joint alignment restricts the ability to generate propulsive power. Moreover, CP patients often show joint contracture and

inappropriate muscle activity. The combined outcome of the aforementioned factors has a deleterious effect on gait. While individual patients show considerable variation in their gait patterns, they all suffer from increases in energy expenditure, discomfort and lack of endurance.

2.3.2 Common Types of Treatment

Foot and ankle treatments are aimed at minimising impairment and pain. The treatment process can be categorised into two types: non-surgical and surgical treatments. Non-surgical treatments include physiotherapy, orthotic devices, accommodative shoes and medications.

In the case of congenital clubfoot, Hippocrates in his writings demonstrated the first therapeutic system, which involved gentle stretching and the use of protective bandaging [65]. In the late 18th century, simple surgery, like Achilles tendon lengthening to reduce equinus, was introduced and with the discovery of anesthesia, the surgical procedures became more complex and diverse [65]. While surgery treated the foot in appearance, stiffness of the foot was a prevalent after-effect [10]. In 1939, Kite [47] addressed the importance of correcting forefoot adduction prior to the equinus. Ponseti [63, 64] developed a therapeutic program which begins with 5-12 weeks of an essential series of manipulations and long-leg casts, followed by an Achilles tenotomy to correct the residual equinus. Sometimes, lateral transfer of the tibialis anterior was required to correct residual inversion [63]. Denis Browne splints [85] were worn for about two years to minimise the chance of recurrence.

Flatfoot treatment is not usually required when symptons are not present. For

flexible flatfoot patients, physiotherapy may be used to provide temporary pain relief, medication such as nonsteroidal anti-inflammatory drugs may be prescribed to reduce inflammation and pain, shoe insoles with arch support may be recommended or custom orthotic devices may be provided to support the arches. In the case of rigid flatfoot patients, surgery is recommended to restore the shape of the foot to allow for natural foot motion. For PTTD patients, the treatment types are similar to those for flexible flatfoot. Immobilisation through a short-leg cast or boot is implemented to allow for the tendon to heal. Furthermore, this is followed by physiotherapy with the aim to help rehabilitate the tendon and muscle. In cases where non-surgical treatments have failed to reduce impairment or pain, surgery may be considered.

The rheumatoid arthritis treatment process mostly involves prescribing medicine to relieve pain. The other common process is the use of orthotic devices and accommodative shoes. They are utilised to provide support when walking and to alleviate pain. Surgeons may aspirate the joint to reduce joint swelling and if none of the aforementioned methods successfully dissipate pain, surgery may be required.

The cerebral palsy treatment process is focused on improving function and assisting motor development. Even though there are numerous physiotherapy techniques, it is unclear as to which is the most effective method. Strengthening exercises are applied to improve weakness in CP patients [88]. Passive stretching exercises are employed to lengthen elastic components of the muscle. Orthoses can be customised to improve function, protect joints and reduce the severity of deformity. The Ankle Foot Orthosis (AFO) is most commonly used for children with CP [9]. Botulinum Toxin is used in conjunction with other treatment techniques to reduce muscle spasticity. Sur-

gical interventions are applied to repair foot alignment and improve function. Surgical interventions such as lengthening of tight and overactive muscles, tendon transfers and bony surgery are implemented in cases with worsening gait and deformity. Since CP is a complex condition, it is unclear which treatment or combination of treatments is most appropriate. Changing the physical and biomechanical properties of a joint can affect other joints. Therefore it is important to understand the joint kinematics in all three dimensions and the corresponding joint coupling before any treatment process is planned. This is where clinical gait analysis can come into play.

2.3.3 Gait Analysis and Treatment Planning

Clinical gait analysis provides information required to assist treatment planning and to evaluate the effects of treatment, tailored to the individual patient. The information constitutes three-dimensional joint kinematics, net joint moments, plantar pressure, electromyography patterns and spatio-temporal parameters.

Three-dimensional kinematic analysis is the study of joint motion, which is illustrated by inter-segmental angles between body segments of interest. In conjunction with the kinematic results, force plate measurements are used in the calculation of kinetic results, such as joint moments, work and power. A pressure plate is used to measure plantar pressure in order to appreciate the distribution of foot pressure throughout the gait cycle. Dynamic electromyography (EMG) measurements show information about when the muscle of interest is active during the gait cycle and its contribution to the overall movement pattern can be inferred. Spatio-temporal parameters of gait include speed, cadence and step and stride length and time. The

overall quality of gait can be assessed using these parameters.

2.4 Human Motion Analysis

2.4.1 Introduction

Human motion analysis is the study of the mechanics of human locomotion. One aspect of human motion analysis is kinematics analysis. This can be achieved by using a motion capture system to track markers attached to the body and computing the angles between adjacent body segments, defined by a biomechanical model, using the marker trajectories. The biomechanical model divides a part of the body into a number of rigid segments so that the body mechanics can be quantified using the principles of classical mechanics.

2.4.2 Calculating Joint Kinematics

A method of calculating joint kinematics has been presented by the International Society of Biomechanics [93, 94]. Global and local coordinate systems are established to define coordinate frames associated with the capture volume and body segments, respectively [13, 93, 94].

The global frame is static and locates the marker coordinates using stereophotogrammetry. There are two types of local frames: technical frame and anatomical frame. The technical frame moves with the body segments to describe the movement [13]. It is reconstructed at each time frame from the instantaneous positions of three or more markers, which are tracked using the stereophotogrammetric system. These markers are called technical markers and are placed on anatomical landmarks and

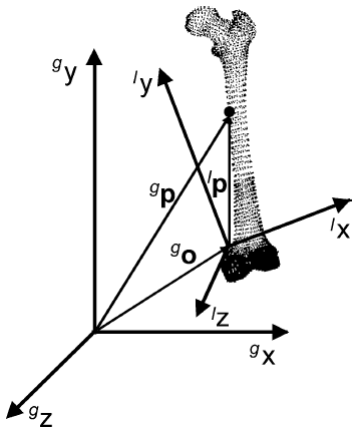

Figure 2.7: A point vector defined by both the global frame and the local frame. Reprinted from [13]

other locations on the corresponding body segment. The anatomical frame is a local frame defined by selected anatomical landmarks, usually bony prominences. The anatomical landmarks that are hidden internally are approximated using the surface markers and predictive models or a functional approach. The position vectors of the markers are measured using the stereophotogrammetric system and are given with respect to the technical frame from an anatomical calibration.

Joint kinematics describes the relative motion of a body segment with respect to its adjacent proximal segment. Figure 2.7 is an illustration of a point vector (p) defined in both the global frame (g_x, g_y, g_z) and local frame (l_x, l_y, l_z). The position vector of a point in global and local frames can be written as ${}^{g}p$ and ${}^{l}p$, respectively. If an orientation matrix and a position vector of the local origin relative to global are ${}^{g}R_l$ and ${}^{g}o$, respectively, the position vector of a point in the global frame, ${}^{g}p$, can be defined as in the equation below.

$$^{g}p = {}^{g}R_{l}{}^{l}p + {}^{g}o \tag{2.1}$$

Using the same notations, the orientation matrices of a local frame with respect to a global frame of a proximal and a distal body segment can be written as ${}^{g}R_{p}$ and ${}^{g}R_{d}$, respectively. Similarly the position vectors of the local origin with respect to the global frame are given as ${}^{g}o_{p}$ and ${}^{g}o_{d}$ for the proximal and the distal segments, respectively. Therefore the joint orientation matrix, R_{j}, and the joint position vector, t_{j}, are defined using the equations below.

$$R_{j} = {}^{g}R_{p}^{T\,g}R_{d} \tag{2.2}$$

$$t_{j} = {}^{g}R_{p}^{T}({}^{g}o_{d} - {}^{g}o_{p}) \tag{2.3}$$

Three joint rotation matrices for the component rotations, as well as the relative orientation of the proximal (x_{p}, y_{p}, z_{p}) and the distal (x_{d}, y_{d}, z_{d}) segment frames can be calculated at any time. The orientation of the distal segment frame with respect to the proximal segment frame can be defined by three sequenced rotations [13]. The orientation matrix of the distal frame rotation by an angle, α, about the x-axis, is given by the equation 2.4.

$$R_{j\alpha} = \begin{pmatrix} 1 & 0 & 0 \\ 0 & \cos\alpha & -\sin\alpha \\ 0 & \sin\alpha & \cos\alpha \end{pmatrix} \tag{2.4}$$

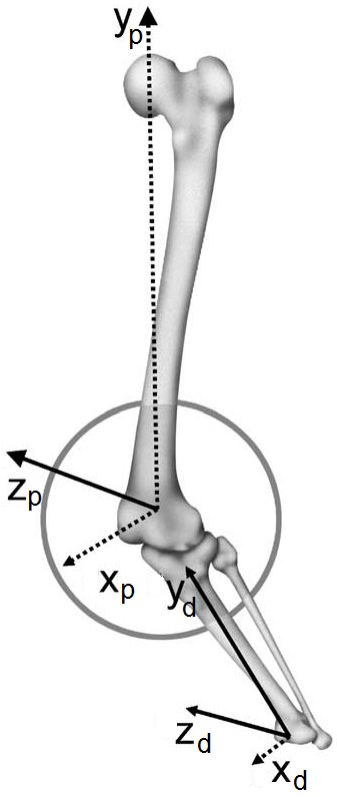

Figure 2.8: Anatomical frames of proximal and distal segment. Reprinted from [13]

Likewise, the orientation matrix of the distal frame rotation by an angle, β, about the y-axis, is given by the equation below.

$$R_{j\beta} = \begin{pmatrix} \cos\beta & 0 & \sin\beta \\ 0 & 1 & 0 \\ -\sin\beta & 0 & \cos\beta \end{pmatrix} \tag{2.5}$$

Finally, the orientation matrix of the distal frame rotation by an angle, γ, about the z-axis, is given by the equation 2.6.

$$R_{j\gamma} = \begin{pmatrix} \cos\gamma & -\sin\gamma & 0 \\ \sin\gamma & \cos\gamma & 0 \\ 0 & 0 & 1 \end{pmatrix} \tag{2.6}$$

To calculate the orientation matrix of a rotation about an axis of the proximal frame, the corresponding rotation can be pre-multiplied to the previous rotation orientation matrix. In contrast, to calculate the orientation matrix of a rotation about an axis of the distal frame, the corresponding rotation can be post-multiplied to the previous rotation orientation matrix. Therefore, the rotation matrix of a rotation about the z_p axis, followed by a rotation about the floating x axis and finally by a rotation the y_d can be calculated by the equations below.

$$R_j = R_{j\gamma}R_{j\alpha}R_{j\beta} = \begin{pmatrix} r_{11} & r_{12} & r_{13} \\ r_{21} & r_{22} & r_{23} \\ r_{31} & r_{32} & r_{33} \end{pmatrix} \tag{2.7}$$

$$R_j = \begin{pmatrix} \cos\gamma\cos\beta - \sin\gamma\sin\alpha\sin\beta & -\sin\gamma\cos\alpha & \cos\gamma\sin\beta + \sin\gamma\sin\alpha\cos\beta \\ \sin\gamma\cos\beta + \cos\gamma\sin\alpha\sin\beta & \cos\gamma\cos\alpha & \sin\gamma\sin\beta - \cos\gamma\sin\alpha\cos\beta \\ -\cos\alpha\sin\beta & \sin\alpha & \cos\alpha\cos\beta \end{pmatrix} \tag{2.8}$$

The angles α, β and γ can be computed using the equations 2.9, 2.10 and 2.11.

$$\alpha = \arcsin r_{32} \tag{2.9}$$

$$\beta = \arcsin\left(\frac{-r_{31}}{\cos\alpha}\right) \tag{2.10}$$

$$\gamma = \arcsin\left(\frac{-r_{12}}{\cos\alpha}\right) \tag{2.11}$$

The sequence of rotations shown above follows the Grood and Suntay [33] Joint Coordinate System (JCS) convention. It defines joint rotations such that the first rotation is about the medial-lateral y-axis of the proximal segment coordinate system, the second rotation is about a floating axis orthogonal to the y-axis of the proximal segment and the z-axis of the distal segment and the third rotation is about the longitudinal z-axis of the distal segment coordinate system.

2.5 Multi-Segment Foot Model

2.5.1 Introduction

The measurement of lower-limb kinematics via stereophotogrammetry is a well established part of clinical decision-making for patients with known gait disabilities. Conventional lower body models, which comprise a rigid pelvis, thigh, shank and foot, do not provide adequate information about foot kinematics during in vivo motion analysis of the foot. Hence this has been a problem for treatment specific to feet. In order to address this issue, many multi-segment foot models have been developed. These models have been tested for clinical significance to justify their clinical use. Multi-segment models have their own set of small segments, defined by strategically placed markers, and systematic procedures for detailed and repeatable attainment of foot kinematic results. A motion capture system is used to record the three-dimensional (3D) coordinates of these markers, that have been affixed to a moving test subject, at a given capture rate. The marker coordinates can be analysed to calculate the segmental axis orientations and hence the inter-segmental angles for each frame.

2.5.2 Conventional Lower Body Model

The conventional lower body model was developed by Kadaba and Davis [23, 40, 41]. It consists of pelvis, thigh, shank and foot. The conventional model represents the foot as a single vector only and therefore does not provide adequate information about foot kinematics during in vivo motion analysis of the foot, especially when foot deformity is present. For example, the conventional model will not be able to detect forefoot dorsiflexion with respect to the hindfoot during late stance while the hindfoot

remains in equinus in a planovalgus foot. However, recent development of motion analysis technology has led to higher resolution and precision in data acquisition. This has allowed clinicians and researchers to scrutinise the relative motion within the foot during gait.

2.5.3 Plug-In Gait

Plug-in Gait (PiG) is the commercial name used by Vicon (Vicon Motion Systems, Oxford, UK) for the implementation of the conventional gait model. It can be divided into four modelling modules: lower body kinematic model, upper body kinematic model, lower body kinetic model and upper body kinetic model. It takes in anthropometric measurement parameters and marker trajectories to calculate joint kinematics and joint kinetics. The anthropometric measurements include body mass, height, leg length, knee width and ankle width. The marker trajectories are obtained by tracking physical markers as well as virtual markers calculated using specific sets of physical markers and subject measurements. Each kinematic model consists of various rigid segments and the segments and corresponding segment axes are defined by surface markers placed on bony landmarks on the foot and leg. The segments are assumed to be rigid and are defined on a frame-by-frame basis.

2.5.4 Multi-Segment Foot Model

Since the conventional lower body model is unsuitable for providing information about multiplanar foot kinematics, multi-segment foot models have been developed to address the issue. Various researchers around the world have proposed multi-segment

foot models with two or more segments. Despite the vast amount of research undertaken so far, a general consensus is yet to be reached on the optimal method of modelling the foot during gait. That said, each model has been tailored to the information required.

Cadaveric studies have shown that accurate models are needed to describe the complex mechanics of the foot and ankle [29, 75]. Kepple et al. [42] made the first attempt to propose a multi-segment foot model. The model consisted of lower leg (tibia) and hindfoot (calcaneus) segments and was tested on five healthy adult subjects to output three-dimensional kinematics. In the 1990s, many other two-segment foot models composed of the lower leg and the hindfoot were proposed [53, 59, 73, 74]. Where they differed was the dynamic inter-segmental angle calculation method. This is epitomised by varying definitions of neutral standing position, represented either as subtalar neutral or as actual angles. The optimum way of referencing to a neutral standing position is still in debate as each method has varying degrees of feasibility for pathologic feet.

From the late 1990s, research groups started proposing multi-segment foot models with three or more segments. Kidder et al. [45] introduced the Milwaukee Foot Model, which consists of the lower leg, hindfoot, forefoot and hallux, in 1996. Other variations of four-segment foot models have also been developed since then but they differ in anatomic classifications of these segments [28, 67]. The Oxford Foot Model, first proposed in 2001 by Carson et al. [14], consisted of the tibia, hindfoot, forefoot and hallux segments. In 2006, Stebbins et al. [78] modified it for wider clinical application. Hunt et al. [37] and Kitaoka et al. [46] proposed models without the

hallux segment, while Wu et al. [92] and Leardini et al. [48, 49] suggested models which included a midfoot segment. Several models separated the forefoot into medial or first metatarsal and lateral segments [16, 39, 49, 66, 88]. MacWilliams et al. [55] proposed a model, composed of 9 segments including the lower leg, calcaneus, talus and navicular, cuboid, lateral forefoot, medial forefoot, lateral toes, medial toes and hallux. Simon et al. [76] introduced the Heidelberg Foot Measurement Method (HFMM), which represented the foot kinematics using two-dimensional angles as opposed to the more widely used approach, three-dimensional segment rotation.

The Shriners Hospital for Children Greenville (SHCG) group proposed a foot model with two segments (hindfoot and forefoot) [21, 22, 72] but this was later modified by Saraswat et al. [71] for easier and wider clinical application. The modified SHCG (mSHCG) foot model increased the number of segments from two to four, now, composed of shank, hindfoot, forefoot and hallux segments. More recently, De Mits et al. [24] proposed a clinically applicable six-segment foot model, known as the Ghent Foot Model (GFM). The GFM consists of lower leg, rearfoot, midfoot, forefoot, medial forefoot and hallux. It is unique in that it tried to find a compromise between the easiness in clinical application, which is a common characteristic of the foot models with less than five segments, and accuracy in describing entire foot kinematics, which is a common characteristic of the foot models with more than five segments.

Motion of the foot in children has only been assessed by a handful of research groups [20, 55, 78]. Assessment of the motion of children's feet poses more difficulty in comparison to that of adult feet, as one has to deal with the smaller surface area of the foot and greater kinematic variability [80]. Also, only a few have published studies

that investigated both stance and swing phases [14, 39, 45, 76, 78, 90, 92] as most studies have focused on the stance phase. Many studies have tested their models on a pathologic population. The Milwaukee Foot Model has been implemented to evaluate ankle arthrosis [44], rheumatoid arthritis [43] and posterior tibialis tendon dysfunction [11, 56, 60]. Woodburn et al. [90] and Siegel et al. [74] have also assessed rheumatoid arthritis, while Tome et al. [86] have also published their study on subjects with PTTD. Several research studies have been conducted using the Oxford Foot Model [14, 78] to assess clubfoot [84], forefoot varus [2] and cerebral palsy [79].

Several studies have looked at the accuracy of skin-mounted marker-based foot kinematics by comparing it with that measured using intra-cortical bone pin markers [5, 57, 65, 92]. The main advantage of using intra-cortical bone pins to measure the foot kinematics is its ability to directly represent the kinematics of the intrinsic bones within the foot. However, the main drawback of this technique is its invasive nature as it requires the subjects to undergo a surgery using anesthetics to insert the bone pins. The inevitable gait adjustments required to accommodate the bone pins and the difficulty in placing the skin markers as well as the bone pin markers make it challenging to quantify the difference between the anatomical and marker-based segments. To compensate for this limitation, videofluoroscopy has been implemented to measure two-dimensional joint kinematics in dynamic trials [55] and compared it against that measured using skin markers. This technique has a major advantage in that it is able to detect the kinematics of the anatomical articulation. For example, it is able to detect the movement of the talus and distinguish tibiotalar from subtalar motion, which would not be possible with skin-mounted markers due to soft tissues

that surround the talus. That said, the main limitations with this method is that the subjects are exposed to the X-ray and is only measured in 2-dimensions. Moreover, the X-ray source of commercially available fluoroscopic image systems generates pulses at a maximum frequency of 25-30 Hz and therefore there is a risk of losing important foot motion during gait cycle.

When proposing new multi-segment foot models, it is vital to substantiate reliability and clinical significance before applying the model in routine clinical practice. Moreover, the following five standards should be met [7]:

1. State the location, accuracy and reliability of marker placement.
2. State the segment definitions.
3. State the definition of segment coordinate systems.
4. State the definition of joint parameters.
5. State the reliability of joint kinematics.

The accuracy of the foot model angle calculations depends on how the markers and segment axes relate to the underlying anatomy and to the assumptions made by the model. Moreover, awareness of the degree of variability found in multiplanar foot and ankle kinematics is critical when making clinical decisions. Large variation has been reported in the transverse plane [42, 49, 59, 74, 78] and this could be due to a lack of consistency of marker placement. Therefore, clear protocols are necessary for minimising the effect of marker placement on kinematic results.

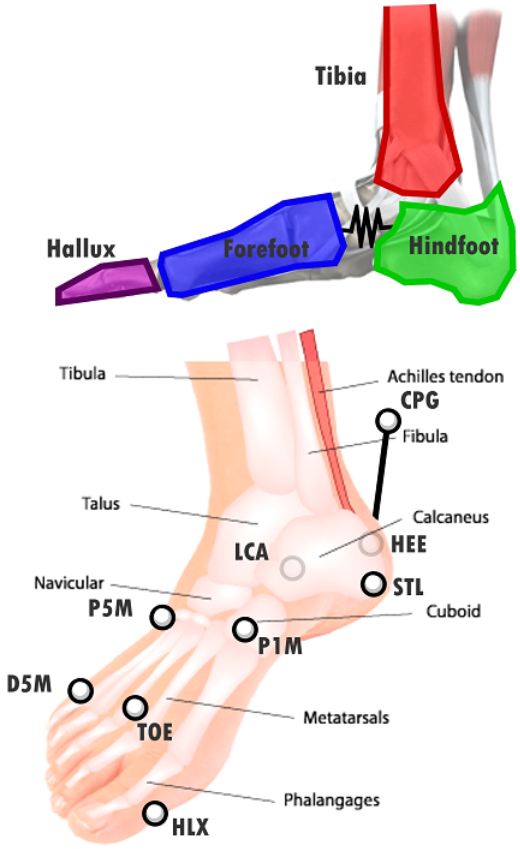

Figure 2.9: Schematic of Oxford Foot Model Segments. Modified from [14]

2.5.5 Oxford Foot Model

The first version of the OFM was tested for reliability on healthy subjects [14] and on children with clubfoot [84]. However these studies were limited to the stance phase only. The adapted version [78] aimed to widen its clinical utility so that it could be implemented on subjects with significant foot deformity like children with cerebral palsy. Stebbins et al. [79] demonstrated that the variability found in children with hemiplegic cerebral palsy using the OFM was similar to that of typically developing children.

The OFM consists of three rigid segments (tibia, hindfoot and forefoot) with the hallux modeled as a vector only (Figure 2.9). The segments are defined by surface markers placed on bony landmarks on the foot and leg. More details on the segment definition and the corresponding axes are discussed in Section 3.1.

2.6 Clinical Utility of Oxford Foot Model

2.6.1 Introduction

The Oxford Foot Model's clinical use ranges from patients with cerebral palsy (CP), to those with clubfeet and various other orthopaedic and neuromuscular disorders. It is used to plan management of their foot deformities and assess outcomes of treatment, as well as to monitor any deterioration in their feet. By 2010, over 400 patients had been assessed with the OFM in one clinical gait service and gait analysis had proved useful in locating dynamic deformity (for example, internal rotation in hindfoot compared with forefoot adduction), clarifying ambiguous findings from the

clinical examination or Plug-in Gait model-derived gait analysis, following up the progression of dynamic deformity and evaluating the quality of treatment outcome [83]. Information such as lower body joint angles, EMG, video data, kinetic data, temporal/spatial data from many different sources is recorded during a gait analysis session, in addition to multi-segment foot model data. All of this data is used to make treatment recommendations, but not all data is useful in every case. In the 50% of cases where foot model data was not directly influential, other sources of data were used instead. Observation of a subject walking via video recordings or the naked eye has limited usefulness in identifying gait dysfunction. For example, it may not be so easy to recognise ankle and/or midfoot plantarflexion for a hemiplegic child with foot drop during swing through simple observation. With the knowledge that the child is only displaying ankle plantarflexion with the forefoot well aligned with the hindfoot, it becomes easier to detect that spasticity of the plantarflexors could be the source of the gait disorder.

2.6.2 Repeatability

The repeatability of the Oxford Foot Model has been investigated. Carson et al. [14] examined between-trial, between-day and between-tester repeatability for two subjects and two testers. The between-trial standard deviation was less than $\pm 2^{\circ}$ for all inter-segment angles, showing good consistency between trials. This implies that skin movement artifacts are repeatable and systematic. The 95% confidence interval (CI) has been calculated for between-day and between-tester analyses. The expected differences between any two days (same tester) were $\pm 2.0^{\circ}$, $\pm 3.0^{\circ}$, $\pm 4.3^{\circ}$ and $\pm 6.5^{\circ}$

for global tibia, ankle joint complex, midfoot and hallux angles, respectively. The between-tester results exhibited similar values, never exceeding by more than 1° the between-day results. In summary, the repeatability of the Oxford Foot Model has been shown to be acceptable and therefore can provide foot kinematic measurements with confidence.

Stebbins et al. [78] carried out a comprehensive repeatability study on 15 healthy children. The results suggested that the sagittal plane angles are the most repeatable while the transverse plane angles are the least repeatable as they exhibited the highest variability out of all planes. Curtis et al. [20] went further to demonstrate that particularly high variability has been observed in the hindfoot rotation where the standard deviation of the between-test repeatability varied from 9.4° to 10.8° for eight healthy children tested. This poor repeatability has been linked with the difficulty in defining and identifying the hindfoot neutral position. Curtis et al. went on to conclude that the Oxford Foot Model demonstrates good inter-centre repeatability in the sagittal plane but needs further investigation to validate the inter-centre repeatability in the other two planes, especially for the hindfoot.

2.7 Accuracy of Oxford Foot Model

2.7.1 Limitations

The accuracy of the OFM angle calculations depends on how the markers and segment axes relate to the underlying anatomy. In the Oxford Foot Model as in other leg and foot models, there is a limitation in that layers of skin, soft tissue and fat cover bony anatomical landmarks. This affects the accuracy of the angle calculations because

markers do not follow the movement of the underlying bony anatomy. Secondly, ligaments and tendons attached to the bones could interfere with the movement between the markers and the underlying anatomy. Thirdly, it may be difficult to pinpoint the exact locations of palpable landmarks. Fourthly, the rigid body assumptions given for the segments could potentially neglect significant movement within the segment. Finally over-simplification of the foot by categorising it into too few segments leads to an inability to measure important foot joint kinematics caused by the relatively small size of the foot and the relatively small range of motion of foot joints.

Furthermore, the challenge correlated to the dynamic assessment of ankle and foot motion during gait in pediatric feet inevitably exists, as one has to deal with smaller surface area of the foot.

2.7.2 Tibia

The Oxford Foot Model Tibia segment is defined using the locations of the ankle joint centre (AJC) and the knee joint centre (KJC). Calculating the KJC requires the global position of the Hip Joint Centre (HJC), lateral thigh (THI), lateral femoral condyle (KNE) markers as well as knee offset (half the knee width), which is measured from clinical examination, and thigh wand angle offset [6]. The KJC is located in the plane defined by the HJC, THI and KNE markers. It is distanced from the KNE marker by the knee offset in a direction perpendicular to the line adjoining the HJC and the KJC in the HJC-THI-KNE plane. This is known as the "chord" function. The Ankle Joint Centre is calculated by taking the mid-point of Medial (MMA) and Lateral (ANK) Malleoli markers. The Tibia is calculated based on the Knee Joint Centre, which

relies on more proximal markers on the knee, thigh and hip. Therefore, the accuracy of the Tibia segment kinematics is dependent on the accuracy of the aforementioned marker placements. On the other hand, the hindfoot is completely independent and thus is not affected by any other segments.

2.7.3 Hindfoot

The Oxford Foot Model hindfoot segment represents the calcaneus and talus complex in the foot. The hindfoot segment is defined using the heel (HEE), lateral calcaneus (LCA), sustentaculum tali (STL) and proximal calcaneus (PCA) markers. The hindfoot segment is an area where relatively thick layers of fatty and soft tissue exist between the surface of skin and the underlying anatomy, especially where the LCA and the STL markers are placed. As there is a lack of palpable bony anatomical landmarks to place the markers on, the agreement between default marker-based segment definitions and the underlying anatomy may not be accurate.

Misplacement of the hindfoot markers will affect the orientation of hindfoot segment axes. However, the difficulty in palpating bony landmarks on lateral and medial sides of the hindfoot means that it is very difficult to accurately locate LCA and STL markers repeatably. The current Oxford Foot Model requires LCA and STL markers to be equidistant from the HEE marker. However in practice, the LCA and STL markers are placed roughly equidistant from the HEE marker without use of any measurement tools or jigs. Potential misplacement of the markers could lead to significant errors in foot kinematic measurement.

In the hindfoot, the HEE marker lies close to the base of the Achilles tendon while

the LCA marker is positioned close to the inferior peroneal retinaculum. Ligaments and tendons attached to the bones cause movement between the markers and the underlying anatomy.

2.8 Conclusion

The measurement of foot kinematics via stereophotogrammetry is a well-established part of clinical decision-making for patients with known gait disabilities. However, there are limitations associated with estimating the orientation of bone from reconstructed skin-marker trajectories. The accuracy of the OFM angle calculations depends on how the markers and segment axes relate to the underlying anatomy. In the Oxford Foot Model as in other models, there is a limitation in that marker axes may not agree well with the underlying anatomy-based axes and that layers of skin, soft tissue and fat cover anatomical landmarks. This affects the accuracy of the angle calculations because markers may not follow the movement of the underlying bony anatomy. This was the motivation behind the present research and the aim of the current thesis was set to investigate the agreement between marker-based and anatomy-based hindfoot and tibia segment axes in the Oxford Foot Model. The experimental methods used to achieve the aim are described in the next chapter.

3 Experimental Methods

The aim of the thesis was to investigate the agreement between marker-based and anatomical hindfoot and tibia segment axes in the Oxford Foot Model. This chapter summarises the experimental data collection and processing protocols implemented in the thesis.

Subject recruitment is outlined to begin with. An experimental data collection section succeeds the subject recruitment section and is divided into clinical examination, gait analysis and medical imaging. The same tester conducted the clinical examination and the gait analysis on the same day for all subjects. The medical imaging session was carried out either straight after the gait analysis session or the next day. Ankle and foot kinematic data collected was processed using the protocol described in the kinematic data processing section. This section also summarises the protocol used to segment and reconstruct CT images. Lastly rigid body transformations used to obtain segment orientations are explained.

3.1 Subject Recruitment

Twenty-one adult females with no known foot deformity were recruited to the study (42 feet in total). The subjects were recruited initially to investigate [50] the development of Patellofemoral Pain Syndrome (PFPS) in long-distance runners and thus, the participants were recruited from running clubs in Oxfordshire and categorised into two groups: a normal group with no previous history of PFPS and a group with a previous history of PFPS. This study was given approval by the National Health Service

(NHS) Research Ethics Committee and the Research and Development Committees of the John Radcliffe Hospital NHS Trust and Nuffield Orthopaedic Centre NHS Trust (Study Reference: 09/H0605/101). The data generated from this study has been granted to be stored by Dr Amy Zavatsky (supervisor) and be used by members of the research team at the Nuffield Department of Orthopaedic, Rheumatology and Musculoskeletal Sciences for 10 years after the end of the study (see Appendix). For the purpose of this study, the groups were combined together as healthy participants with no foot deformities or injuries.

Out of the twenty-one participants, one had to be excluded from the study as she developed patellar tendonitis four weeks into testing and another had to be excluded from the study as she fell on the treadmill during testing and the testing was terminated for health and safety reasons.

Inclusion criteria required that subjects were 18 years or older and that they were injury-free at the time of testing. Exclusion criteria required that subjects had no previous history of lower-limb surgery, knee joint swelling or patellar dislocation. In addition, it was required that subjects did not suffer from severe claustrophobia, had no medical implants and were not pregnant at the time of the testing for medical imaging purposes. A subject was recruited if both inclusion and exclusion criteria were met and two consent forms were signed.

A detailed participant information leaflet was sent to all subjects who showed interest in participating in the study and there was an offer to discuss the investigation with the Principal Investigator.

3.2 Anthropometric Data Collection

The clinical examination and gait analysis were conducted at the Oxford Gait Laboratory (Nuffield Orthopaedic Centre NHS Trust, Oxford, UK).

Anthropometric measurements were taken, as the subject lay supine. A designated tester took measurements for all subjects. Leg length, the distance from the anterior superior iliac spine (ASIS) to the medial femoral condyle, plus the distance from the medial femoral condyle to the medial malleolus, were measured using a measuring tape. The knee width, ankle width and the distance between the left and the right ASIS were measured using a digital caliper. Height was measured using a stadiometer while mass was equal to the vertical ground reaction force, measured using a force plate during quiet standing. These anthropometric data were required as input for the Plug-in Gait Model and the Oxford Foot Model.

3.3 Gait Analysis

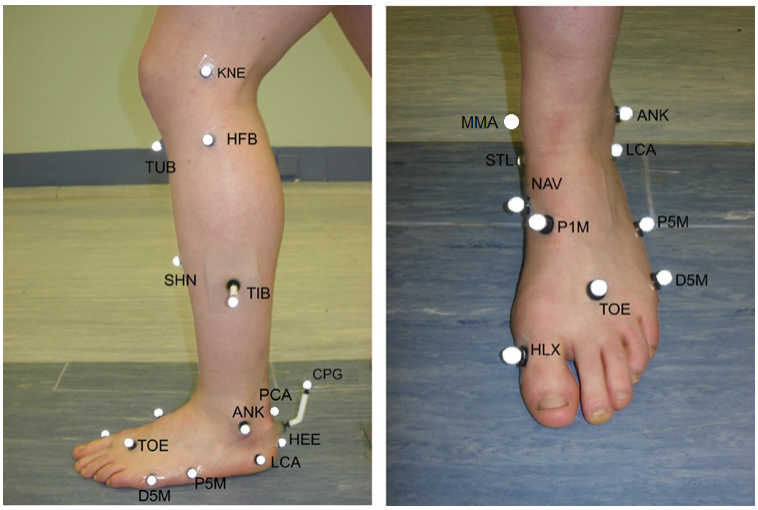

Figure 3.1: Lateral (left) and anterior (right) view of Oxford Foot Model tibia and foot markers

Spherical reflective markers of 9 mm diameter were attached (figure 3.1 and table 3.1) using double-faced tape to the locations specified by the Oxford Foot Model (for foot, ankle and tibia) and the Plug-in Gait model (for other parts of the lower body). The same tester placed the markers for all subjects. Prior to the placement of the markers on the foot and ankle, the locations were marked with a permanent pen so that the radio-opaque markers later used for the medical imaging could be placed on the same locations as the reflective surface markers.

Each subject's lower limb 3D kinematics were recorded at 200 Hz using a 12-camera VICON MX system (Vicon Motion Systems Ltd., Oxford, UK). The laboratory was calibrated through a standard process. Static trials were performed on each subject with the OFM and PiG markers placed on their pelvis and lower limbs. The

Table 3.1: Oxford Foot Model markers and their respective positions

Name	Position	Segment
KNE	Lateral femoral condyle	Femur
TUB	Tibial tuberosity	Tibia
HFB	Head of fibula	Tibia
ANK	Lateral malleolus	Tibia
MMA	*Medial Malleolus*	*Tibia*
SHN	Anterior aspect of shin	Tibia
TIB	Lateral aspect of lower-leg (wand marker)	Tibia
HEE	Posterior distal aspect of heel	Hindfoot
PCA	*Posterior proximal aspect of heel*	*Hindfoot*
CPG	Wand marker on posterior calcaneus	Hindfoot
LCA	Lateral calcaneus	Hindfoot
STL	Sustentaculum tali	Hindfoot
P1M	Base of first metatarsal	Forefoot
P5M	Base of fifth metatarsal	Forefoot
D1M	*Head of first metatarsal*	*Forefoot*
D5M	Head of fifth metatarsal	Forefoot
TOE	Between second and third metatarsal heads	Forefoot
HLX	1st phalanx hallux	Hallux

Markers marked in italics are used in the static trial only and are removed for dynamic trials.

subjects were asked to stand still on a force plate (Model OR6, AMTI, MA, USA) with weight evenly distributed over both feet. For dynamic trials, the subjects were asked to walk barefoot at self-selected pace along a 10 m walkway. Without forcing the feet to make contact with the force plates, located in the walkway, the subjects walked across it until five satisfactory left and right force plate foot strikes were recorded. Ground reaction force data was collected at 1000 Hz using the force plate as the subject made each force plate strike. The force plate data was synchronised with the motion capture system.

After the gait analysis session, the markers were removed and the subjects were taken to the Radiography Department for medical imaging.

3.4 Imaging

Medical imaging was carried out at the Churchill Hospital (Oxford Radcliffe Hospitals NHS Trust, Oxford, UK). Radio-opaque monitoring electrodes (Type 2223, 3M Healthcare, Neuss, Germany) were placed on the feet at the locations marked by a permanent marker from the gait analysis session. CT images (GE 64-slice Lightspeed VCT scanner) were acquired, as the subjects lay supine with their feet in a semi-weight-bearing posture. Tube voltage and tube current were 100 kV and 110 mA, respectively. The scan was taken using the standard bone and soft tissue scan algorithm and the slice thickness and slice distance were both 0.625 mm.

The semi-weight bearing posture was achieved using a custom-built rig that applied 40% body-weight to the lower extremity (Figure 3.2). The rig was made from wood and was designed to fit into both a CT and an MRI scanner. It consisted of a

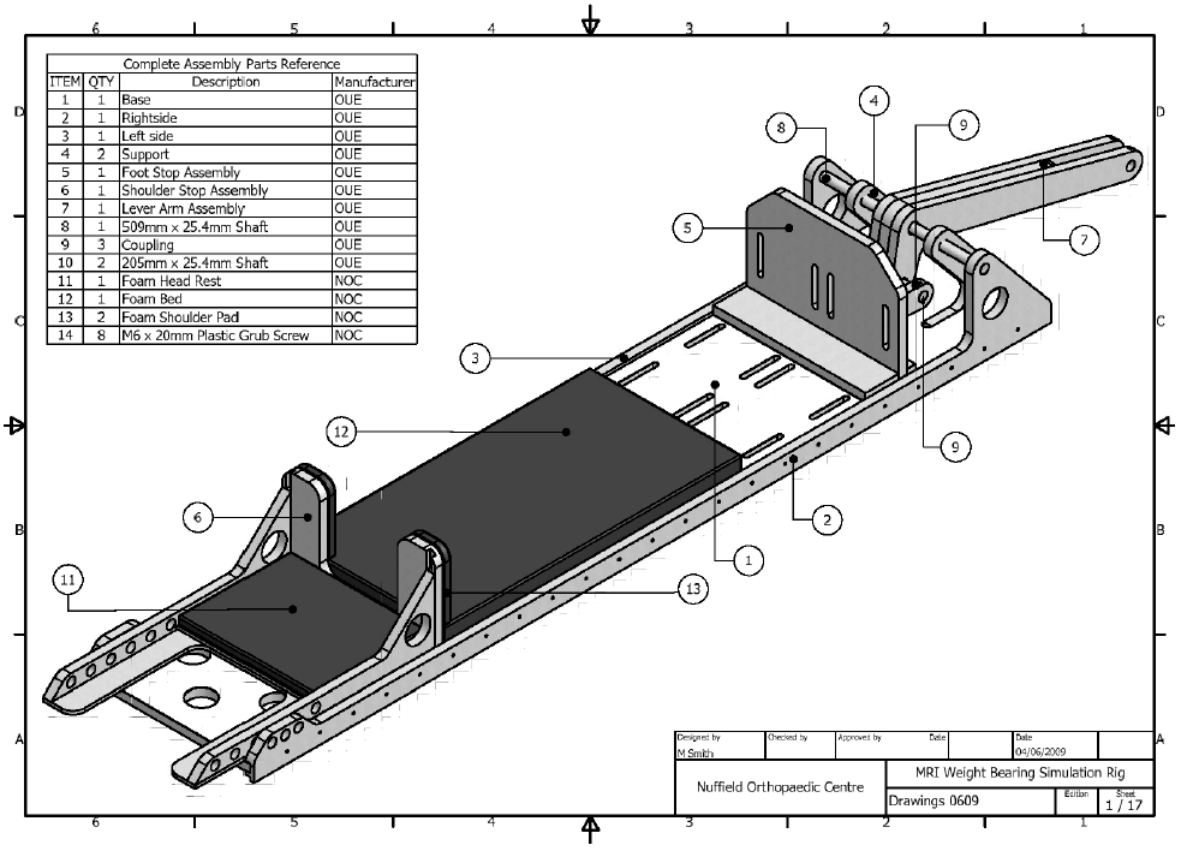

Figure 3.2: Drawing of the custom-built rig [50]

support bed, a footplate lever and an adjustable shoulder support. Foam pads were inserted on the support bed and the shoulder support to provide comfort. The subject lay supine in such a way that the shoulders were rested against the shoulder support and the plantar surfaces of the feet were in contact with the footplate with both knees flexed to about 30°. To enhance image quality, each foot was scanned individually, which was achieved by maximally flexing the opposite knee to move the contralateral leg out of the image capture volume.

Load was applied to the footplate lever using a container filled with water. The applied load was 40% body weight. The subjects had to push against the footplate to counterbalance the load applied to the foot. The CT images were captured in this posture and the same procedure was repeated for the opposite foot. There are two assumptions when replicating the position of the foot in standing with 40% bodyweight. The first is that the alignment of the foot bones is in the same position with 40% loading as in standing (100% bodyweight), and the other is that applying a load in lying down might distribute the load across the sole of the foot differently compared to standing. Kothari et al. (unpublished work) verified that 40% load accurately replicated the arch position compared to standing. Therefore it is better than comparing to a completely unloaded condition, which clearly would be different. Another limitation is that the subjects were assumed to be in a position that replicated standing/weightbearing, but this was not fully verified.

3.5 Kinematic Data Processing

Vicon Nexus (Vicon Nexus Version 1.5.1, Vicon Motion Systems, Oxford, UK) was used to collect and process the coordinate data from the static and the level walking trials. The anthropometric measurements collected during the clinical examination were specified. A standard Vicon Skeleton Template was created that represented the generic marker set from the Oxford Foot Model. The static trial was reconstructed, the markers were labeled and the marker coordinate data were low-pass filtered using quintic-spline smoothing. The skeleton template file was then scaled to the individual subject to create a Vicon Skeleton. The static trial was processed using the Plug-In Gait and Oxford Foot Model Static gait models. The three-dimensional coordinate data for the walking trials were reconstructed, labeled and low-pass filtered using quintic spline smoothing. Foot-strike and toe-off times were detected from the vertical component of the ground-reaction-force with a cut-off value of 10 N. Knee, ankle and foot joint angles were calculated using the Oxford Foot Model. The marker trajectory data and three-dimensional joint angles were exported to Matlab (V7.13, The Mathworks Inc., Natick, MA, USA) for further analysis.

The knee flexion-extension axis is dependent on the position of the thigh wand marker. If this marker is misaligned then due to cross-talk, the angles may not reflect true knee motion. Misplaced thigh wand markers can be accounted for by including a rotational offset (about the long axis of the thigh). This offset is determined by assuming minimal knee motion in the frontal plane, and iteratively changing the offset until frontal plane knee motion is minimized [6]. Baker et al. [6] proposed a method of applying a correction for the thigh wand marker misalignment. It first calculates the

knee ab-adduction angle based on the thigh wand marker position. Then a new knee ab-adduction angle is calculated by shifting the marker by a pre-determined offset. Through an iterative process, the thigh offset that gives the minimum amplitude of the knee ab-adduction angle is identified. This offset is applied to correctly realign the thigh wand marker and thus to minimise kinematic crosstalk. This procedure was implemented to process the kinematic data used in this investigation.

3.6 Image Data Processing

The objectives of the image data processing was to obtain the principal axes of the subjects' calcanei and tali and to obtain the 3D coordinates of the radio-opaque markers and the bony anatomical landmarks corresponding to the ideal marker locations.

Based on the CT images, the calcanei of all 38 feet were segmented using Mimics software (Materialise NV, Leuven, Belgium). Then 3D models of the calcanei and tali were created and these were used to create STL files, which is a file format suitable for Computer Aided Design (CAD) software. The STL files were imported into Solidworks (Dassault Systèmes SolidWorks Corp., Vélizy, France) to create 3D CAD models of the calcanei and tali. The mass properties tool in Solidworks allowed the unit vectors of the principal axes and the coordinates of the centre of mass to be obtained. The CT global coordinate system was retained when creating the Solidworks model from the STL files. The first principal axis of the calcaneus was regarded as the most clinically relevant way to represent the orientation of this bone. The principal axis is implied in the Oxford Foot Model as it is assumed that the Oxford Foot Model hindfoot Anterior-Posterior axis is representing the long axis of the calcaneus.

The OFM hindfoot segment models the calcaneus and talus. However, the hindfoot markers are all placed on the calcaneus, not on the talus and therefore the markers only replicate the calcaneus. Even so, a layer of soft tissue exists between the calcaneus and the markers and thus hinders accurate representation of the movement of the calcaneus. Accurate knowledge of calcaneus rotation provides useful clinical information and minimises making inappropriate treatment recommendations. For example, if the marker-based kinematic data showed the hindfoot to be rotated, clinicians might recommend surgical intervention (calcaneal osteotomy), when in reality there is no calcaneal rotation. To find the long axis of the calcaneus, it was required to calculate its first principal axis, assuming uniform density, since the principal axis of a body with uniform density is an axis of rotational symmetry.

Moreover, the 3D coordinates of the radio-opaque markers and, where relevant, the bony coordinates corresponding to the ideal marker coordinates were obtained from the CT images using the Mimics software. For each radio-opaque marker, the slice that located its central point was identified in all three planes and the corresponding coordinates were recorded. To extract the bony coordinates, the slice that located the appropriate, and typically the most prominent, point was identified for all three planes and the corresponding coordinates were recorded.

3.7 Rigid Body Transformation

In 1993, Söderkvist and Wedin [77] introduced a method of calculating a best-fit rigid-body transformation matrix from noisy marker coordinates using the Singular Value Decomposition (SVD) method. This method can be used to calculate a 4×4

transformation matrix from a matrix of the instantaneous positions of the markers at a given time frame and a matrix of the static reference positions of the markers. In short, the method first takes the information of the XYZ coordinates of the marker positions to find a point that marks the centre of each of a body of markers at a given time frame and a body of markers at the static reference position. It then centres each body by subtracting one central point from another. The transpose of the matrix that comprises the subtracted marker positions of the body at a given time frame is pre-multiplied by the matrix that comprises the subtracted marker positions of the body at the static reference position. The singular value decomposition of the resultant matrix outputs a transformation matrix. The transformation matrix contains a 3×3 rotation matrix and a 3×1 translation vector and therefore the amount of rotation and translation required to transform from the reference position of a rigid body to its instantaneous position can be computed. By comparing this information with the kinematic data gathered from gait analysis, one can test the rigid body assumption of the Oxford Foot Model segments. More detailed information on the method is presented in chapter 4.

The accuracy of this method is influenced by the rigidity assumption of a body segment. If the markers move significantly relative to each other due to skin motion artifact, the corresponding body segment cannot be approximated as a rigid body.

3.8 Conclusion

In total, of twenty-one subjects recruited into the study, nineteen subjects were eligible for analysis. With the experimental data available from clinical examination,

gait analysis and CT imaging, it was possible to investigate how well the marker-based and the anatomical-based hindfoot and tibia segment axes align statically. This static comparison of marker-based hindfoot and tibia segment axes and anatomical definition is described in the next chapter. Moreover, investigation of how marker misplacement affects the static hindfoot and tibia anatomical segment definition was carried out. This analysis is also presented in the next chapter.

4 Static Comparison of Marker Based Hindfoot and Tibia Segment Axes and Anatomical Definition

4.1 Introduction

The Oxford Foot Model hindfoot segment represents the calcaneus and the talus while the tibia segment represents the tibia and fibula. For the hindfoot segment, there is a lack of palpable bony surfaces to place the markers on and therefore the markers can only be placed on areas where there are relatively thick layers of soft tissue and fat. This potentially hinders an accurate description of the movement of the calcaneus and talus. For the tibia segment, the axes are defined using the Knee Joint Centre and medial and lateral malleoli markers. The Knee Joint Centre is an derived anatomical landmark, whereas medial and lateral malleoli are palpable anatomical landmarks. Even for palpable landmarks, the question remains as to how well the markers describe the underlying anatomy. Therefore the purpose of this study was to investigate how well the marker-based and the anatomy-based hindfoot and tibia segment axes align. In this chapter, the marker-based hindfoot anterior-posterior axis was also compared with the calcaneus and talus first principal axes, while the marker-based tibia longitudinal axis was compared with that defined from the malleoli coordinates and the Knee Joint Centre.

4.2 Tibia Segment Definition as Defined by OFM

- **Origin**: Midpoint between the Medial (MMA) and Lateral (ANK) Malleoli markers. Defined as Ankle Joint Centre (AJC).

$$\overrightarrow{o}_{\mathrm{T}} = \overrightarrow{P}_{\mathrm{AJC}} = \frac{\overrightarrow{P}_{\mathrm{MMA}} + \overrightarrow{P}_{\mathrm{ANK}}}{2} \tag{4.1}$$

- **Proximal-Distal (P-D) Axis, y**: Vector from the origin to the Knee Joint Centre* (KJC). The positive direction points proximally for both legs.

$$\overrightarrow{y}_{\mathrm{T}} = \frac{\overrightarrow{P}_{\mathrm{KJC}} - \overrightarrow{P}_{\mathrm{AJC}}}{\left\| \overrightarrow{P}_{\mathrm{KJC}} - \overrightarrow{P}_{\mathrm{AJC}} \right\|_2} \tag{4.2}$$

- **Interim Medial-Lateral Axis, i**: Vector from the MMA to ANK.

$$\overrightarrow{i}_{\mathrm{T}} = \frac{\overrightarrow{P}_{\mathrm{ANK}} - \overrightarrow{P}_{\mathrm{MMA}}}{\left\| \overrightarrow{P}_{\mathrm{ANK}} - \overrightarrow{P}_{\mathrm{MMA}} \right\|_2} \tag{4.3}$$

- **Anterior-Posterior (A-P) Axis, x**: Perpendicular to the P-D axis and the interim medial-lateral axis. The positive direction is taken to point anteriorly so for a left leg, it is necessary to take $\overrightarrow{x_T} = -\overrightarrow{x_T}$.

$$\overrightarrow{x}_{\mathrm{T}} = \overrightarrow{y}_{\mathrm{T}} \times \overrightarrow{i}_{\mathrm{T}} \tag{4.4}$$

- **Medial-Lateral (M-L) Axis, z**: Cross product of the A-P and P-D axes. The positive direction points laterally for a right leg. For the left leg, it is positive medially.

Figure 4.1: Schematics of the Chord Function to Locate the Knee Joint Centre [97]

$$\overrightarrow{z}_{\mathrm{T}} = \overrightarrow{x}_{\mathrm{T}} \times \overrightarrow{y}_{\mathrm{T}} \tag{4.5}$$

*Knee Joint Centre (KJC) (Figure 4.1): Calculating the KJC requires the global position of the Hip Joint Centre (HJC), lateral thigh (THI), and lateral femoral condyle (KNE) markers as well as knee offset (half the knee width), which is measured from clinical examination, and thigh wand angle offset [6]. The KJC is located in the plane defined by the HJC, THI and KNE markers. It is distanced from the KNE marker by the knee offset in a direction perpendicular to the line joining the HJC and the KJC. This is described as the "chord" function by Vicon [97].

4.3 Hindfoot Segment Definition

- **Origin**: Distal Heel (HEE) marker.

$$\overrightarrow{o}_{\mathrm{H}} = \overrightarrow{P}_{\mathrm{HEE}} \tag{4.6}$$

- **Mid-point (MID)**: Mid-point between the Sustentaculum Tali (STL) and Lateral Calcaneus (LCA).

$$\overrightarrow{P}_{\mathrm{MID}} = \frac{\overrightarrow{P}_{\mathrm{STL}} + \overrightarrow{P}_{\mathrm{LCA}}}{2} \tag{4.7}$$

- **Anterior-Posterior (A-P) Axis, x**: The vector from the origin to MID and parallel to global x-y plane (i.e. the floor). The positive direction points anteriorly for both legs.

$$\overrightarrow{x}_{H} = \frac{\overrightarrow{P}_{\mathrm{MID}}(1:2) - \overrightarrow{P}_{\mathrm{HEE}}(1:2)}{\left\| \overrightarrow{P}_{\mathrm{MID}}(1:2) - \overrightarrow{P}_{\mathrm{HEE}}(1:2) \right\|_2}, \overrightarrow{x}_{H}(3) = 0 \tag{4.8}$$

- **Interim Proximal-Distal Axis, i**: Vector from the origin to the Posterior Heel (PCA) marker.

$$\overrightarrow{i}_{\mathrm{H}} = \frac{\overrightarrow{P}_{\mathrm{PCA}} - \overrightarrow{P}_{\mathrm{HEE}}}{\left\| \overrightarrow{P}_{\mathrm{PCA}} - \overrightarrow{P}_{\mathrm{HEE}} \right\|_2} \tag{4.9}$$

- **Medial-Lateral (M-L) Axis, z**: Perpendicular to the A-P axis and the interim proximal-distal axis. The positive direction is taken to point laterally for a right leg and medially for a left leg.

$$\overrightarrow{z}_{\mathrm{H}} = \overrightarrow{x}_{\mathrm{H}} \times \overrightarrow{i}_{\mathrm{H}} \tag{4.10}$$

- **Proximal-Distal (P-D) Axis, y**: Cross product of the M-L and A-P axes. The positive direction points proximally for both legs.

$$\overrightarrow{y}_{\mathrm{H}} = \overrightarrow{z}_{\mathrm{H}} \times \overrightarrow{x}_{\mathrm{H}} \tag{4.11}$$

4.4 Subjects

Twenty-one adult females participated in the study. However, due to the reasons explained in Section 3.1, only nineteen subjects were eligible for analysis. Moreover, eight feet had to be excluded as the heel marker had been displaced from its original position due to contact with the CT loading rig plate. Therefore only thirty feet were available for analysis (see Appendix). The right and left feet results were pooled together, as there were no consistent differences between them.

4.5 Methods

4.5.1 Hindfoot

Based on the CT images, the bony landmark coordinates and the marker coordinates in the CT global coordinate system were recorded and the calcanei and tali of all thirty feet were segmented using Mimics (Materialise NV, Leuven, Belgium). The method of identifying palpable bony landmark coordinates in the CT images required locating the bony prominence on all three sagittal, transverse and coronal

slices. A detailed protocol for each bony prominence was developed. Inter and Intra-rater reliability was established for locating each landmark (mean inter-rater error was 0.43mm, and intra-rater error was 0.39mm). Then 3D models of the calcanei and tali were created once the segmentation process was completed and these were used to create STL files, which is a file format suitable for Computer Aided Design (CAD) software. The STL files were imported into Solidworks (Dassault Systèmes SolidWorks Corp., Vélizy, France) to create 3D CAD models of the bones. The mass properties tool in Solidworks allowed the unit vectors of the principal axes and the coordinates of the centre of mass to be obtained. A uniform mass distribution was assumed. The CT global coordinate system was retained when creating the Solidworks model from the STL files. The principal axis of a body with constant density is, in short, an axis of rotational symmetry. A rigid body requires a torque to rotate it about a rotational axis with a certain angular acceleration and this is known as the moment of inertia. The moments of inertia relative to the centre of mass about the three coordinate axes can be described in the form of an inertia matrix. The inertia matrix can be decomposed into the product of a rotation matrix and a diagonal matrix. Here, the columns of the rotation matrix define the principal axes of the rigid body. The first principal axis of the calcaneus was regarded as the most clinically relevant way to represent the orientation of this bone. The OFM hindfoot segment models the calcaneus and talus. However, the hindfoot markers are all placed on the calcaneus, not on the talus and therefore the markers only replicate the calcaneus. Even so, a layer of soft tissue exists between the calcaneus and the markers and thus hinders accurate representation of the movement of the calcaneus. Accurate knowl-

edge of calcaneus rotation provides useful clinical information and minimises making inappropriate treatment recommendations. For example, if the marker-based kinematic data showed the hindfoot to be rotated, clinicians might recommend surgical intervention (calcaneal osteotomy), when in reality there is no calcaneal rotation.

After looking at the hindfoot marker positions, both relative to the bones and on the skin relative to the posterior plate of the loading rig, it was found that the heel markers on eight feet had been displaced from their original position due to contact with the plate. Therefore it was agreed that these feet could justifiably be excluded from the study of the hindfoot axes, as already mentioned.

The marker-defined OFM hindfoot A-P axis was compared to that of the first principal axis of the calcaneus in the horizontal projection. Both axes were also compared to the long axis of the foot, which was defined by the Heel-Toe axis (H-T axis) projected into the plantar plane, which extends from the HEE marker to the TOE marker (located at the mid-point of the heads of the second and third metatarsals). Like the A-P axis, the H-T axis in 3D was defined. Superscript I refers to the image coordinate system while the subscript H refers to the hindfoot.

$$ {}^{\mathrm{I}}\overrightarrow{HT}_{\mathrm{H}} = \frac{{}^{\mathrm{I}}\overrightarrow{P}_{\mathrm{TOE}} - {}^{\mathrm{I}}\overrightarrow{P}_{\mathrm{HEE}}}{\left\| {}^{\mathrm{I}}\overrightarrow{P}_{\mathrm{TOE}} - {}^{\mathrm{I}}\overrightarrow{P}_{\mathrm{HEE}} \right\|_2} \tag{4.12} $$

Since the transverse plane projection of the angular difference was the required outcome, the unit vectors of the A-P, H-T and first principal axes axes had to be recalculted to make the axes 2-Dimensional (2D) by accounting for removal of their vertical coordinates (y-component).

3-Dimensional (3D) axis $\overrightarrow{A}$ consists of unit vectors in x, y and z components.

$$\overrightarrow{A} = \begin{bmatrix} x \\ y \\ z \end{bmatrix} \tag{4.13}$$

To make the axis 2-Dimensional, the x and y component unit vectors need to be recalculated.

$$x' = \frac{x}{\sqrt{x^2 + z^2}} \tag{4.14}$$

$$z' = \frac{z}{\sqrt{x^2 + z^2}} \tag{4.15}$$

Therefore the axis A in 2D is given by:

$$\overrightarrow{A}' = \begin{bmatrix} x' \\ z' \end{bmatrix} \tag{4.16}$$

Each static axis was made 2-Dimensional before calculating the 2D angular difference between the axes.

Moreover, the A-P axis, the H-T axis, and the first principal axes of the calcanei, obtained from the Solidworks model, were plotted in Matlab, taking the origin to be the centre of mass of the calcaneus (Figure 4.2). Finally, the angles theta between the plantar-plane projections of the axes, say $\overrightarrow{a}$ and $\overrightarrow{b}$ were calculated by the dot product equation given by:

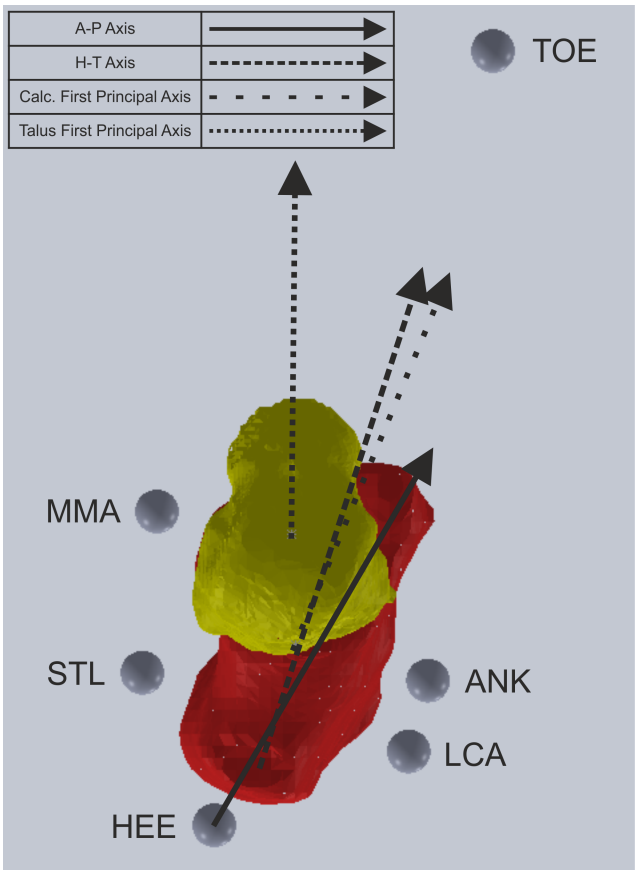

Figure 4.2: Plantar Projection of an example Subject's Hindfoot Segment Axes.

$$\theta = \arccos\left(\frac{\overrightarrow{a} \cdot \overrightarrow{b}}{\|\overrightarrow{a}\| \left\|\overrightarrow{b}\right\|}\right) \tag{4.17}$$

The angle in the horizontal plane between the A-P axis and the first principal axis, the A-P and the H-T axis and the first principal axis and the H-T axis were computed for all feet. It is important to note that a positive sign was used when the A-P axis or the first principal axis pointed more laterally than the H-T axis. To interpret these results, limits of agreement analysis [8] was carried out to investigate the level of agreement between the two axes.

The orientation of first principal axis of the talus relative to the first principal axis of the calcaneus was analysed as a verification to check that the subjects did not have any hindfoot deformity. The orientation of the long axis of the talus is more medial than that of the H-T and the calcaneus first principal axis. Coughlin, Saltzman and Mann [18] state that healthy feet have an anterior-posterior talocalcaneal angle (Kite's angle) ranging from 15 to 30 degrees. An angle greater than 30° would indicate hindfoot valgus whereas an angle less than 15° would indicate hindfoot varus.

To find the Kite's angle, equation 4.17 was used. The first principal axis of the talus was put into 2D projected into the plantar plane, as the other axes were. Kite's angle was calculated for all thirty feet.

4.5.2 Tibia

In addition to defining a marker-based OFM tibia segment axis, an anatomy-based tibia axis can be defined using the coordinates of the malleoli in the CT scans, which

can be referred to as the ideal positions for the malleoli markers (ANK and MMA). The coordinates of the malleoli as well as the radio-opaque markers on the malleoli in the CT image coordinate system can be extracted from the CT images. Two directions in the plane of the CT scan can be defined using identified landmarks. To register the CT scan in three-dimensional space, the third, out of plane, direction also needs to be defined and this was achieved using a direction normal to the CT plane. However, while the coordinates of the radio-opaque markers on the malleoli were available in the CT coordinate system, the coordinates of the Knee Joint Centre were not available in the CT coordinate system. In order to define marker-based tibia segment axes, the KJC and malleoli markers are required and therefore the tibia marker-based axes were defined using the KJC and the malleoli markers in the global coordinate system. In order to make direct comparison between the marker-based axis and the anatomy-based axis, the same coordinate system must be used. The method employed to achieve it was by transforming the malleoli coordinates in the CT coordinate system into the global coordinate system. In order to transform the malleoli coordinates, a transformation matrix, T, is required and one way to obtain it is by applying a rigid body transformation method [77].

The principle of the rigid body transformation method was mentioned in Section 3.7 and is described in further detail below.

Assume that there are n landmarks in a rigid body and let $\{x_1,\dots ,x_n\}$ be the 3D positions of these landmarks before movement (say in a reference position) and $\{y_1,\dots ,y_n\}$ be the positions after the movement (say, in any other position). Finding rotation matrix R and a translation vector d that map the positions x_i to the points

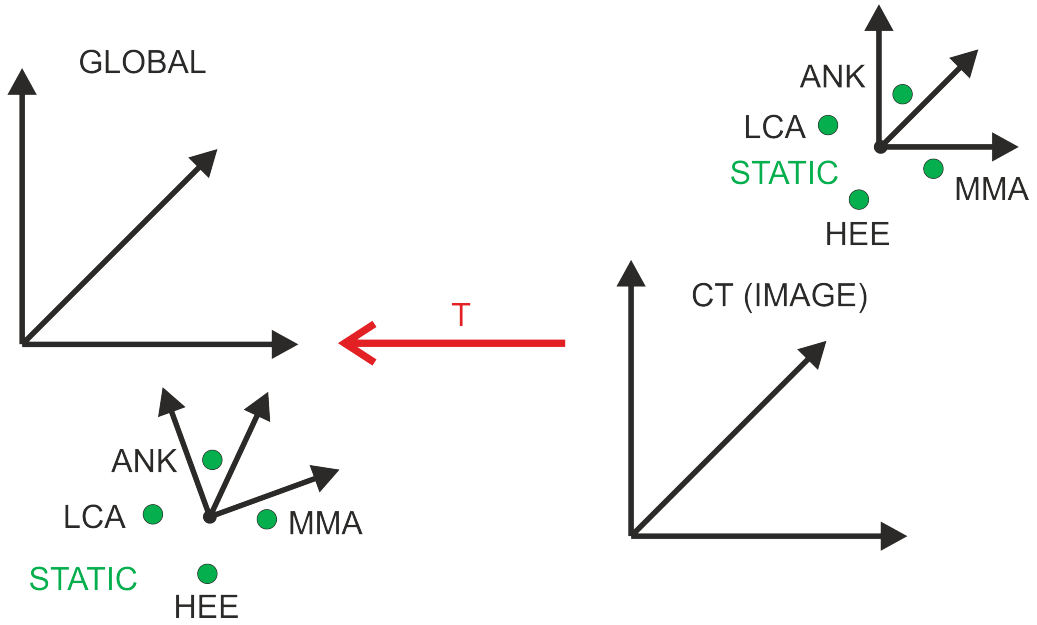

Figure 4.3: Schematics of Rigid Body Transformation Method of Transforming Tibia Segment Markers in Image Coordinate System to Global Coordinate System

y_i, i=1,... ,n is required. Measurement errors cause the mapping to be not exact and thus the following least-squares problem is used:

$$\min_{R\in\Omega,d} \sum_{i=1}^{n} \|Rx_i + d - y_i\|^2 \tag{4.18}$$

Where,

$$\Omega = \{R|R^T R = RR^T = I_3; det(R) = 1\} \tag{4.19}$$

Arun et al. [5] and Hanson and Norris [34] show that the singular value decomposition of the matrix $C = BA^T$ can be used to determine the solution to the problem. The computation steps is described by the algorithm below [77].

1. $\bar{x} = \frac{1}{n}\sum_{i=1}^{n} x_i$

2. $\bar{y} = \frac{1}{n}\sum_{i=1}^{n} y_i$

3. $A = [x_i - \bar{x}, \ldots, x_n - \bar{x}]$

4. $B = [y_i - \bar{y}, \ldots, y_n - \bar{y}]$

5. $C = BA^T$

6. $P\Gamma Q^T = C$. (Computations of the singular value decomposition of C, i.e. P and Q are 3×3 orthogonal matrices and $\Gamma = \text{diag}(\sigma_1(C), \sigma_2(C), \sigma_3(C))$. The numbers $\sigma_i(C)$ are the singular values of the matrix C and satisfy $\sigma_1(C) \geq \sigma_2(C) \geq \sigma_3(C)$).

7. $R = P$ diag(1,1,det$(PQ^T))Q^T$

8. $d = \bar{y} - R\bar{x}$

9. Transformation matrix, $T = [R, d; 0001]$.

The malleoli coordinates in the image coordinate system can be converted to those in the global coordinate system by first working out the rotation matrix and translation vector (Figure 4.3). The x's mentioned above are the image coordinates while the y's refer to the global coordinates. Since the static coordinates of HEE, LCA, ANK and MMA markers are known in both the image and global coordinate systems, those coordinates were used to work out the transformation matrix, T. The rotation matrix and translation vector were then implemented to convert the malleoli coordinates

from the image to the global coordinate system. This assumes that the four markers mentioned define a rigid segment. The subscript i represents ideal coordinates.

$$\begin{bmatrix} {}^{\mathrm{G}}\overrightarrow{x}_{\mathrm{ANK_i}} \\ {}^{\mathrm{G}}\overrightarrow{y}_{\mathrm{ANK_i}} \\ {}^{\mathrm{G}}\overrightarrow{z}_{\mathrm{ANK_i}} \\ 1 \end{bmatrix} = {}^{G}_{I}T \begin{bmatrix} {}^{\mathrm{I}}\overrightarrow{x}_{\mathrm{ANK_i}} \\ {}^{\mathrm{I}}\overrightarrow{y}_{\mathrm{ANK_i}} \\ {}^{\mathrm{I}}\overrightarrow{z}_{\mathrm{ANK_i}} \\ 1 \end{bmatrix} \tag{4.20}$$

$$\begin{bmatrix} {}^{\mathrm{G}}\overrightarrow{x}_{\mathrm{MMA}} \\ {}^{\mathrm{G}}\overrightarrow{y}_{\mathrm{MMA}} \\ {}^{\mathrm{G}}\overrightarrow{z}_{\mathrm{MMA}} \\ 1 \end{bmatrix} = {}^{G}_{I}T \begin{bmatrix} {}^{\mathrm{I}}\overrightarrow{x}_{\mathrm{MMA}} \\ {}^{\mathrm{I}}\overrightarrow{y}_{\mathrm{MMA}} \\ {}^{\mathrm{I}}\overrightarrow{z}_{\mathrm{MMA}} \\ 1 \end{bmatrix} \tag{4.21}$$

$${}^{\mathrm{G}}\hat{P}_{\mathrm{ANK_i}} = \begin{bmatrix} {}^{\mathrm{G}}\overrightarrow{x}_{\mathrm{ANK_i}} \\ {}^{\mathrm{G}}\overrightarrow{y}_{\mathrm{ANK_i}} \\ {}^{\mathrm{G}}\overrightarrow{z}_{\mathrm{ANK_i}} \end{bmatrix} \tag{4.22}$$

$${}^{\mathrm{G}}\hat{P}_{\mathrm{MMA_i}} = \begin{bmatrix} {}^{\mathrm{G}}\overrightarrow{x}_{\mathrm{MMA_i}} \\ {}^{\mathrm{G}}\overrightarrow{y}_{\mathrm{MMA_i}} \\ {}^{\mathrm{G}}\overrightarrow{z}_{\mathrm{MMA_i}} \end{bmatrix} \tag{4.23}$$

With the malleoli positions from the CT images in the global coordinate system, the anatomical definition of Ankle Joint Centre can be calculated from equation 4.1 and is labeled as ideal AJC ($\mathrm{AJC_i}$). Thus, enough information is available to define both marker-based and anatomy-based tibial coordinate axes in the global coordinate system using the axis definitions in Section 4.2.

Since the transverse plane hindfoot-tibia kinematics is the area of interest, the transverse plane projection of the tibia antero-posterior axes were scrutinised. The corrected anterior-posterior axis was used to visually and analytically compare with the marker based tibia anterior-posterior axis. The plantar plane projections of the unit vectors of the axes were calculated using equations 4.13 - 4.16 to compare in 2D.

For convenience, the various axes are referred to in the rest of this chapter by the acronyms listed in Table 4.1.

Table 4.1: List of Axes in Chapter 4

Coordinate System	Segment	Acronym	Definition
Image	Hindfoot	A-P	Anterior-Posterior Axis
		H-T	Heel-Toe Axis
		FPAC	Calcaneus First Principal Axis
		FPAT	Talus First Principal Axis
Global	Tibia	AP	Anterior-Posterior Axis
		APC	Corrected Anterior-Posterior Axis

4.6 Results

4.6.1 Hindfoot

The H-T axis was assumed as the long axis of the foot and was used as a reference axis, against which the other two axes are compared. Also it was assumed that the H-T axis for each foot is "correct" or without error. Table 4.2 shows that the mean static A-P axis and the calcaneus first principal axis orientations relative to the H-T axis are 2.8° and 1.7° laterally, respectively. The bias between the measurements can be estimated by the difference in the means and it was shown that the A-P axis was laterally biased in comparison to the first principal axis by 0.9°. The static angle

Table 4.2: Table of Results for A-P Axis and First Principal Axis Angles Measured From H-T Axis. FPAC = Calcaneus First Principal Axis; FPAT = Talus First Principal Axis; FPAC from FPAT also known as Kite's Angle; SD = Standard Deviation; SE = Standard Error. Note that a positive sign was given when A-P or calcaneus First Principal Axis pointed more laterally than H-T. Also a positive sign was given when the A-P pointed more laterally than the calcaneus First Principal Axis.

	A-P - H-T (°)	FPAC - H-T (°)	A-P - FPAC (°)	FPAC - FPAT
Mean	2.8	1.7	0.9	21.5
SD	9.9	5.0	8.8	6.2
SE	1.8	0.9	1.6	1.1

difference between the calcaneus and talus first principal axes is known as the Kite's angle and its mean value is 21.5°. A representative subject, shown in Figure 4.2, is in agreement with this finding. The SD value of the A-P axis relative to the H-T axis (9.9°) suggest that the A-P axis orientation relative to the H-T axis is random and highly variable. Similarly, the SD value of the A-P axis relative to the calcaneus first principal axis is 8.8°, which, again, shows that the agreement between the A-P axis and the calcaneus first principal axis is random and highly variable. In contrast, the variation of the first principal axis relative to the H-T axis is more modest as the SD values of 5.0° shows. Moreover, the mean and standard deviation value of the Kite's angle were 21.5° and 6.2°. As mentioned in Section 4.5.1, the Kite's angle of healthy feet ranges from 15° to 30°, which indicates that most of the subjects tested had healthy feet. Overall, the findings imply that for healthy feet, the H-T axis is a better representation of the calcaneus first principal axis than the A-P axis. Standard errors of the measurements were calculated to find the standard deviation of the sample mean based on the population mean. It was shown that the first principal

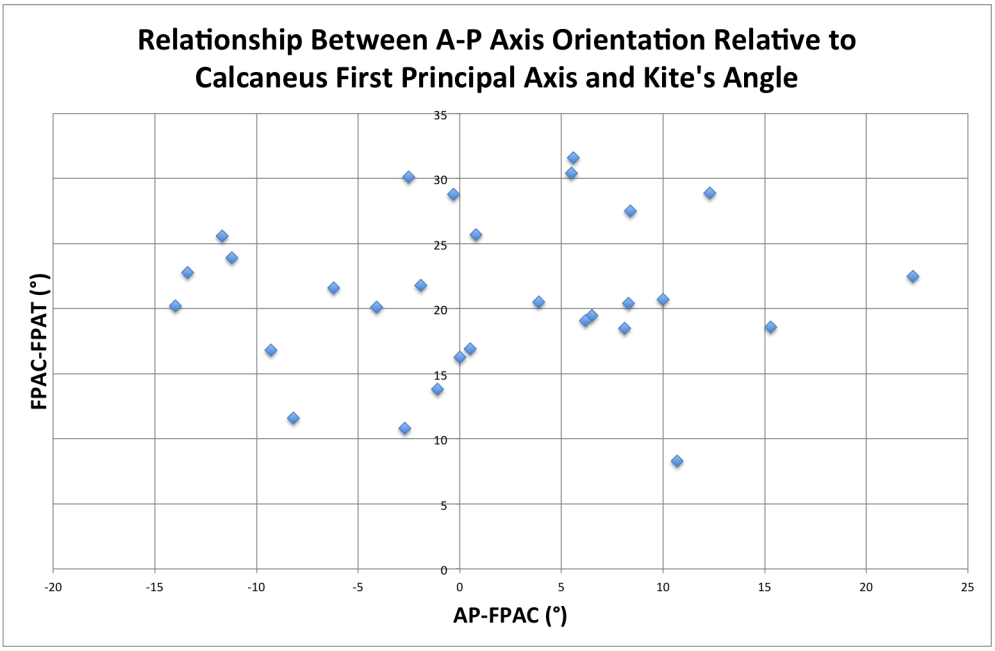

Figure 4.4: Relationship Between Hindfoot A-P Axis Orientation Relative to Calcaneus First Principal Axis and Kite's Angle

axis relative to the H-T axis exhibited the least sample bias with the standard error of less than 1. On the other hand, the data of the A-P axis relative to the H-T axis showed the most sample bias with the standard error of 1.8. This illustrates that the first principal axis relative to the H-T axis data was the most true to its original population while the A-P axis relative to the H-T axis data the least true to its original population.

Figure 4.4 shows relationship between the hindfoot A-P axis orientation relative to calcaneus first principal axis and Kite's angle. There is no apparent relationship between the two factors and therefore suggests that the healthiness of the foot does not affect the static orientation of the hindfoot A-P axis relative to the calcaneus first

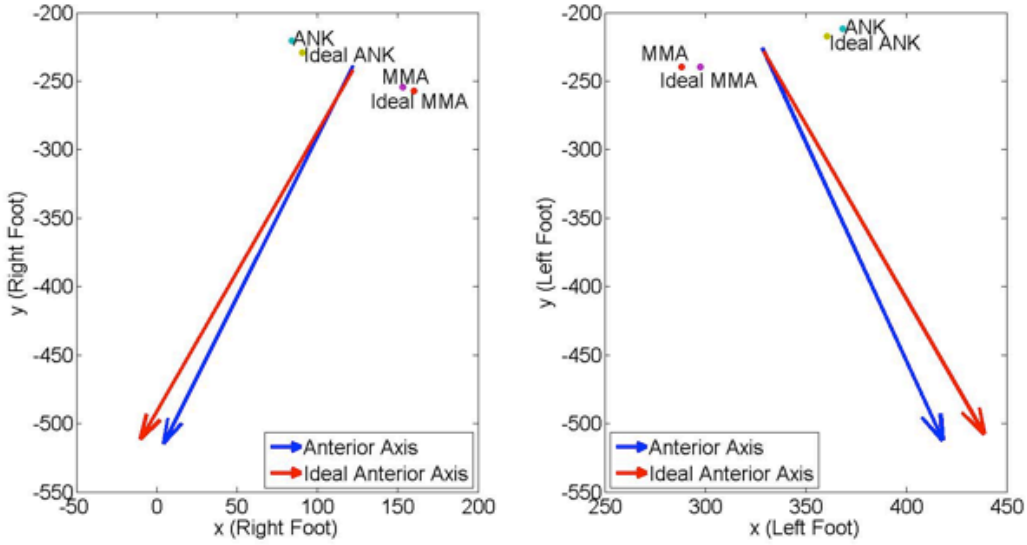

Figure 4.5: Plantar Projection of an example Subject's Tibia Segment Axes. Blue and red arrows represent anterior and corrected anterior axis, respectively

principal axis. As a result, it was decided not to include the feet for which Kite's angle fell outside the healthy range (15° to 30°) in this investigation.

4.6.2 Tibia

From Figure 4.5 it is visible that the corrected anterior axis (APC) lies more externally rotated in comparison to the anterior axis (AP). While this was the case for the representative subject, this occurrence was also observed in most of the other subjects. The absolute distances between the ANK and MMA markers and their corresponding anatomical coordinates were measured for all feet and the statistical results are outlined in Table 4.3. These absolute distances are referred to as ANK error and MMA error for convenience. The corrected anterior-posterior axis was calculated

Table 4.3: Table of Results for Corrected Tibia Anterior-Posterior Axis (APC) From Tibia Anterior-Posterior Axis (AP). SD = Standard Deviation; SE = Standard Error

	ANK Error (mm)	MMA Error (mm)	APC - AP (°)
Mean	3.9	3.5	4.4
SD	2.3	2.3	3.4
SE	0.4	0.4	0.6

using default knee joint centre and ideal ankle joint centre, defined as the midpoint of the anatomical coordinates of the medial and lateral malleoli. The mean ANK and MMA errors are 3.9 mm and 3.5 mm, respectively and these values contributed to 4.4° of static orientation difference between the corrected tibia anterior-posterior axis and the default tibia anterior-posterior axis. It is clear that the mean values of the ANK and MMA errors (Table 4.3) are similar in magnitude. Moreover, the SD values of the ANK and MMA errors (Table 4.3) are small. This suggests that both malleoli marker placements were consistent and true to their ideal locations, assuming that inevitable human errors of approximately 5 mm exist. Likewise, the consistent placement of malleoli markers has led to a consistent and small static orientation difference between the corrected tibia anterior-posterior axis and the default tibia anterior-posterior axis as the standard deviation value of 3.4 demonstrate (Table 4.3). The ANK and MMA error measurements showed low sampling bias as the standard error value of 0.4 for both, indicate. This illustrates that both sets of data were true to their corresponding population sets.

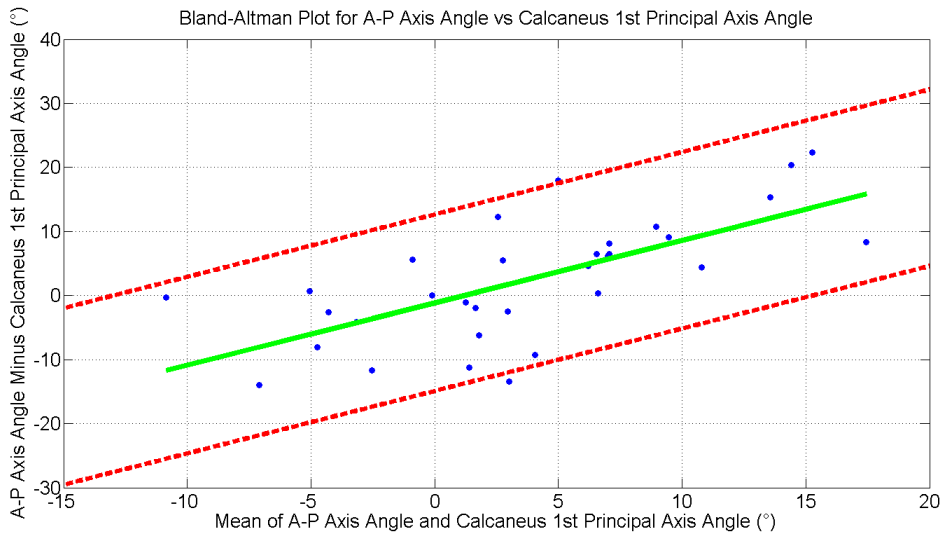

Figure 4.6: Difference against Mean Plot of the A-P Axis and First Principal Axis Angle. The solid green line represents the best-fit line through the points while the dotted red lines represent the 95% limits of agreement.

4.7 Discussion

4.7.1 Hindfoot

The mean and standard deviation values of the difference in angle between the calcaneus and the talus first principal axes (Kite's angle) were 21.5° and 6.2°, respectively (Table 4.2). This shows that most of the subjects' feet fall in the category of healthy feet (15° to 30°) and are suitable for assessment.

A starting point of this analysis was to find the differences between the measurements of A-P axis and the first principal axis orientation relative to the H-T axis of the same subject. It is possible that one measurement consistently exceeds the other and this type of occurrence is called bias. This can be approximated by the mean of the measurements. Also, the variation about this mean value can be estimated

by the standard deviation. However assumptions that the bias and variability are uniform throughout the measurements must hold for the estimates to be reasonable. The credibility of this assumption can be checked graphically.

A histogram of the values of the differences was plotted to see if they were normally distributed or not and it showed that they were approximately normally distributed. Hence it would be expected for 95% of the differences to lie within the range defined by $\bar{d} = 1.96 s_d$ where d and s_d are the mean and the standard deviation of the differences, respectively. The boundaries that define the range are referred to as 95% limits of agreement.

Graphical presentation of agreement can be implemented to show the agreement of the A-P and the first principal axis in a more explicit way (Figure 4.6). The solid green linear regression line in Figure 4.6 demonstrates that the difference between A-P and first principal axis and the mean of the A-P and first principal axis are positively correlated. In other words, the difference between the two axes is expected to increase, as the two axes lie further away from the Heel-Toe axis. This implies that the difference between the A-P axis and the first principal axis is likely to be greater for feet with deformity in the hindfoot than in healthy feet. Moreover, the width of limits of agreement line band is about 30° and this suggests that there is a large variation in the difference of A-P axis and first principal axis data. It can be concluded that the two measurements weakly agree with each other and that the OFM hindfoot segment A-P axis is not an ideal representation of the first principal axis of the calcaneus. In theory, it could be possible to take offset values to predict the first principal axis from the A-P axis using the regression line but the variation

is too large for this practice to be implemented.

The most obvious application of the results found in this chapter relates to the relationship between the A-P axis relative to the calcaneus first principal axis and the H-T axis relative to the calcaneus first principal axis. This means that the more deformed the foot, potentially the more inaccurate the A-P axis definition, therefore this is potentially amplified in deformed feet like clubfoot and justifies further investigation. One of the explanations as to why there appears to be a systematic effect of the angle of the hindfoot on the error between estimates of the A-P axis and the calcaneus first principal axis may be related to the method of the application of markers by the clinicians. It is possible that the clinicians tend to place the hindfoot markers so that the A-P axis is in line with the H-T axis, which is found to be closely approximated by the calcaneus first principal axis for the healthy feet. However, in deformed feet where the discrepancy between the H-T axis and the calcaneus first principal axis is likely to be greater, the difference in orientation between the A-P axis and the first principal axis would also likely to be amplified. It could also be that the first principle axis of the calcaneus is not aligned with the marker placement protocol of making STL and LCA equidistant from HEE. This might be an anatomical bias compared to the marker definition.

There are limitations associated with the methodology. The process of removing motion capture system markers and reapplying radio-opaque markers for image acquisition creates potential errors. Firstly, there may be discrepancy between where the marker was originally and where the radio-opaque marker was placed, although the skin was marked prior to applying motion capture markers to limit this error.

Secondly, the diameter of the motion capture marker and that of the radio-opaque marker were different, meaning that the coordinates of the centre of the markers will be slightly different even if they were placed on the exact same location. However, this would only affect the distance away from the skin surface, which was mostly not a variable of interest for this study. The combination of the two aforementioned limitations may limit the reliability of the results found in this chapter.

Another main limitation comes from application of 40% bodyweight to the sole of the foot to replicate the loads around the foot in standing.

4.7.2 Tibia

Table 4.3 demonstrates that the mean angular difference in static tibia anterior-posterior axis and the corrected anterior-posterior axis is 4.4°. The mean values of the absolute distance between the ANK and MMA markers and their ideal locations were 3.9 mm and 3.5 mm, respectively (Table 4.3). Hence marker misplacement as small as 5 mm is enough to change the projected axes angle of the Oxford Foot Model tibia segment anterior-posterior axis by more than 5°.

Additionally, the standard deviation values for marker errors were 2.3 mm and 2.3 mm for ANK and MMA markers, respectively and this contributed towards 3.4° of standard deviation of the angular difference between the static tibia anterior-posterior axis and the corrected counterpart. This indicates varying marker placement and consequently the accuracy of tibia anterior-posterior axis orientation is compromised. Therefore a method or a tool that ensures accurate placement of ANK and MMA markers would be a good idea.

It can be inferred from Table 4.3 that there is a tendency for the corrected anterior-posterior axis to be externally rotated in comparison to the anterior-posterior axis as the mean value of the angular difference between the two measures was 4.4°. Moreover, the standard deviation of 3.4° demonstrates that there is a good consistency in the way the corrected anterior-posterior axis aligns with respect to the anterior-posterior axis. This is a static representation of the axis, and that this may not wholly represent the functional axis of the ankle, but this is difficult to ascertain anyway, as stated by Leitch et al. [51]. Clinically, the findings imply that the clinicians tend to place the malleoli markers such that the transmalleolar axis is more internally rotated than it ought to be. The implication this has on transverse plane hindfoot-tibia kinematics is to be investigated in the dynamic analysis.

It is important to note that the Knee Joint Centre in the image coordinate system was recreated using hindfoot markers. Whilst it would have been more ideal to use tibia markers to transform the KJC in the global coordinate system to the image coordinate system, it was not possible as the acquired images were only available to just above the ankle. Therefore the KJC in the image coordinate system was recreated with the assumption that the segment defined by the markers from the hindfoot are equally rigid as that defined by the markers around the tibia and the knee. Inevitably, this assumption induces some error to the estimation of the KJC in the image coordinate system and therefore weakens the reliability of the results found in this chapter.

4.8 Conclusion

This chapter provided a comprehensive analysis of static comparison of marker-based and anatomy-based hindfoot and tibia segment anterior-posterior axes. The first objective of the thesis was investigated in this chapter. It demonstrated that there was good agreement between the marker-based and anatomy-based axes in the mean values (less than 1 degree difference) but with a larger inter-subject variation (SD of 8.8 degrees). Given there is a general agreement in the gait community that errors of less than 5 degrees of gait kinematics are acceptable, this would appear to be outside of those limits. The tibia segment exhibited better agreement between the marker-based and the anatomy-based segment axes. In relation to this analysis, it is also useful to know how marker misplacement affects the static alignment of the hindfoot anatomy-based segment definition. This is scrutinised in the next chapter. Furthermore, the effect of any static misalignment between the marker-based and the hindfoot and tibia anatomy-based segment axes on joint angles during motion will be discussed in detail in chapter 6.

5 Sensitivity Analysis

5.1 Introduction

The purpose of the sensitivity analysis was to observe how the marker placement error of the hindfoot markers affects the orientation of the hindfoot segment axes. It was performed on heel, lateral calcaneus and sustentaculum tali markers to examine how the difference in distance between these markers from their corresponding ideal locations affects the orientation of the hindfoot antero-posterior axis. Bony landmarks on the lateral and medial sides of the hindfoot are not easily palpable, meaning that there are no obvious locations at which to site foot-model markers. The current OFM requires LCA and STL markers to be equidistant from the HEE marker. However in practice, the LCA and STL markers are placed only roughly equidistant from the HEE marker without use of any measurement tools or jigs. Sensitivity analysis was performed to find out how much error was caused by the difference in distance between the LCA (from HEE) and the STL (from HEE) markers and also the difference in distance between the HEE and its ideal counterpart.

5.2 Methods

5.2.1 Hindfoot - Assuming HEE correct (MID Corrected)

Figure 5.1 is a transverse plane projection of the hindfoot markers of a subject's right foot where the foot is pointing upwards. This is a schematic of a case when the STL and LCA markers are not equidistant from the HEE marker; in this example, the STL marker is located closer to HEE than the LCA.

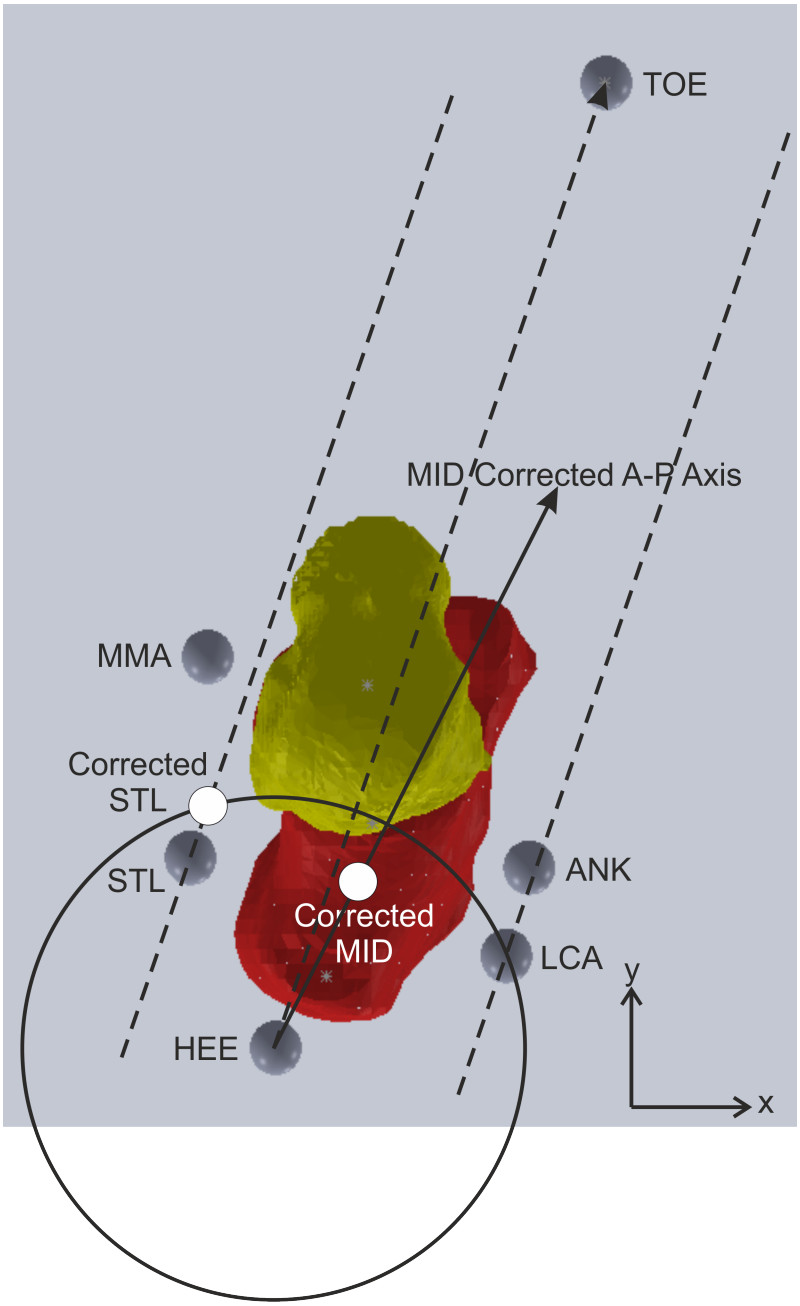

Figure 5.1: Method of Determining Correct Right Foot STL Position

It was assumed that the LCA and STL markers can only be re-positioned along the sides of the calcaneus, which in this study were taken to be parallel to the Heel-Toe axis. Lines passing through LCA and STL markers and parallel to the H-T axis were mathematically defined, as follows.

- Define radius of the circle based on LCA and HEE:

$$r_{LCA} = \sqrt{({}^{I}x_{LCA} - {}^{I}x_{HEE})^2 + ({}^{I}y_{LCA} - {}^{I}y_{HEE})^2} \tag{5.1}$$

- Define radius of the circle based on STL and HEE:

$$r_{STL} = \sqrt{({}^{I}x_{STL} - {}^{I}x_{HEE})^2 + ({}^{I}y_{STL} - {}^{I}y_{HEE})^2} \tag{5.2}$$

- Define gradient of the HEE-TOE line:

$$m = \frac{{}^{I}\overrightarrow{HT}_{H}(2)}{{}^{I}\overrightarrow{HT}_{H}(1)} \tag{5.3}$$

- Find the y-axis intercept of the line through STL and parallel to H-T:

$$c_{STL} = {}^{I}y_{STL} - m\,{}^{I}x_{STL} \tag{5.4}$$

- Find the y-axis intercept of the line through LCA and parallel to H-T:

$$c_{LCA} = {}^{I}y_{LCA} - m \cdot {}^{I}x_{LCA} \tag{5.5}$$

Then a circle extending from the HEE marker to the calcaneal marker further away from the HEE marker, which in this example (Figure 5.1) is the LCA marker, was also mathematically defined. There are two intersection points between the LCA-based circle and the STL-based line but the point closer to the marker's actual position is defined as the ideal marker position and in this example, the point is the "ideal STL" marker position in Figure 5.1. The steps in the calculation are:

- See which radius of the two circles is bigger and use the circle with bigger radius:

  if $\overrightarrow{r}_{LCA} > \overrightarrow{r}_{STL}$, $r = r_{LCA}$, otherwise $r = r_{STL}$

- Calculate the x-coordinates of the points intersecting between the circle, $(x - x_{HEE})^2 + (y - y_{HEE})^2 = r^2$, and the line, $y = mx + c$.

- Now, substitute equation $y = mx+c$ into equation $(x-x_{HEE})^2+(y-y_{HEE})^2 = r^2$ to solve for x. Note that the points are in image coordinate system.

$$x_{1,2} = \frac{2(x_{HEE} - m \cdot c + m \cdot y_{HEE})}{2(m^2+1)} \pm \frac{\sqrt{4(x_{HEE} - m \cdot c + m \cdot y_{HEE})^2 - 4(m^2+1)(x_{HEE}^2 + (c - y_{HEE})^2) - r^2}}{2(m^2+1)} \tag{5.6}$$

if $m > 0$, $x_{LMC} = x_2$

else, $x_{LMC} = x_1$

where, LMC refers to either of the ideal lateral or medial calcaneus points. This guarantees that the distance between STL/LCA and ideal STL/ideal LCA is a minimum.

- Calculate the y-coordinate of the ideal point.

$$y_{LMC} = mx_{LMC} + c_{LMC} \tag{5.7}$$

- Calculate the z-coordinate of the ideal point.

For ideal STL,

$$z_{LMC} = {}^{I}z_{STL} \tag{5.8}$$

For ideal LCA,

$$z_{LMC} = {}^{I}z_{LCA} \tag{5.9}$$

- Hence the ideal LCA/STL (LMC) is given by:

$${}^{I}\overrightarrow{P}_{LMC} = \begin{bmatrix} x_{LMC} \\ y_{LMC} \\ z_{LMC} \end{bmatrix} \tag{5.10}$$

Once the coordinates of the ideal LCA or STL marker were obtained, the A-P axis which passed through HEE and the mid-point of a line segment connecting the ideal marker and its opposite calcaneal marker were computed. For convenience, this is referenced as "MID corrected A-P axis". These MID corrected A-P axes were first graphically compared against the uncorrected A-P axis and then their angular differences were calculated. The steps in the calculations were:

- Assign the ideal MID.

  For ideal STL,

$${}^{I}\overrightarrow{P}_{MID_i} = \frac{{}^{I}\overrightarrow{P}_{LCA} + {}^{I}\overrightarrow{P}_{LMC}}{2} \tag{5.11}$$

  where, subscript i, for ideal, was given to indicate ideal MID point.

  For ideal LCA,

$${}^{I}\overrightarrow{P}_{MID_i} = \frac{{}^{I}\overrightarrow{P}_{STL} + {}^{I}\overrightarrow{P}_{LMC}}{2} \tag{5.12}$$

- Calculate the MID ideal A-P axis (APM) parallel to the plantar surface of the foot.

$$ {}^{I}\overrightarrow{x}_{H}^{APM} = \frac{{}^{I}\overrightarrow{P}_{MID_i}(1:2) - {}^{I}\overrightarrow{P}_{HEE}(1:2)}{\left\| {}^{I}\overrightarrow{P}_{MID_i}(1:2) - {}^{I}\overrightarrow{P}_{HEE}(1:2) \right\|_2}, x(3) = 0 \tag{5.13} $$

The next procedure consisted of computing the difference in length, in the $z = 0$ (plantar) plane, between the distance from HEE to LCA and the distance from HEE to STL. It is important to note the sign convention here; a positive sign was assigned when the distance of the LCA marker measured from the HEE marker was longer than the distance of the STL marker measured from the HEE marker.

5.2.2 Hindfoot - Assuming LCA and STL correct (HEE Corrected)

The orientation of the A-P axis is also determined by placement of the HEE marker. Therefore, a further sensitivity analysis was carried out to find out how misplacement of the HEE marker affects the orientation of the A-P axis.

The misplacement of the HEE marker was defined by the difference in distance between the centre of the HEE marker and the corresponding anatomical definition which represents where the HEE marker should be.

The coordinates of the HEE marker centres were obtained from the CT images. The method of attaining the coordinates of the ideal location, represented by the anatomical representation of the HEE marker, is outlined below and is illustrated in figures 5.2 and 5.3.

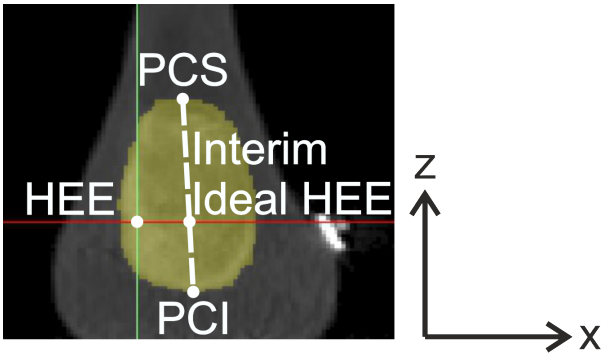

Figure 5.2: Illustration of Identifying the Interim Ideal Location of HEE Marker

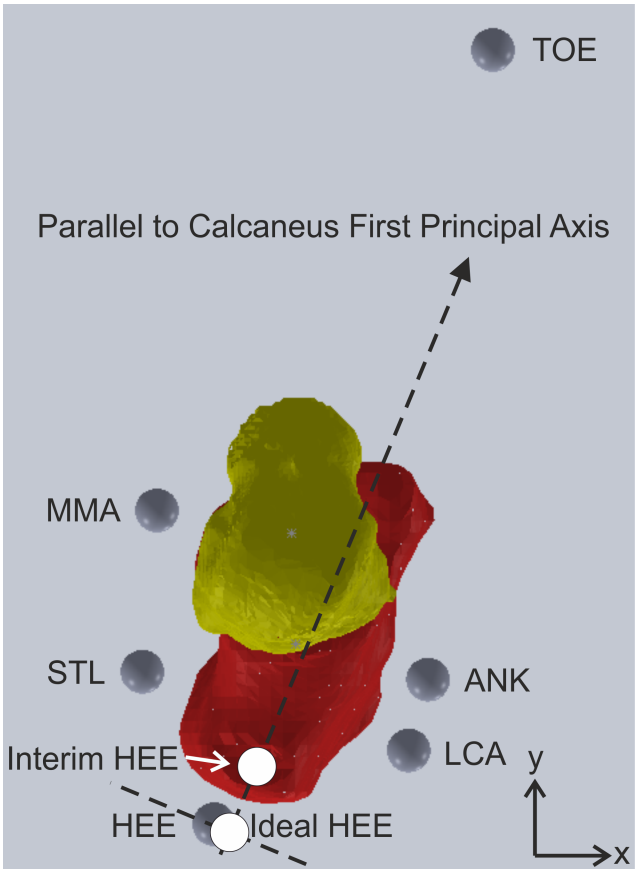

Figure 5.3: Illustration of Identifying the Ideal Location of HEE Marker

1. View the CT image of the calcaneus in the coronal plane.

2. Identify the slice that gives the largest surface area of the calcaneus.

3. Record the coordinates of the superior (PCS) and inferior (PCI) mid line of the calcaneus.

4. Using Matlab, calculate the coordinates of the point of the same height (z-coordinate) as the HEE marker along the line joining the superior and inferior calcaneus (Figure 5.2). It was assumed that the ideal HEE and the ideal PCA markers would be somewhere along the line joining the superior and inferior calcaneus. The reason for making this assumption was to ensure that the hind-foot Proximal-Distal axis, defined by the HEE and the PCA markers, would replicate the true varus/valgus inclination of the calcaneus. This would not be achieved if the limits of the posterior limits of the calcaneus based on the first principal axis or the planes perpendicular to it were used to define the ideal HEE marker location. Moreover, it was aimed to replicate clinical practice of placing the markers on the mid point of the posterior surface of the calcaneus, not on the most posterior point.

   The superior and inferior calcaneus points share the same y-coordinates (same in the anterior-posterior direction).

   The gradient, n, of a line in the $x-z$ plane adjoining the superior and inferior calcaneus points is given by:

$$n = \frac{{}^{I}z_{PCS} - {}^{I}z_{PCI}}{{}^{I}x_{PCS} - {}^{I}x_{PCI}} \tag{5.14}$$

The z-axis intercept, k, of the line can be calculated by substituting the coordinates of the superior calcaneus into the equation of the line.

$$k = {}^{I}z_{PCS} - n \cdot {}^{I}x_{PCS} \tag{5.15}$$

The point of interest (interim ideal HEE in Figure 5.2) shares the same z-coordinate as the HEE marker and is on the line with slope n and intercept k.

$${}^{I}z_{HEE'_i} = {}^{I}z_{HEE} \tag{5.16}$$

Its x-coordinate can be calculated by substituting in the z-coordinate of the HEE marker into the equation of the line, $z = nx + k$, to give

$${}^{I}x_{HEE'_i} = \frac{{}^{I}z_{HEE} - k}{n} \tag{5.17}$$

In addition, the y-coordinate, as mentioned earlier, is the same as that of both superior and inferior calcaneus.

$${}^{I}y_{HEE'_i} = {}^{I}y_{PCS} = {}^{I}y_{PCI} \tag{5.18}$$

The interim ideal HEE (HEE'_i) marker position, is therefore:

$$ {}^{I}\overrightarrow{P}_{HEE'_i} = \begin{bmatrix} {}^{I}x_{HEE'_i} \\ {}^{I}y_{HEE'_i} \\ {}^{I}z_{HEE'_i} \end{bmatrix} \tag{5.19} $$

5. In order to locate the ideal HEE marker on the surface of the hindfoot, the location found from the previous stage, ${}^{I}P_{HEE'}$, was shifted posteriorly along a line parallel to the first principal axis of calcaneus until it met a line through the HEE marker perpendicular to the calcaneus first principal axis (Figure 5.3).

   The gradient, m, of the first principal axis in the transverse plane is given by:

$$ m = \frac{{}^{I}\overrightarrow{FPA}_H(2)}{{}^{I}\overrightarrow{FPA}_H(1)} \tag{5.20} $$

   The y-axis intercept of a line parallel to the first principal axis through the interim ideal HEE is:

$$ c = {}^{I}y_{HEE'_i} - m \cdot {}^{I}x_{HEE'_i} \tag{5.21} $$

   The gradient of a line perpendicular to the first principal axis is:

$$ d = -\frac{1}{m} \tag{5.22} $$

   The y-axis intercept of the line through HEE and perpendicular to the first principal axis through the interim ideal HEE is:

$$e = {}^{I}y_{HEE} - d \cdot {}^{I}x_{HEE} \tag{5.23}$$

The x-coordinate of the intersection point between the first principal axis through the interim ideal HEE and the perpendicular line through HEE is defined as the x-coordinate of the ideal HEE marker.

$${}^{I}x_{HEE_i} = \frac{e - c}{m - d} \tag{5.24}$$

The y-coordinate of the intersection point between the first principal axis through the interim ideal HEE and the perpendicular line through HEE is defined as the y-coordinate of the ideal HEE marker.

$${}^{I}y_{HEE_i} = m \cdot {}^{I}x_{HEE_i} + c \tag{5.25}$$

The ideal HEE marker shares the same z-coordinate as the HEE marker.

$${}^{I}z_{HEE_i} = {}^{I}z_{HEE} \tag{5.26}$$

6. This point is theorised as the ideal location.

$${}^{I}\overrightarrow{P}_{HEE_i} = \begin{bmatrix} {}^{I}x_{HEE_i} \\ {}^{I}y_{HEE_i} \\ {}^{I}z_{HEE_i} \end{bmatrix} \tag{5.27}$$

HEE Corrected A-P (APH) is therefore given by:

$$ {}^{I}\overrightarrow{x}_{H}^{APH} = \frac{{}^{I}\overrightarrow{P}_{MID}(1:2) - {}^{I}\overrightarrow{P}_{HEE_i}(1:2)}{\left\| {}^{I}\overrightarrow{P}_{MID}(1:2) - {}^{I}\overrightarrow{P}_{HEE_i}(1:2) \right\|_2}, x(3) = 0 \tag{5.28} $$

5.2.3 Hindfoot - PCA corrected

The Oxford Foot Model hindfoot segment is defined using not only the HEE, LCA and STL markers but also the PCA (proximal calcaneus) marker. The PCA marker is used to define the interim proximal-distal axis and consequently the medial-lateral and the proximal-distal axes of the hindfoot. Therefore these axes will be sensitive to the position of the PCA marker and sensitivity analysis was carried out to quantify how misplacing the PCA marker can affect the hindfoot axes.

To analyse how the Hindfoot P-D axis is sensitive to PCA and HEE marker positions, ideal locations of the PCA and HEE markers were computed. The ideal locations were used to calculate the fully corrected Hindfoot axes and were compared to the orientation of the actual Hindfoot axes (see Section 5.2.4). However, many feet had missing PCA marker locations on the CT images and with several feet removed for inaccurate placement of the HEE markers, only 13 feet were eligible for analysis.

The misplacement of the PCA marker is defined by the distance between the centre of the PCA marker and that of the PCA marker on a proposed ideal location. This ideal PCA marker location is the point that most truly reflects the underlying anatomy.

The CT images were used to obtain the coordinates of the ideal PCA marker location. Since there is no clear palpable anatomical landmark for the PCA marker, the

following method was proposed. The method is replicated from the HEE methodology (see Section 5.2.2), except using PCA z-coordinate.

5.2.4 Hindfoot - Fully corrected axes

The corrected A-P axis based both on the ideal HEE marker point and the corresponding ideal MID point was determined.

$$ {}^{I}\overrightarrow{x}_{H}^{APC} = \frac{{}^{I}\overrightarrow{P}_{MID_i}(1:2) - {}^{I}\overrightarrow{P}_{HEE_i}(1:2)}{\left\| {}^{I}\overrightarrow{P}_{MID_i}(1:2) - {}^{I}\overrightarrow{P}_{HEE_i}(1:2) \right\|_2}, x(3) = 0 \tag{5.29} $$

The MID corrected A-P axis, HEE corrected A-P axis and fully corrected A-P axis were first graphically compared against the uncorrected A-P axis and then their angular differences when projected into the plantar ($z = 0$) plane were calculated in 2D in global coordinate system.

In addition, the difference in absolute distance between the centre of HEE and PCA markers and their ideal locations were calculated. A positive sign was given when the location of the HEE or PCA marker was more lateral in relation to the ideal position.

The final stage involved quantifying the A-P axis error by determining the 2D angular differences between the MID corrected A-P axis, HEE corrected A-P axis and fully corrected A-P axis with the uncorrected A-P axis. Again, the new unit vectors of the axes in 2D were calculated and the angles between the axes were calculated using the dot product equation, mentioned earlier. A positive sign was used in the cases where the corrected A-P axis pointed more laterally than the uncorrected A-P axis. The angle between MID corrected A-P axis against uncorrected A-P axis data was

plotted against data of the difference in distance between the LCA (from HEE) and the STL (from HEE) markers to see the correlation between the two measurements. A linear regression line was plotted as a tool to predict A-P axis error for a given difference in distance between the LCA (from HEE) and the STL (from HEE) markers. Similarly, the angle between HEE corrected A-P axis against uncorrected A-P axis data was plotted against data of the difference in distance between the HEE marker and its ideal definition to see the correlation between the two measurements. A linear regression line was plotted as a tool to predict A-P axis error for a given difference in distance between the HEE marker and its ideal representation.

Furthermore, the M-L and P-D axes based on the ideal HEE and PCA marker locations were calculated.

1. The corrected interim P-D axis is given by:

$$\overrightarrow{i}_{H_i} = \frac{\overrightarrow{P}_{PCA_i} - \overrightarrow{P}_{HEE_i}}{\left\| \overrightarrow{P}_{PCA_i} - \overrightarrow{P}_{HEE_i} \right\|_2} \tag{5.30}$$

2. The fully corrected M-L axis is perpendicular to the fully corrected A-P axis and the interim P-D axis. The positive direction points laterally for a right leg and medially for the left leg.

$$\overrightarrow{z}_{H_i} = \overrightarrow{x}_H^{APC} \times \overrightarrow{i}_{H_i} \tag{5.31}$$

3. The fully corrected P-D axis is the cross product of the fully corrected M-L and the fully corrected A-P axes. The positive direction points proximally for both legs.

$$\overrightarrow{y}_{H_i} = \overrightarrow{z}_{H_i} \times \overrightarrow{x}_{H}^{APC} \tag{5.32}$$

For convenience, the various axes are referred to in the rest of this chapter by the acronyms listed in Table 5.1.

Table 5.1: List of Axes in Chapter 5

Coordinate System	Segment	Acronym	Definition
Image	Hindfoot	AP	Anterior-Posterior Axis
		APM	MID Corrected Anterior-Posterior Axis
		APH	HEE Corrected Anterior-Posterior Axis
		APC	Fully Corrected Anterior-Posterior Axis
		PD	Proximal-Distal Axis
		PDC	Corrected Proximal-Distal Axis

5.2.5 Summary

Sensitivity analysis was carried out to investigate how misplacing markers from their corresponding ideal locations affect the hindfoot segment axes. Four difference cases were investigated. The first case examined how the hindfoot A-P axis was influenced by correcting the MID point with HEE marker held constant. The second case scrutinised how the hindfoot A-P axis was determined by correcting the HEE marker with MID held constant. The third case investigated how the hindfoot P-D axis was affected by correcting the PCA marker with HEE marker held constant. The first, second and third cases were aimed to find out how the hindfoot axes are sensitive to individual hindfoot markers. The last case involved finding out how the hindfoot axes were changed by correcting all MID, HEE and PCA markers. Correcting the MID point and the HEE marker together enables assessment of the combined effect on the

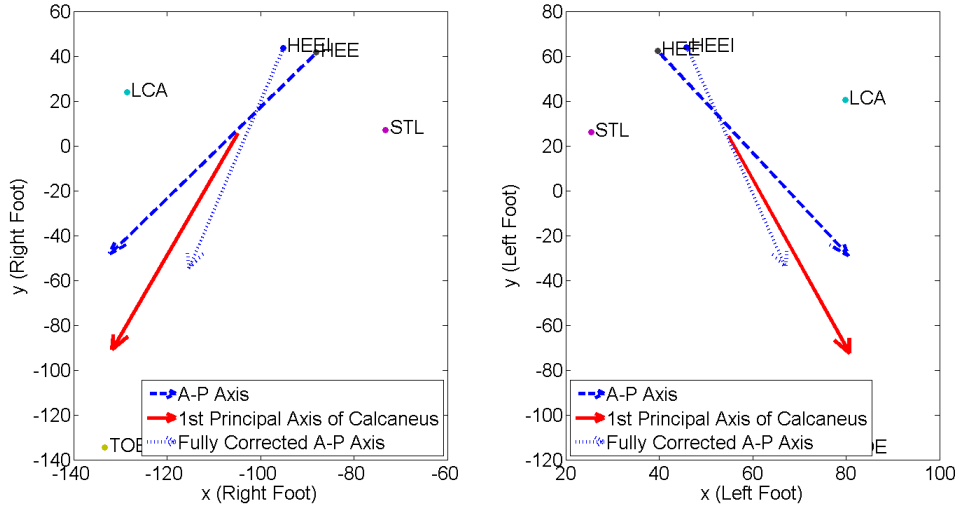

Figure 5.4: A Representative Subject's Plantar Projection of Hindfoot Axes and Fully Corrected A-P Axis. Blue, red, green and black arrows represent A-P axis, fully corrected A-P axis, first principal axis of calcaneus and H-T axis, respectively

hindfoot A-P axis. Similarly, correcting both the HEE and PCA markers allows the combined effect on the hindfoot P-D axis to be observed. Therefore when gauging the combined effect of the multiple interactions between variables on the hindfoot axes, the two aforementioned combinations cannot be ruled out. That said, the combined interaction between the MID point and the PCA marker can be ruled out as the two variables do not directly influence one particular hindfoot axis.

5.3 Results

5.3.1 Hindfoot

A representative subject (Figure 5.4) demonstrates that the fully corrected A-P axis lies closer to the first principal axis than the default marker-based A-P axis. While this

Table 5.2: Angular differences between the AP, APH (HEE corrected A-P), APM (MID corrected A-P), and APC (Fully corrected A-P) axes.

	APM – AP(°)	APH – AP (°)	APC – AP (°)
Mean	-0.4	-1.6	-1.4
SD	1.2	13.0	11.8

phenomenon occurred in most of the other subjects, some cases showed the corrected A-P axis to be situated further away from the first principal axis than the A-P axis. Hence it would be misleading to hypothesise that A-P axis correction always improves the estimation of the first principal axis. The corrected marker locations only refer to the locations corresponding to the underlying bony anatomy the markers are trying to represent. This is a test to see what happens to the orientation of the axes if the markers are put where they are intended to put. Therefore, the axes formed by these markers do not necessarily have to agree with the calcaneus first principal axis, as this is a separate question dealing with whether bony alignment and "true" marker placement agree. Levels of agreement between A-P axis and its corrected counterpart were assessed and this has been elaborated in the discussion section.

Tables 5.2 and 5.3 are statistical summaries of results of the A-P axis error and the difference in distance between the LCA (from HEE) and the STL (from HEE) markers. For convenience, the difference in distance between the LCA (from HEE) and the STL (from HEE) markers was referred to as MID error. The error in MID and HEE is equivalent, but the resulting effect on the angle error (APM-AP and APH-AP) appears to be disproportionate.

Figure 5.5 is a linear regression analysis of how marker misplacement influences

Table 5.3: HEE and MID placement error

	MID Error (mm)	HEE Error (mm)
Mean	1.7	1.6
SD	4.8	7.0

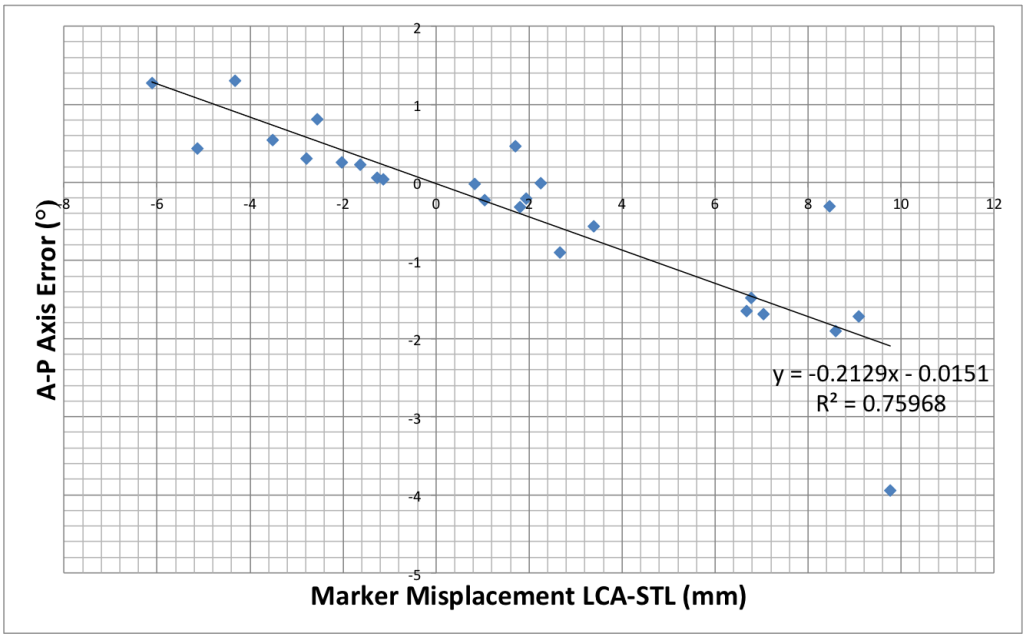

Figure 5.5: How Marker Misplacement Influences A-P Axis Orientation Error

the A-P axis orientation error.

The explanatory variable is the difference in distance between the LCA (from HEE) and the STL (from HEE) markers and the dependent variable is A-P axis error. There is a good negative correlation ($R^2 = 0.76$) between the two variables. Because the equation of this line is known ($y = -0.21x - 0.02$), the amount of A-P axis error for a given difference in distance between the LCA (from HEE) and the STL (from HEE) markers can be predicted.

Figure 5.6 is a linear regression analysis of how the HEE error influences the A-P

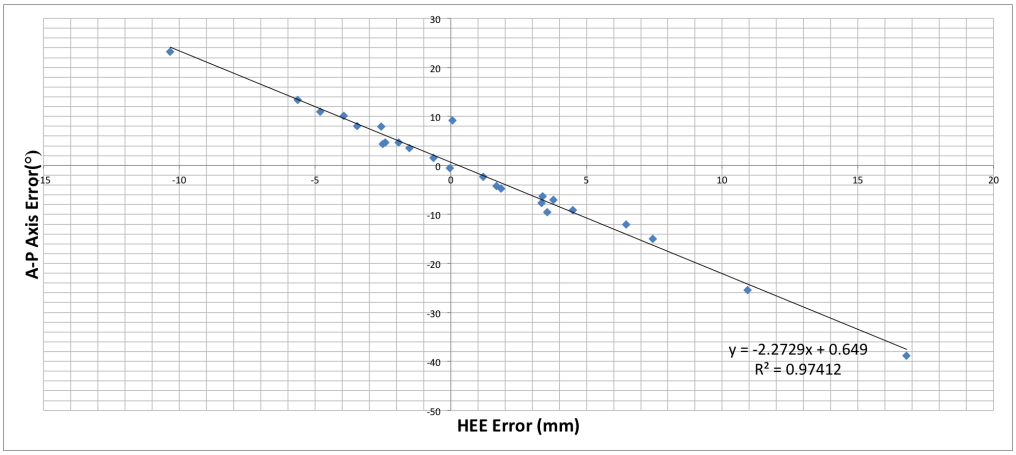

Figure 5.6: How HEE Error Affects A-P Axis

Table 5.4: PCA and HEE placement error and 2D angular difference between the PD and PDC (Fully corrected P-D) axes.

	PDC vs PD (°)	PCA Error (mm)	HEE Error (mm)
Mean	-2.6	1.5	1.7
SD	11.8	5.0	7.4

axis orientation error.

Here, the explanatory variable is the difference in distance between the HEE marker and its ideal location whereas the dependent variable is A-P axis error. It is evident that there is a good negative correlation ($R^2 = 0.97$) between the two variables. As the equation of the regression line is given by $y = -2.3x + 0.6$, the amount of A-P axis error can be predicted for a given difference in distance between the HEE marker and its corresponding ideal location.

Table 5.4 is statistical summary of the static sensitivity analysis results of PCA and HEE marker placement.

A positive sign was assigned when the corrected P-D axis was lateral relative to

Table 5.5: Results of P-D axis multiple linear regression analysis

	Values	Coefficients
Adjusted R^2	0.83	-
Intercept	-	-2.22
PCA Error	-	1.17
HEE Error	-	1.52

the default P-D axis. For the PCA and HEE errors, positive signs were given when the location of the ideal marker was more lateral in relation to the actual position.

The feasibility of putting on markers accurately and how much influence this had on P-D axis orientation was investigated. This was done using multiple linear regression analysis with PCA error and HEE error as regressors and P-D axis error as dependent variable.

The results show that there is a good positive correlation (Adjusted $R^2 = 0.83$) between the regressors and the dependent variable. The equation of the regression line is $y = -2.22 + 1.17x_1 - 1.52x_2$, where, y, x_1 and x_2 are estimated P-D axis error, PCA error and HEE error, respectively. Using this equation, the static P-D axis error can be estimated for given values of PCA and HEE marker placement errors.

5.4 Discussion

5.4.1 Hindfoot

Sensitivity analysis involved finding the difference in distance between the LCA (from HEE) and the STL (from HEE) markers and A-P axis error. Corresponding measurements were plotted and a suitable linear regression line was calculated to describe the linear relationship between the two factors (Figure 5.5). The equation of the linear

regression line was found to be $y = -0.21x - 0.02$ and therefore 10 mm of difference in distance between the LCA (from HEE) and the STL (from HEE) markers would affect the A-P axis by about -2.3 degrees. Table 5.3 shows that the mean difference in distance between the LCA (from HEE) and the STL (from HEE) markers value were only 1.7 mm which only accounts for -0.4°. The standard deviation of 4.8 mm to 7.0 mm imply that the differences in distance between the LCA (from HEE) and the STL (from HEE) markers of more than 10 mm or less than -10 mm were rare occurrences. If 5° is an accepted level of error [57], it can therefore be deduced by extrapolating Figure 5.5 that the difference in distance between the LCA (from HEE) and the STL (from HEE) markers of more than 23.4 mm or less than -23.6 mm would yield significant error in A-P axis orientation. However in reality, it would be rare for clinicians well-trained in marker placement to yield such large error. Hence it can be concluded that the difference in distance between the LCA (from HEE) and the STL (from HEE) markers induces minimal influence on A-P axis orientation and is not likely to be the determining factor for large intra-subject variability in hindfoot rotation.

The results (Table 5.3 and Figure 5.5) suggest that correcting the position of either the LCA or the STL marker induced less than 1° of change in the anterior-posterior (A-P) axis for most feet.

When the HEE marker position was aligned with the correct anatomical location, the orientation of the A-P axis was affected as the standard deviation value of APH-AP infers. There was large variation in its orientation relative to the original A-P axis with a slight medial bias as the mean HEE error of 1.6 mm lateral validates.

When the HEE marker was corrected, the effect it had on the orientation of the A-P axis was found to be more profound than when the LCA and STL markers were corrected. The mean and standard deviation values of 1.6 mm and 7.0 mm (Table 5.3) demonstrate that the HEE error can vary both medially and laterally with respect to the ideal location with a slight lateral bias. This implies that the clinicians have a tendency to place the HEE marker slightly medial to its ideal location but the bias is only 1.6 mm. The standard deviation value of the static angular difference between the HEE corrected A-P axis (APH) and the default A-P axis is 13.0° whereas that of the static angular difference between the MID corrected A-P axis (APM) and the default A-P axis is only 1.2°. Likewise, the fully corrected A-P axis (APC) is also affected by the HEE marker alignment error as the 11.8° of standard deviation value infers. It implies that while the HEE error mean is similar in order of magnitude to that of the MID error, the effect it has on the orientation of the A-P axis is much greater. Linear regression analysis was conducted to investigate how sensitive the A-P axis is to the HEE marker error. From Figure 5.6 it can be inferred that there is a very good negative correlation ($R^2 = 0.97$) and since the equation of the line is known, $y = -2.3x + 0.6$, the A-P axis error for a given HEE error can be predicted but with caution. Therefore if the HEE marker is placed 1 mm laterally with respect to the corresponding ideal location, it would result in approximately 2.9° of A-P axis error. If static axis error of 5° is perceived as clinically significant [57], it would only require 1.9 mm of lateral HEE marker bias to cause significant A-P axis error. In consequence, while there is yet to be a practical device or a method that identifies the ideal location from surface anatomy, placing the HEE marker on its corresponding

ideal location would ensure accurate orientation of the A-P axis.

Sensitivity analysis of PCA as well as HEE marker placement involved calculating PCA and HEE marker placement errors and how these affected the orientation of the hindfoot Proximal-Distal axis. Table 5.4 show that there was a large variation in corrected P-D axis orientation relative to the original A-P axis with a lateral bias as the mean and standard deviation values infer. The mean and standard deviation values for the PCA error were 1.5 mm and 5.0 mm (Table 5.4), respectively. This suggests that the PCA marker can vary both medially and laterally with respect to the ideal location. The mean and standard deviation values for the HEE error were 1.7 mm and 7.4 mm (Table 5.4), respectively, which also means the HEE marker can vary both medially and laterally with respect to its ideal location with a medial bias. These results are consistent with the understanding that if the PCA marker has no bias in its placement and the HEE marker is consistently placed medially with respect to its ideal location, it would make the orientation of the Proximal-Distal axis be more lateral to the corresponding axis produced with ideal PCA and HEE marker positions. Multiple linear regression analysis was conducted to estimate the P-D axis error for given PCA and HEE marker placement errors and the results are presented in Table 5.5. The equation of the linear regression line was found to be $y = -2.22 + 1.17x_1 - 1.52x_2$ and therefore 10 mm of PCA and HEE marker misplacement would induce -5.72° of static P-D axis error. Table 5.4 shows that the mean values of the PCA and HEE errors were only 1.5 mm and 1.7 mm, respectively. Substituting these values into the regression equation, it estimates -3.1° of static P-D axis error. Whether or not if this is significant enough to cause significant dynamic

angle errors is unknown at this stage but given that the well-trained clinicians are not likely to make more than 10 mm of marker placement errors, the static P-D axis error is not likely to exceed 5°.

The major limitation to this analysis was the assumptions used to define the ideal marker positions. When finding the XZ planar slice with the largest surface area to find the location of either the interim HEE or the interim PCA markers, it is important to note that the slice is not perpendicular to the calcaneus first principal axis. This results in skewness to the XY plane and thus the ideal marker locations will inevitably be affected by how tilted the calcaneus first principal axis is to the XZ plane.

5.5 Conclusion

This chapter provided a comprehensive analysis of how marker misplacement affects the static agreement of the hindfoot and tibia anatomical segment definition. The fourth objective of the thesis was investigated in this chapter. It demonstrated that while the LCA and STL marker misplacement had minimal influence on the orientation of the marker-based hindfoot anterior-posterior axis, the HEE marker misplacement was found to affect it significantly. In addition, while the HEE and the PCA marker misplacement had some effect on the orientation of the hindfoot medial-lateral and proximal-distal axes, they were not found to be large enough to concern the accuracy in defining the axes. To proceed from this analysis, how marker misplacement affects the kinematics of the hindfoot and tibia segment is scrutinised in the next chapter.

6 Dynamic Comparison of Marker Based Hindfoot and Tibia Segment Axes and Anatomical Definition

6.1 Introduction

Chapter 4 scrutinised the static agreement between the marker-based and the anatomy-based hindfoot and tibia segment axes. Chapter 5 investigated the severity of marker misplacement and how it affected the static orientation of the hindfoot and tibia anatomical segment definitions. To examine how clinically significant these static results are, dynamic analysis was performed and is presented in this chapter. There are three main objectives to achieve this aim: The first objective is to investigate how appropriate the rigidity assumption is in estimating the hindfoot and tibia anatomy-based segment definition from the corresponding marker-based definition. The second objective is to investigate the effect of marker misplacement on dynamic joint angles. Finally, the last objective is to investigate how closely the "best" representation of the OFM, with all markers corrected, represents underlying anatomy during gait.

6.2 Methods

The ideal HEE marker coordinates calculated from chapter 5 are given in the image coordinate system. However, the hindfoot medial-lateral and proximal-distal axes are required for analysis of the dynamic angles and in order to refer static results with the dynamic analysis results, the markers and coordinate system used in the overall

investigation were made consistent.

From the singular value decomposition method, the transformation matrix required to transform the ideal HEE marker coordinates from the image coordinate system to the Global coordinate system can be computed. Since the static coordinates of HEE, LCA, ANK and MMA markers are known in both the image and Global coordinate systems, those coordinates were used to work out the transformation matrix, T. With the transformation matrix, T, the ideal HEE marker coordinates in the Global coordinate system can be easily calculated.

$$\begin{bmatrix} {}^{G}x_{HEE_i} \\ {}^{G}y_{HEE_i} \\ {}^{G}z_{HEE_i} \\ 1 \end{bmatrix} = T \begin{bmatrix} {}^{I}x_{HEE_i} \\ {}^{I}y_{HEE_i} \\ {}^{I}z_{HEE_i} \\ 1 \end{bmatrix} \tag{6.1}$$

$${}^{G}\overrightarrow{P}_{HEE_i} = \begin{bmatrix} {}^{G}x_{HEE_i} \\ {}^{G}y_{HEE_i} \\ {}^{G}z_{HEE_i} \end{bmatrix} \tag{6.2}$$

To calculate dynamic angles, the following approach was used:

1. Define the Axes of the Hindfoot and Tibia when the subject is stationary (using the static markers from Vicon).

    - Define Oxford Foot Model Hindfoot Segment Axes (OFM)
    - Define First Principal Axis Based Hindfoot Segment Axes (FPA)

    The first principal axis based hindfoot segment axes in the CT coordinate system

can be converted to the global coordinate system. From the singular value decomposition method, the transformation matrix required to transform the first principal axis based hindfoot segment axes in the CT coordinate system to the global coordinate system can be computed. Since the static coordinates of HEE, TOE, LCA and STL markers are known in both the CT and global coordinate system, those coordinates were used to work out the transformation matrix, T. With the transformation matrix, T, the first principal axis based hindfoot segment axes in the Global coordinate system can be easily calculated:

$$\begin{bmatrix} {}^{G}\overrightarrow{x}_{H}^{FPA} \\ {}^{G}\overrightarrow{y}_{H}^{FPA} \\ {}^{G}\overrightarrow{z}_{H}^{FPA} \end{bmatrix} = T(1:3,1:3) \begin{bmatrix} {}^{I}\overrightarrow{x}_{H}^{FPA} \\ {}^{I}\overrightarrow{y}_{H}^{FPA} \\ {}^{I}\overrightarrow{z}_{H}^{FPA} \end{bmatrix} \tag{6.3}$$

- Define Corrected Oxford Foot Model Hindfoot Segment Axes (CH, FCH)
- Define Oxford Foot Model Tibia Segment Axes (OFM)
- Define Corrected Oxford Foot Model Tibia Segment Axes (CT)
- Define Fully Corrected Axes (COFM, FCOFM)

For convenience, the various axes are referred to in the rest of this chapter by the acronyms listed in Table 6.1.

1. Compare successive time frame marker coordinates from the various dynamic trials to produce rigid-body transformation matrices for the hindfoot and tibia for each time frame. For the hindfoot, HEE, PCA, LCA and STL markers are used whereas for the tibia, HFB, SHN, TIB and TUB markers are used as

Table 6.1: List of Axes in Chapter 6

Coordinate System	Analysis	Acronym	Definition
Global	Before PCA Corrected	OFM	Uncorrected Hindfoot - Uncorrected Tibia
		CH	AP Corrected Hindfoot - Uncorrected Tibia
		CT	Uncorrected Hindfoot - Corrected Tibia
		COFM	AP Corrected Hindfoot - Corrected Tibia
		FPA	Calcaneus First Principal Axis Based Hindfoot - Uncorrected Tibia
	After PCA Corrected	OFM	Uncorrected Hindfoot - Uncorrected Tibia
		CH	AP Corrected Hindfoot - Uncorrected Tibia
		FCH	Fully (with PCA) Corrected Hindfoot - Uncorrected Tibia
		COFM	AP Corrected Hindfoot - Corrected Tibia
		FCOFM	Fully (with PCA) Corrected Hindfoot - Corrected Tibia

recommended by Leitch et al. [51]. Since PCA marker coordinates in the CT images were not available in many subjects, the PCA marker was replaced by the TOE marker.

The technique only treats discrete movements from one frame to another (and not a continuous displacement path). Therefore one describes the relative movement of the segment for each time frame by comparing the X, Y, Z coordinates of a set of markers (defined as the "actual" segment) to the position of corresponding markers in the static trial (the "reference" segment). The outcome of the singular value decomposition Matlab program produced a transformation matrix T for each segment at each time frame.

2. Use the transformation matrices and static trial axes to find the orientations of the segment axes at each time point and then the relative dynamic angles of the ankle joint.

   A Matlab code was designed to take, at each time frame, the transformation matrix T for both hindfoot and tibia and the static hindfoot and tibia axes to calculate the joint rotations: plantarflexion/dorsiflexion, internal/external rotation, and inversion/eversion. The following equations were referenced from the Cole et al. Standardisation Proposal [17].

   Floating axis is defined at every time point t by:

$$ {}^{G}\overrightarrow{j} = {}^{G}\overrightarrow{z}_{T} \times {}^{G}\overrightarrow{x}_{H} \tag{6.4} $$

   Where subscripts H and T denote hindfoot (distal segment) and tibia (proximal

segment) respectively.

$$\text{internal/external} = \phi_y = \arccos\left(\frac{{}^{G}\overrightarrow{r} \,.\, {}^{G}\overrightarrow{x}_{H}}{\|{}^{G}\overrightarrow{r}\| \, \|{}^{G}\overrightarrow{x}_{H}\|}\right) \tag{6.5}$$

Where,

$${}^{G}\overrightarrow{r} = {}^{G}\overrightarrow{z}_{T} \times {}^{G}\overrightarrow{j} \tag{6.6}$$

$$\text{inversion/eversion} = \phi_x = \arccos\left(\frac{{}^{G}\overrightarrow{j} \,.\, {}^{G}\overrightarrow{y}_{H}}{\left\|{}^{G}\overrightarrow{j}\right\| \, \|{}^{G}\overrightarrow{y}_{H}\|}\right) \tag{6.7}$$

$$\text{plantar/dorsiflexion} = \phi_z = \arccos\left(\frac{{}^{G}\overrightarrow{j} \,.\, {}^{G}\overrightarrow{x}_{T}}{\left\|{}^{G}\overrightarrow{j}\right\| \, \|{}^{G}\overrightarrow{x}_{T}\|}\right) \tag{6.8}$$

3. Use the mean and Root Mean Square Difference to quantify differences between axes.

   One method of comparison between the different axes is to calculate the Root Mean Square Difference (RMSD). By comparing each axis rotation to the default Oxford Foot Model (here assumed to be a reference) with this method, a single value can be produced, which serves as a simple measure of the difference. If n is the total number of time frames, then the RMS value for each component rotation is defined as:

$$RMSD_{model} = \sqrt{\frac{\sum_{i=1}^{n} \left[\phi_{model}(i) - \phi_{OX}(i)\right]^2}{n}} \tag{6.9}$$

Where ϕ_{OX} and ϕ_{model} are the dynamic angles of the Oxford Foot Model and any other axes, respectively.

To find out how the PCA error contributes to the Oxford Foot Model dynamic angles, the kinematics of the fully corrected hindfoot segment (both the HEE and PCA corrected) with respect to the tibia segment were calculated using the rigid body segment approach, outlined in the previous section. To isolate the effect of the P-D axis error on the dynamic angles, it was decided to compare the fully corrected hindfoot segment kinematics with the default hindfoot segment and HEE corrected hindfoot segment kinematics. As mentioned in Section 5.2.3, many feet had missing PCA marker locations on the CT images and with several feet removed for inaccurate placement of the HEE markers, only 13 feet were eligible when analysing how the PCA marker misplacement affects the kinematics of the hindfoot and tibia anatomical segment definition.

6.3 Results

Due to reasons mentioned in Section 4.4, only thirty feet were available for analysis. The right and left feet results were pooled together, as it did not appear that there was any consistent bias in results between feet for individual subjects.

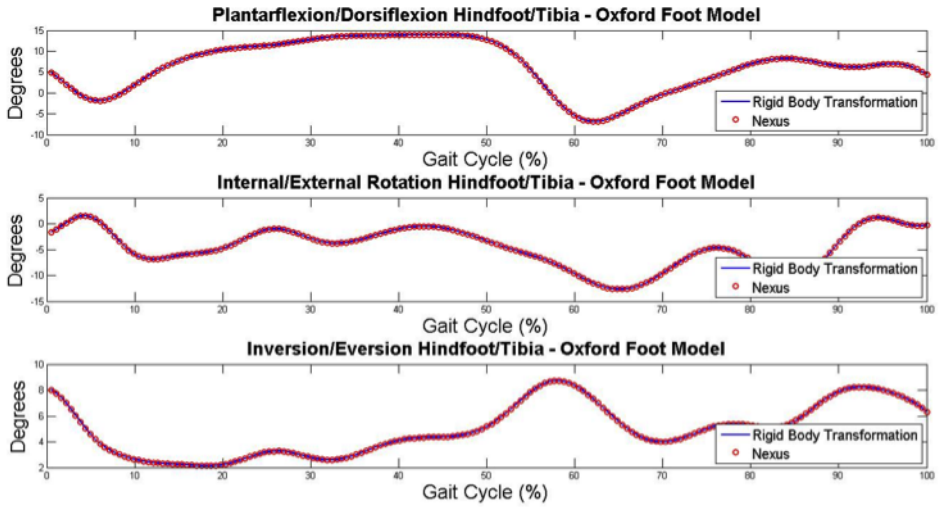

Figure 6.1: Verification of Rigid Body Method of Calculating a Representative Subject's Right Ankle Angles during Level Walking Trial. Nexus refers to the Vicon Nexus ankle joint output.

6.3.1 Hindfoot – Tibia

To test the validity of the singular value decomposition method, the default Oxford Foot Model hindfoot segment kinematics were predicted using this approach. The uncorrected marker-based OFM hindfoot-tibia kinematics were calculated frame by frame, using the marker coordinates as output by default from Nexus software. The hindfoot-tibia angles were calculated in Matlab and then compared with the Vicon Nexus kinematic output. From Figure 6.1, it is evident that the two kinematic waveforms overlap for all sagittal, transverse and coronal planes. This finding was similar for all feet.

The kinematics of the uncorrected Oxford Foot Model hindfoot against uncorrected Oxford Foot Model tibia, fully corrected A-P axis based hindfoot against un-

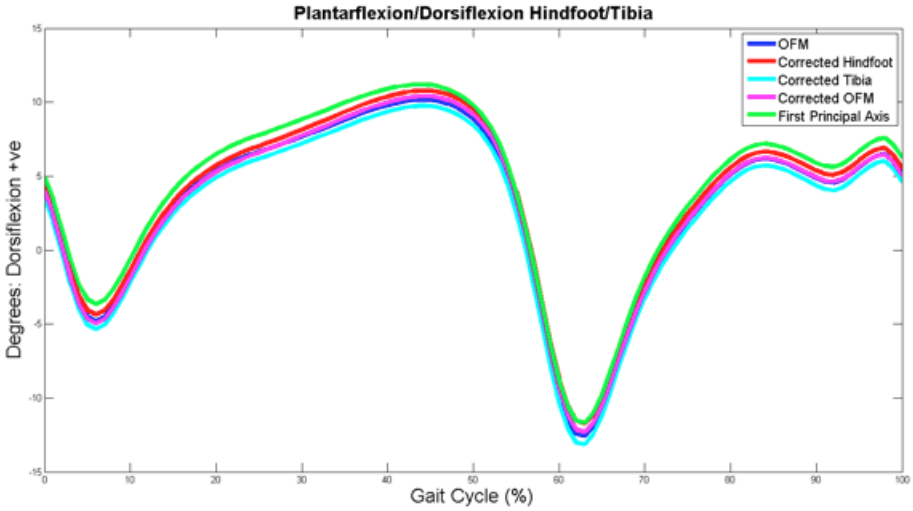

Figure 6.2: A Representative Subject's Right Hindfoot Plantar/Dorsiflexion with Respect to Tibia during Level Walking Trial

corrected tiba, uncorrected hindfoot against A-P corrected tibia, corrected hindfoot against corrected tibia and calcaneus first principal axis (projected into transverse plane) based hindfoot against uncorrected tibia were calculated (Table 6.1). Figures 6.2, 6.3 and 6.4 are the mean kinematics of all five aforementioned permutations of segments. Visually, whilst they show similar kinematic waveforms it is evident that the offsets between the axes are the greatest in the transverse plane kinematics.

To quantify the spread in distribution of the axes tested, the Root Mean Squared Differences (RMSD) against the Vicon Nexus output were calculated for all thirty feet. The RMSD was chosen to quantify deviation between the waveforms because it is sensitive to the shape of the waveform. Alternative methods such as comparing the means or certain points of the waveforms lack sensitivity to the shape of the waveform. Therefore they do not provide the implicit information found in the shapes

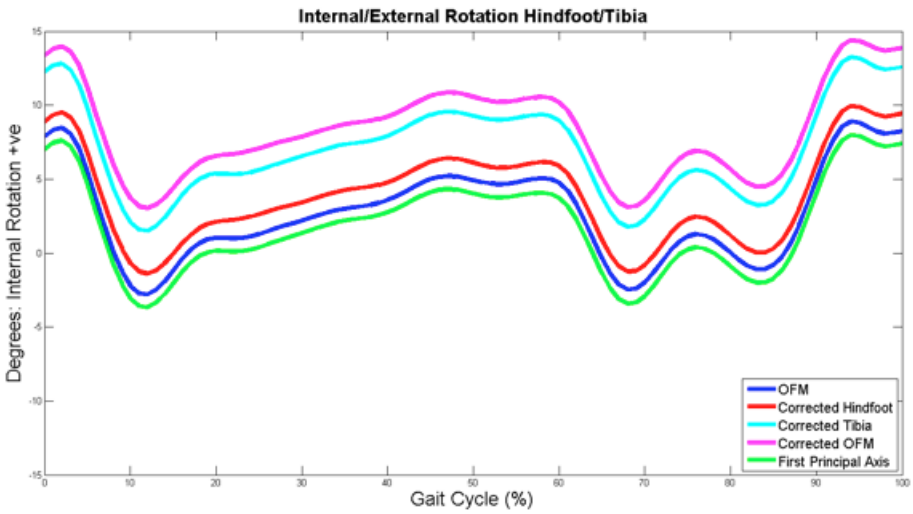

Figure 6.3: A Representative Subject's Right Hindfoot Internal/External Rotation with Respect to Tibia during Level Walking Trial

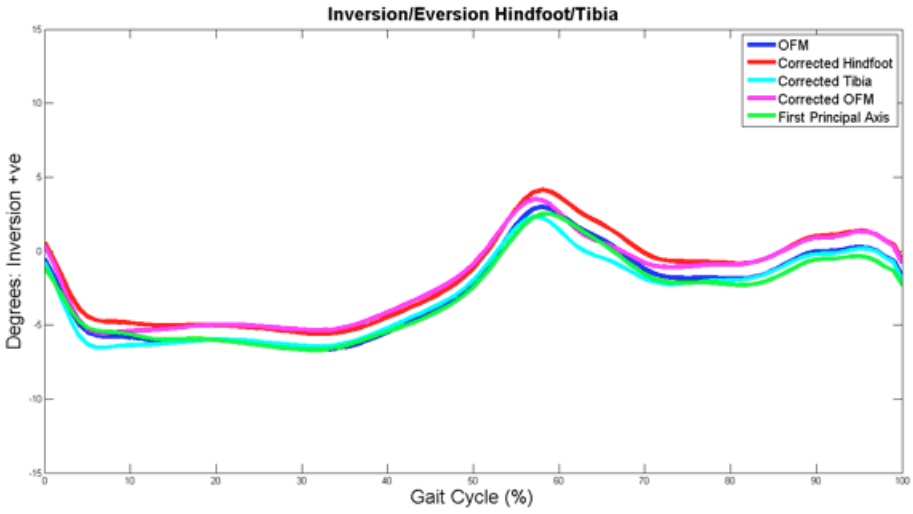

Figure 6.4: A Representative Subject's Right Hindfoot Inversion/Eversion with Respect to Tibia during Level Walking Trial

of the waveforms. This is vital in gait analysis as the waveforms describe the inter-segmental joint kinematics. Tables 6.2, 6.3 and 6.4 summarised the RMSD values in tables and Figures 6.5, 6.6 and 6.7 are boxplots of the RMSD distribution. Figures 6.5, 6.6 and 6.7 show that the spread in distribution of the RMSD values was the greatest in the transverse plane. This statement is backed up by the interquartile range and standard deviation values in Tables 6.2, 6.3 and 6.4. The calcaneus first principal axis based hindfoot against uncorrected tibia RMSD show the greatest SD value. This finding is in agreement with the static comparison of the uncorrected hindfoot A-P axis and the calcaneus first principal axis with the high SD value, 8.8° (Table 4.2 from Section 4.6.1).

Table 6.2: OFM, AP Corrected Hindfoot (CH), AP Corrected Tibia (CT), AP Corrected OFM (COFM), Hindfoot First Principal Axis (FPA) Plantar-Dorsiflexion RMSD in Comparison to Vicon Nexus Output

	OFM-Nexus	CH-Nexus	CT-Nexus	COFM-Nexus	FPA-Nexus
Mean	-1.98E-04	0.25	-0.52	-0.27	1.38
Median	-2.18E-05	0.47	-0.51	-0.46	0.42
IQR	5.79E-05	0.63	0.41	0.69	4.95
SD	1.03E-03	1.28	0.34	1.40	5.26

Table 6.3: OFM, AP Corrected Hindfoot (CH), AP Corrected Tibia (CT), AP Corrected OFM (COFM), Hindfoot First Principal Axis (FPA) Internal-External Rotation RMSD in Comparison to Vicon Nexus Output

	OFM-Nexus	CH-Nexus	CT-Nexus	COFM-Nexus	FPA-Nexus
Mean	-1.08E-05	0.47	4.74	5.22	-4.33E-01
Median	-2.61E-05	0.17	4.96	5.10	-6.42E-01
IQR	3.61E-05	6.71	4.25	8.95	11.10
SD	1.11E-04	3.42	3.42	6.93	9.51

Table 6.4: OFM, AP Corrected Hindfoot (CH), AP Corrected Tibia (CT), AP Corrected OFM (COFM), Hindfoot First Principal Axis (FPA) Inversion-Eversion RMSD in Comparison to Vicon Nexus Output

	OFM-Nexus	CH-Nexus	CT-Nexus	COFM-Nexus	FPA-Nexus
Mean	-5.47E-05	0.57	-0.15	0.20	2.36
Median	7.98E-06	0.27	0.40	0.50	1.43
IQR	1.27E-04	0.72	1.17	2.01	2.91
SD	6.36E-04	2.06	1.47	2.52	5.79

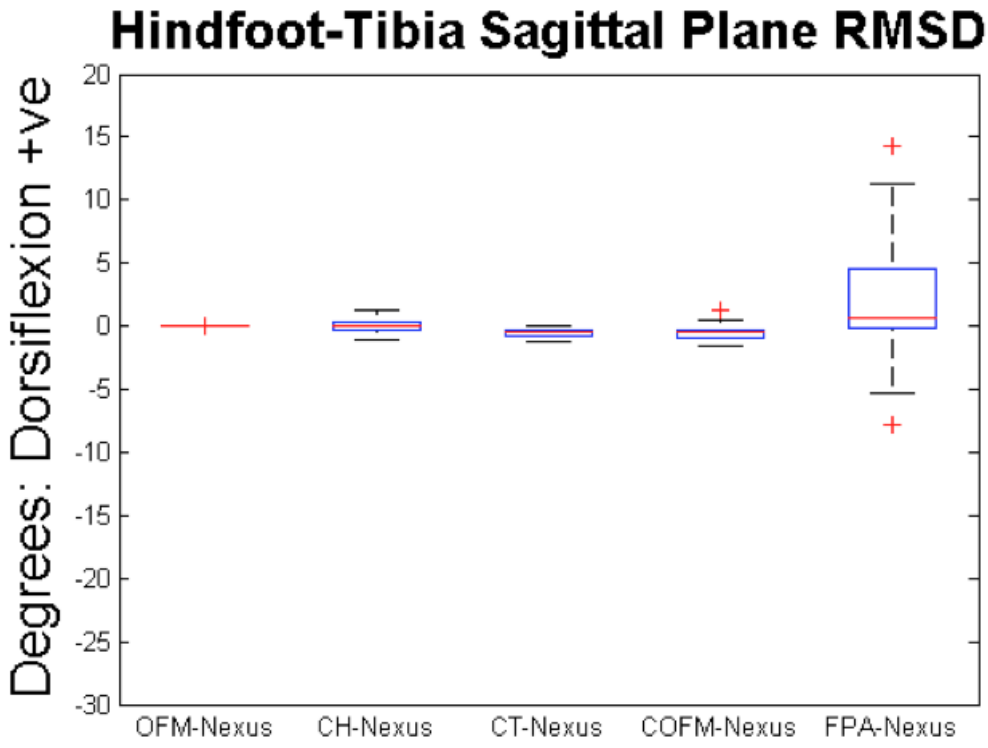

Figure 6.5: OFM, AP Corrected Hindfoot (CH), Corrected Tibia (CT), AP Corrected OFM (COFM), First Principal Axis (FPA) Sagittal Plane RMSD in Comparison to Vicon Nexus Output

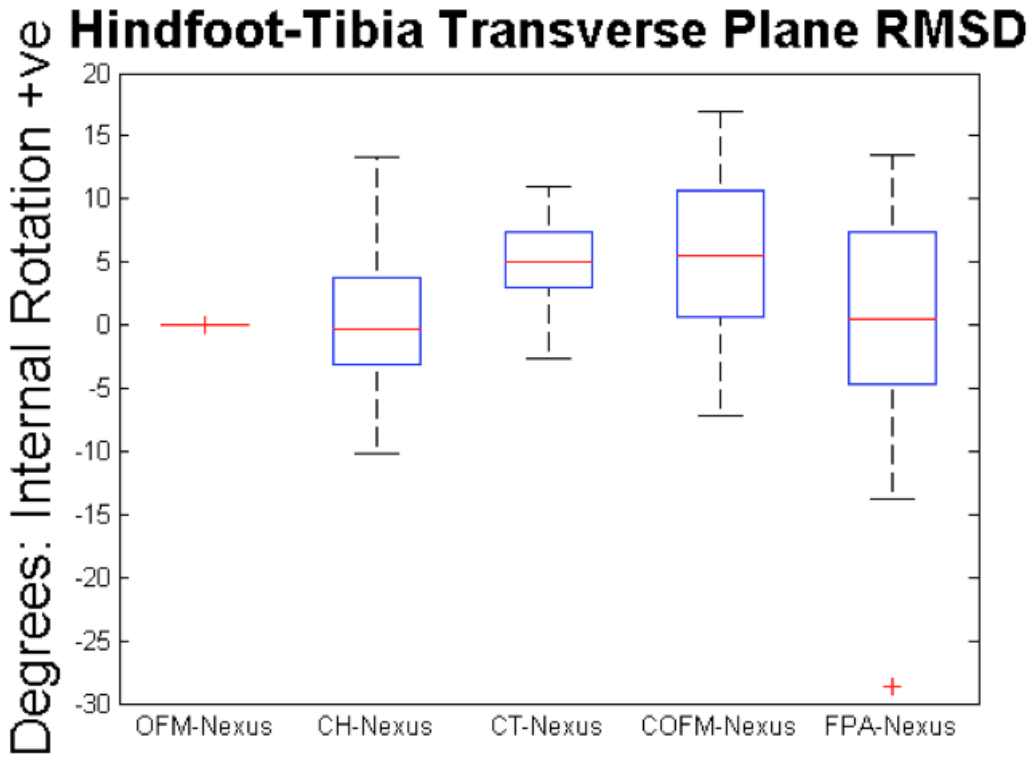

Figure 6.6: OFM, AP Corrected Hindfoot (CH), Corrected Tibia (CT), AP Corrected OFM (COFM), First Principal Axis (FPA) Transverse Plane RMSD in Comparison to Vicon Nexus Output

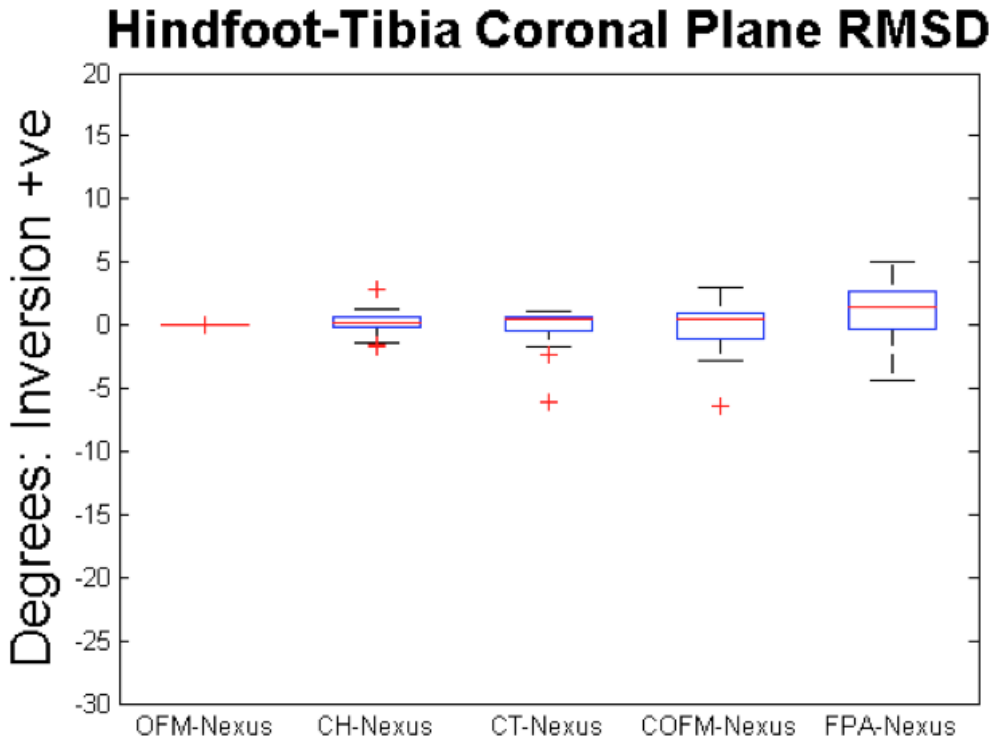

Figure 6.7: OFM, AP Corrected Hindfoot (CH), Corrected Tibia (CT), AP Corrected OFM (COFM), First Principal Axis (FPA) Coronal Plane RMSD in Comparison to Vicon Nexus Output

For analysis on how the PCA marker misplacement affects the kinematics of the hindfoot and tibia anatomical segment definition, kinematics of the uncorrected Oxford Foot Model hindfoot against uncorrected Oxford Foot Model tibia, fully corrected A-P axis based hindfoot against uncorrected tiba, fully corrected hindfoot against uncorrected tibia, fully corrected A-P axis based hindfoot against uncorrected tibia and fully corrected hindfoot against corrected tibia were computed for the thirteen feet available for the analysis (Table 6.1). Figures 6.8, 6.9 and 6.10 are the mean kinemat-

ics of all five aforementioned permutations of segments. Visually, whilst they show similar kinematic waveform it is evident that the offsets between the axes are the greatest in the transverse plane kinematics.

To quantify the spread in distribution of the axes tested, the Root Mean Squared Differences against the Vicon Nexus output were calculated for all thirteen feet. Tables 6.5, 6.6 and 6.7 summarised the RMSD values in tables and Figures 6.11, 6.12 and 6.13 are boxplots of the RMSD distribution. Figures 6.11, 6.12 and 6.13 show that the spread in distribution of the RMSD values was the smallest in the sagittal and the greatest in the transverse plane. This statement is backed up by the interquartile range and standard deviation values in Tables 6.5, 6.6 and 6.7. This suggests that correcting the HEE and PCA markers will affect the transverse plane kinematics more so than in other planes. Moreover, in the coronal plane, only the fully corrected hindfoot against corrected tibia and the fully corrected hindfoot against uncorrected tibia showed significant RMSD distribution as both exhibited IQR and SD values of more than 5°. This is consistent with the knowledge that correcting HEE and PCA will affect the orientation of the hindfoot proximal-distal axis, which will consequently affect the coronal plane hindfoot-tibia kinematics.

Table 6.5: Statistical Summary of OFM, AP Corrected Hindfoot (CH), Fully Corrected Hindfoot (FCH), AP Corrected OFM (COFM), Fully Corrected OFM (COFM) Sagittal Plane RMSD in Comparison to Vicon Nexus Output

	OFM-Nexus	CH-Nexus	FCH-Nexus	COFM-Nexus	FCOFM-Nexus
Mean	3.26E-05	-0.11	0.15	-0.63	-4.53E-02
Median	-1.86E-05	-0.15	2.66E-02	-0.82	-0.26
IQR	4.30E-05	0.43	0.63	0.84	1.10
SD	2.34E-04	0.56	1.19	0.74	1.63

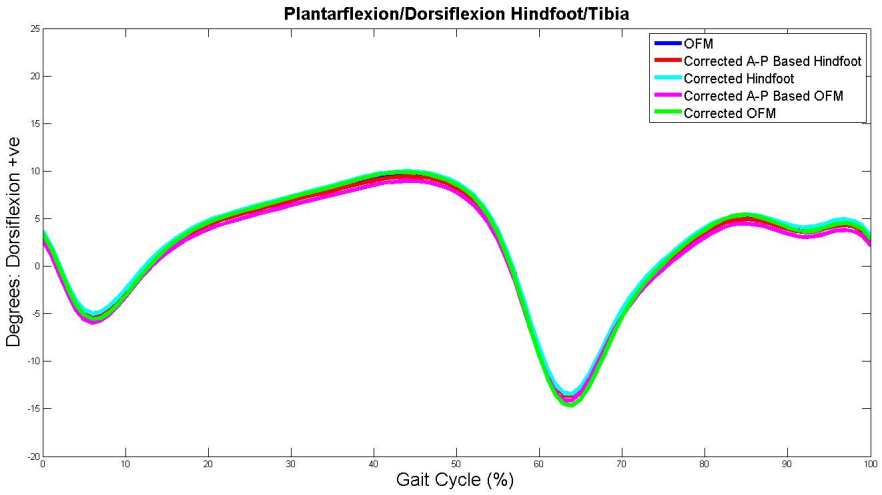

Figure 6.8: Mean Hindfoot Plantar/Dorsiflexion with Respect to Tibia during Level Walking Trial

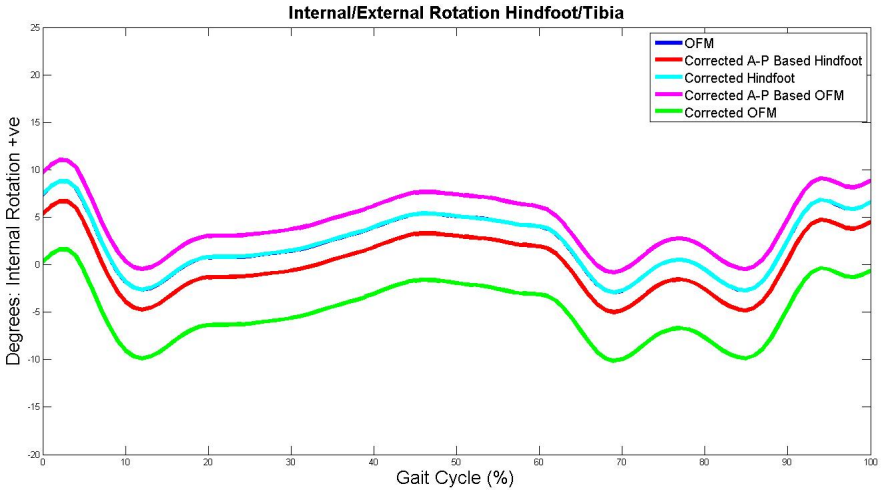

Figure 6.9: Mean Hindfoot Interal/External Rotation with Respect to Tibia during Level Walking Trial

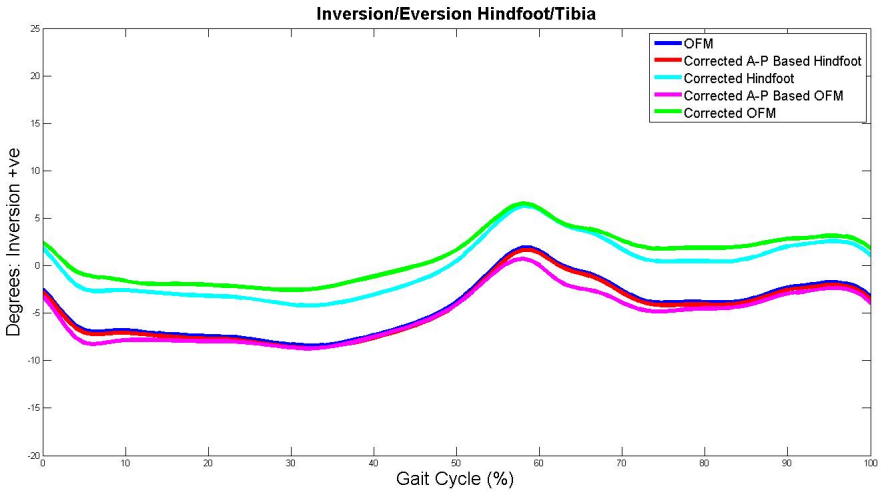

Figure 6.10: Mean Hindfoot Inversion/Eversion with Respect to Tibia during Level Walking Trial

Table 6.6: Statistical Summary of OFM, AP Corrected Hindfoot (CH), Fully Corrected Hindfoot (FCH), AP Corrected OFM (COFM), Fully Corrected OFM (COFM) Transverse Plane RMSD in Comparison to Vicon Nexus Output

	OFM-Nexus	CH-Nexus	FCH-Nexus	COFM-Nexus	FCOFM-Nexus
Mean	3.83E-06	-2.08	1.85E-02	2.21	-7.13
Median	-1.97E-05	-2.92	-0.35	1.67	-2.62
IQR	5.77E-05	3.57	10.0	7.68	20.3
SD	8.52E-05	5.93	12.7	6.28	20.5

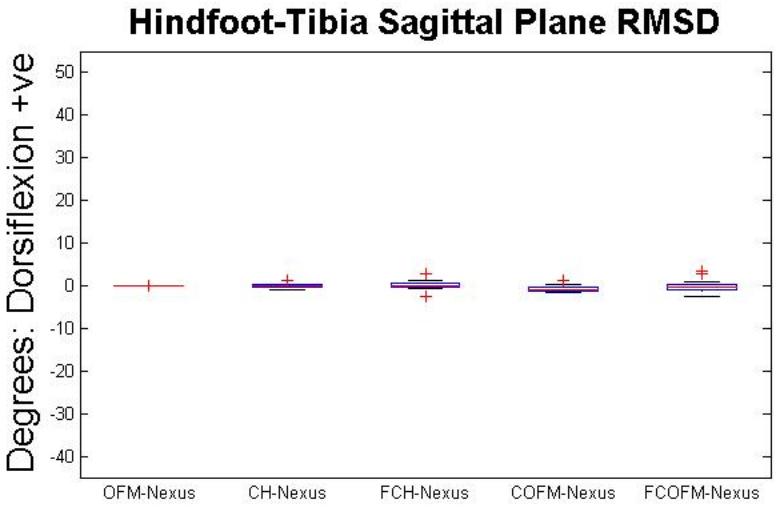

Figure 6.11: Boxplots of OFM, AP Corrected Hindfoot (CH), Fully Corrected Hindfoot (FCH), AP Corrected OFM (COFM), Fully Corrected OFM (COFM) Plantar-Dorsiflexion RMSD in Comparison to Vicon Nexus Output

Table 6.7: Statistical Summary of OFM, AP Corrected Hindfoot (CH), Fully Corrected Hindfoot (FCH), AP Corrected OFM (COFM), Fully Corrected OFM (COFM) Coronal Plane RMSD in Comparison to Vicon Nexus Output

	OFM-Nexus	CH-Nexus	FCH-Nexus	COFM-Nexus	FCOFM-Nexus
Mean	-2.04E-04	2.47E-04	6.69	-0.86	5.48
Median	7.42E-06	0.11	3.90	-0.68	-1.37
IQR	1.28E-04	0.87	7.67	2.13	13.6
SD	6.22E-04	1.10	16.2	2.25	18.0

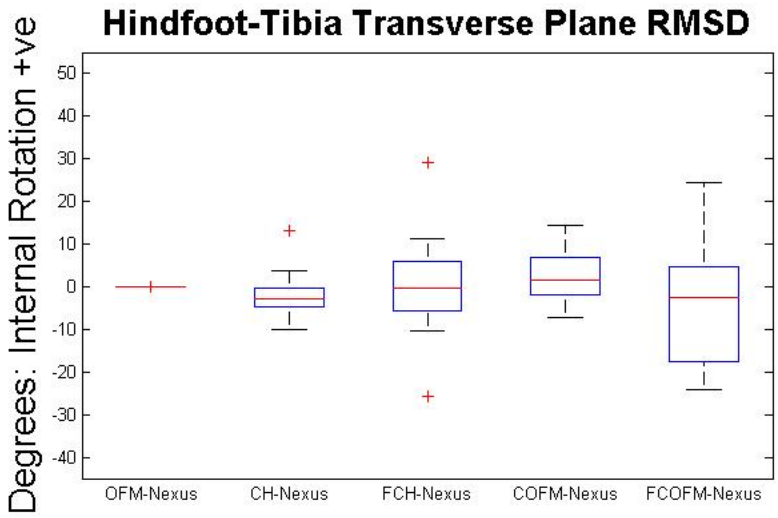

Figure 6.12: Boxplots of OFM, AP Corrected Hindfoot (CH), Fully Corrected Hindfoot (FCH), AP Corrected OFM (COFM), Fully Corrected OFM (COFM) Internal-External Rotation RMSD in Comparison to Vicon Nexus Output

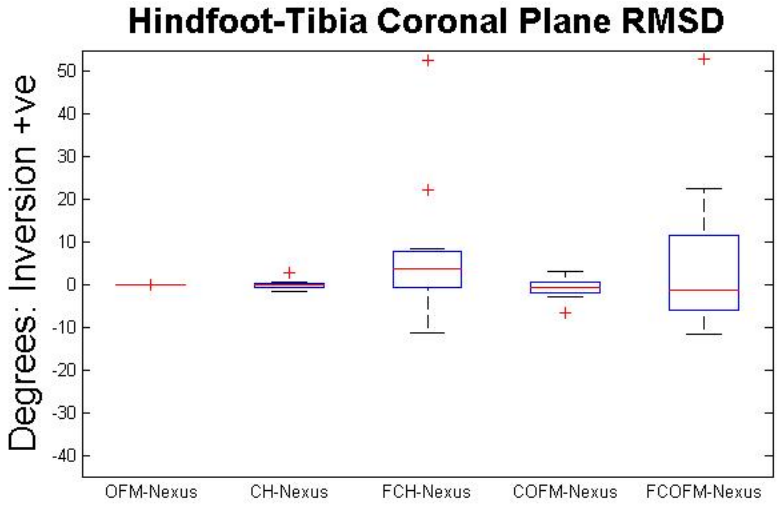

Figure 6.13: Boxplots of OFM, AP Corrected Hindfoot (CH), Fully Corrected Hindfoot (FCH), AP Corrected OFM (COFM), Fully Corrected OFM (COFM) Inversion-Eversion RMSD in Comparison to Vicon Nexus Output

6.4 Discussion

6.4.1 Hindfoot – Tibia

The purpose of dynamic analysis was to find out how the static differences observed in hindfoot and tibia marker and anatomy-based axes influence dynamic angles. In this analysis, the singular value decomposition method was used to predict the kinematic patterns of the hindfoot and tibia axes and their root mean squared difference values with respect to Vicon Nexus kinematic output were compared.

The way Vicon Nexus outputs the dynamic angles is by, first, calculating the hindfoot and tibia segment axes at each time frame and then computing the Euler angles between the two sets of axes. As mentioned in section 3.7, the way the rigid body transformation method calculates the dynamic angles is by first, calculating a transformation matrix from a matrix of the instantaneous positions of the markers at each time frame and a matrix of the static reference positions of the markers. It then uses a singular value decomposition technique to calculate the best-fit transformation matrix and this transformation matrix can be multiplied to the matrix of the static reference position of markers to predict its instantaneous rigid body positions at each time frame. The estimated instantaneous positions can then be used to calculate the segment axes for both the hindfoot and tibia and computing the Euler angles between the two sets of axes outputs the dynamic intersegmental angles. To validate the accuracy of the rigid body method, the dynamic angles calculated using this approach were verified against the Vicon Nexus outputs (Figure 6.1). This notion is backed up by the results in Tables 6.2, 6.3 and 6.4; the median RMSD values for sagittal, transverse and coronal planes were mere -2.2×10^{-5}, -2.6×10^{-5} and 8.0×10^{-6}

respectively. Hence it can be safely substantiated that the rigid body assumptions for the hindfoot and tibia are valid and that the singular value decomposition technique can be used alternatively to calculate kinematics.

The sagittal, transverse and coronal plane interquartile range values for the A-P corrected hindfoot segment were 0.6, 6.7 and 0.7 degrees, respectively. This has a clinical implication in that the hindfoot markers, has a significant effect on the accuracy of the transverse plane OFM hindfoot-tibia kinematics, assuming that a change in dynamic angle of 5 degrees or more is clinically significant [57].

The sagittal, transverse and coronal plane interquartile range values for the corrected A-P axis based tibia segment were 0.4, 4.1 and 1.1 degrees, respectively (Table 6.2, 6.3 and 6.4). While the effect is not as pronounced as that of the corrected hindfoot segment, it is still evident that accurate placement of tibia markers is pivotal in obtaining accurate OFM hindfoot-tibia kinematics.

Furthermore, the kinematics of the corrected OFM hindfoot against the corrected OFM tibia was computed to observe the overall effect of marker placement in OFM hindfoot-tibia kinematics. Figures 6.2, 6.3 and 6.4 as well as the boxplots in Figures 6.5, 6.6 and 6.7 illustrates the significance of the consistent and accurate placement of hindfoot and tibia markers as the spread of the distribution is quite large for the transverse plane; from Table 6.2, 6.3 and 6.4 the sagittal, transverse and coronal plane interquartile range values are 0.7, 9.0 and 2.0 degrees, respectively. These results exhibit evidence to suggest that marker placement can be the source of large variability in transverse plane hindfoot-tibia kinematics, as stated in past literatures [42, 49, 59, 74, 78].

When the hindfoot was fully corrected (including correction of the P-D axis), it was found that coronal plane kinematics were affected as well as the transverse plane. This is intuitive as correcting HEE and PCA will affect the orientation of the hindfoot proximal-distal axis, which will consequently affect the coronal plane hindfoot-tibia kinematics. The mean sagittal, transverse and coronal plane fully corrected hindfoot-tibia kinematic RMSD values are 0.15, 0.019 and 6.69 degrees while the fully corrected hindfoot-fully tibia kinematic RMSD values are -0.045, -7.13 and 5.48 degrees, respectively (Tables 6.5, 6.6 and 6.7 and figures 6.11, 6.12 and 6.13). This suggests that correcting all hindfoot markers significantly affects the coronal plane hindfoot-tibia kinematics. Figure 6.10 shows that fully correcting the hindfoot segment axes will result in more inversion around the ankle. This is not consistent with the result of the static comparison of the default hindfoot proximal-distal axis and the corrected hindfoot proximal-distal axis, as mentioned in Section 5.3 (Table 5.4), where the corrected proximal-distal axis was found to be everted on average by 2.6 degrees in relation to the default proximal-distal axis. The inter-quartile range values of the coronal plane fully corrected hindfoot-tibia kinematic RMSD and fully corrected hindfoot-fully tibia kinematic RMSD values are 7.7 and 13.6 degrees, respectively (Table 6.7 and figures 6.13). This large spread in distribution suggests why dynamic angles show inversion when static angles show eversion. Hence, we are under-estimating inversion.

Figures 6.5 illustrates that the sagittal plane FPA-Nexus error is clearly larger than any other variables. With the interquartile range around 5 degrees, this relationship suggests that the marker-based hindfoot axes significantly differ from the anatomy-

based hindfoot axes. However, fully correcting the hindfoot and/or tibia markers do not affect the sagittal plane hindfoot-tibia motion. This implies that even correcting the markers does not improve the agreement between the marker-based and anatomy-based hindfoot and tibia segments. Since the Oxford Foot Model as well as many other multi-segment foot models uses markers to represent the calcaneus, this is a significant finding as it suggests that the calcaneus first principal axis cannot be replicated well using markers. Hence, the hindfoot kinematic results derived from these models may be unreliable to make accurate clinical interpretations. That said, an explanation for why the FPA-Nexus error was so large is the error in transforming the first principal axis in the CT image coordinate system to the global coordinate system. Essentially, this means that there were discrepancies between the locations of the markers in the global coordinate system and those in the image coordinate system. This is as a result of the process of removing motion capture system markers and reapplying radio-opaque markers for image acquisition creates potential errors, as stated in section 4.7.1, and the corresponding limitation is made apparent, here. Therefore, this may limit the reliability of the results found in this chapter. Tables 6.2, 6.3 and 6.4 show that the mean sagittal, transverse and coronal plane kinematic RMSD values for FPA-Nexus are 1.38, -0.43 and 2.36, respectively. This hints that the coronal plane is where the marker-based and anatomy-based segment kinematics differs the most while the transverse plane differ the least. However, figures 6.2, 6.3 and 6.4 as well as the boxplots shown as Figures 6.5, 6.6 and 6.7 explicitly suggest that the spread in distribution of the RMSD values for the transverse plane is greater than for either sagittal or coronal planes and this is backed up by the interquartile

range and standard deviation values in Tables 6.2, 6.3 and 6.4. The sagittal, transverse and coronal plane interquartile range values for the calcaneus first principal axis based hindfoot segment are 4.9, 11.1 and 2.9 degrees, respectively. It can be inferred that the Oxford Foot Model does not consistently embody the movement of the calcaneus, the represented bone of the hindfoot segment, especially the transverse plane movement. This finding was in contrast to the finding of Reinschimdt et al. [69], who investigated the tibiocalcaneal motion during walking using external and skeletal markers. They found that the mean sagittal, transverse and coronal RMSD values for five subjects tested were 3.1, 2.5 and 3.4 degrees, respectively. While the order of magnitudes are similar, the results showed that the kinematic difference was smallest in the transverse plane. This difference may be explained by the fact that the subjects in the study by Reinschmidt et al. [69] walked shod with markers placed on the shoes.

There are limitations associated with predicting the kinematics of the corrected OFM and anatomy-based segments. The kinematics of the corrected OFM and calcaneus based hindfoot segment were predicted using the rigid body methodology. While the embedded rigid body movement assumption was found to be quite accurate, the kinematics could only be predicted not measured. Since the current 3D motion analysis technology does not allow the underlying bones to be measured, the rigid body movement prediction was thought to be the best approach to observe the kinematic patterns of the subcutaneous bones.

Another limitation is that the skin artefact was not accounted for in this comparison. The skin artefact affects the marker movement relative to the underlying bone and therefore will prevent the markers replicate true movement of the underlying

bone. This provides a future scope of this investigation to quantify the skin motion artefact and how it affects the dynamic angles. That said, the rigid-body prediction was good and therefore suggests little skin movement.

6.5 Conclusion

This chapter followed from the work of the previous chapters and outlined the dynamic comparison of marker-based hindfoot and tibia segment axes and anatomy-based segment definitions. The second, third and the fourth objectives of the thesis were investigated in this chapter. It has been demonstrated that the agreement between the marker-based and the anatomy-based segment axes was worst in the transverse plane, showing more than 5 degrees of dynamic angle RMSD difference and that heel and malleoli marker misplacement was found to affect the hindfoot-tibia kinematics. However, it was shown that the hindfoot and tibia rigidity assumption was valid in estimating the motion of the underling anatomy from the marker-based segment axes definition.

7 Conclusion

The measurement of foot kinematics via stereophotogrammetry is a well-established part of clinical decision-making for patients with known gait disabilities. However, there are limitations associated with estimating the orientation of bone from reconstructed skin-marker trajectories. The accuracy of the OFM angle calculations depends on how the markers and segment axes relate to the underlying anatomy. In the Oxford Foot Model, there is a limitation in that layers of skin, soft tissue and fat cover anatomical landmarks. This affects the accuracy of the angle calculations because markers do not follow the movement of the underlying bony anatomy. The aim of the current thesis was to investigate the agreement between marker-based and anatomical hindfoot and tibia segment based axes in the Oxford Foot Model. The thesis investigated marker-placement error but did not investigate skin-movement error.

Overall, twenty-one healthy female adults were recruited to this study but due to various reasons, only nineteen subjects were eligible for analysis. Moreover, seven feet had to be excluded as the heel marker has been displaced from its original position due to contact with the foot loading plate. The loading rig was used to provide a simulation of the loaded ankle. As mentioned in section 3.4, there are two assumptions when replicating the position of the foot in standing with 40% bodyweight. The first is that the alignment of the foot bones is in the same position with 40% loading as in standing (100% bodyweight), and the other is that applying a load in lying down might distribute the load across the sole of the foot differently compared to standing. Kothari et al. (unpublished work) verified that 40% load accurately replicated the

arch position compared to standing. Based on this result, it is reasonable to recommend future studies to perform measurements under loading. CT images of the subjects' feet were acquired to measure the anatomical segment axes of the hindfoot. Gait analysis was implemented to obtain three-dimensional angles at the foot and ankle for all subjects.

The first objective was to investigate the static agreement between the marker-based and the anatomical hindfoot and tibia segment based axes. The second objective was to investigate the dynamic agreement between the marker-based and the anatomical hindfoot and tibia segment based axes. Overall, it can be concluded that there is enough evidence that there is a discrepancy between the Oxford Foot Model hindfoot A-P axis and the corresponding anatomical definition in the transverse plane, both statically and dynamically. The relationship between the A-P axis the calcaneus first principal axis and the H-T axis and the calcaneus first principal axis suggested that the more deformed the foot, potentially the more inaccurate the A-P axis definition and therefore this is potentially amplified in deformed feet such as the clubfoot. This implies that when planning for treatments, clinicians can provide inappropriate treatment recommendation to the patients with deformed feet and potentially result in an unsuccessful treatment outcome. The third objective was to investigate how appropriate the rigidity assumption is in estimating the hindfoot and tibia anatomical segment definition from the corresponding marker based definition. The root mean square difference between the hindfoot-tibia kinematics derived from a standard stereophotogrammetric procedure (frame by frame reconstruction) and that estimated by the rigid body transformation method was insignificant. This

implies that the hindfoot and tibia rigidity assumption was valid in estimating the motion of the underling anatomy from the marker-based segment axes definition. The fourth objective was to investigate how marker misplacement affects the description of the hindfoot and tibia anatomical segment definition. The results showed that there was a discrepancy between the OFM hindfoot and tibia axes and the corrected OFM hindfoot and tibia axes in the transverse plane, both statically and dynamically. The results imply that the aforementioned reasons cause the large variability in transverse plane hindfoot-tibia kinematics, as stated in past literatures [42, 49, 59, 74, 78]. Since many multi-segment foot models [45, 49] use similar hindfoot and tibia definitions as those of the Oxford Foot Model, a new paradigm of the hindfoot and tibia segment definitions would be needed to accurately describe the motion of the underlying anatomy.

Predicting the kinematics of the corrected hindfoot, calcaneus first principal axis based hindfoot and corrected tibia segment using the rigid body methodology has limitations. The fact that the kinematics could only be predicted not measured and the assumption that each segment is perfectly rigid will always induce errors. However, as the results show, the rigid body assumption was found to be quite accurate and since the current 3D motion analysis technology does not measure the kinematics of the underlying bones, the rigid body approach was accepted as the optimal method to calculate the kinematic patterns of the subcutaneous bones.

Furthermore, measurement of skin motion artefact and the kinematic errors caused by it was not within the scope of this study. Quantifying the skin movement error would show how much influence it has on the joint kinematics. If there is a consistent

and significant skin movement error, clinicians can offset the skin movement error from the kinematic data and interpret based on it. Measuring the skin motion artefact and how it affects the dynamic angles could potentially help the clinicians in making accurate interpretation of the dynamic Oxford Foot Model angles.

7.1 Recommendations for Future Work

As stated from the conclusion of this study, improving marker placement, especially the HEE marker, would enhance prediction of the motion of the underlying anatomy. In practice, it is time consuming and costly to get all patients have their feet CT scanned, identify the ideal location of the markers and place the markers on these ideal locations. One practical way of placing the markers consistently and accurately on the ideal locations is to manufacture the base plates, which the markers are attached to, more form fitting. The default base plates are flat and therefore it is difficult to place the markers on specific locations, at times. If they are made to follow closely to the curvature of the surface of the marker locations, the marker placement might be more consistent and true to the ideal locations.

Moreover, measuring the skin movement error can be added to the scope of future study. As mentioned previously, the knowledge of the effect of the skin motion artefact on the dynamic Oxford Foot Model angles could help clinicians make more accurate interpretation of the dynamic angles and consequently make more appropriate treatment decisions. One way of quantifying the skin motion artefact is to measure the movement of the markers on the surface of the skin, approximated by a plane defined using nearby markers. For example, to measure skin movement underneath the HEE

marker, HEE, PCA and STL and LCA markers can be used to define a plane and calculate the HEE movement vectors in that plane.

The current Oxford Foot Model assumes the forefoot segment as a single rigid segment [14, 78]. The forefoot is made up of more bones than other segments and therefore behaves less rigidly than other segments. The forefoot is an area with little previous research. Just like the previous analysis, the forefoot should be analysed to find out the accuracy of the forefoot segment in describing the motion of the forefoot. Appropriate modifications to the marker sets should be suggested, if necessary. It is known that the forefoot is not as rigid as other segments like the hindfoot or the tibia. However, the Oxford Foot Model assumes it as a single rigid segment. Hence, it is hypothesised that there will be some differences in the marker-based forefoot segment kinematic data and that predicted from the rigid body transformation method.

8 Bibliography

1. Allard P, Thiry PS, Duhaime M, Geoffroy G. Kinematics of the foot. Can J Neurol Sci 1982;9(2):119–25.

2. Alonso-Vazquez A, Villarroya MA, Franco MA, Asín J, Calvo B. Kinematic assessment of paediatric forefoot varus. Gait Posture 2009;29(2):214–9.

3. Andriacchi TP, Alexander EJ. Studies of human locomotion: past, present and future. J Biomech 2000;33(10):1217–24.

4. Arndt A, Wolf P, Liu A, Nester C, Stacoff A, Jones R, Lundgren P, Lundberg A. Intrinsic foot kinematics measured in vivo during the stance phase of slow running. J Biomech 2007;(40):2672–2678.

5. Arun K, Huang TS, Blostein SD. Least-squares fitting of two 3-d point sets. IEEE Transactions on Pattern Analysis and Machine Intelligence 1987;Pami-9(5):698-700.

6. Baker RJ, Finney L, Orr J. A new approach to determine the hip rotations profile from clinical gait analysis data. Human Movement Science 1999;18: 655-667.

7. Bishop C, Paul G, Thewlis D. Recommendations for the reporting of foot and ankle models. J Biomech 2012;45(13):2185-94.

8. Bland JM and Altman DG. Measuring agreement in method comparison studies. Statistical Methods in Medical Research 1999;8(2):135-160.

9. Bleck E. Orthopaedic Management in Cerebral Palsy. Mac Keith Press, Oxford, 1987.

10. Bost F, Schottstaedt E, Larsen L. Plantar dissection: an operation to release the soft tissues in recurrent or recalcitrant talipes equinovarus. J Bone Joint Surg Am. 1960;42-A(1):151-176.

11. Brodsky JW, Charlick DA, Coleman SC, Pollo FE, Royer CT. Hindfoot motion following reconstruction for posterior tibial tendon dysfunction. Foot Ankle Int 2009;30(7): 613–8.

12. Cappozzo A, Catani F, Leardini A, Benedetti MG, Della Croce U. Position and orientation of bones during movement: experimental artefacts. Clin Biomech 1996;11(2):90–100.

13. Cappozzo, A., Della Croce, U., Leardini, A., and Chiari, L. Human movement analysis using stereophotogrammetry: Part 1: Theoretical background. Gait and Posture 2005;21(2):186–196.

14. Carson MC, Harrington ME, Thompson N, O'Connor J, Theologis T. Kinematic analysis of a multi-segment foot model for research and clinical applications: a repeatability analysis. J Biomech 2001;34(10):1299–307.

15. Chumanov E, Wall-Scheffler C, Heiderscheit B. Gender differences in walking and running on level and inclined surfaces. Clinical Biomechanics 2008;23(10):1260–1268.

16. Cobb SC, Tis LL, Johnson JT, et al. The effect of low-mobile foot posture on multisegment medial foot model gait kinematics. Gait Posture 2009;30(3):334–9.

17. Cole GK, Nigg BM, Ronsk JL, Yeadon MR. Application of the joint coordinate system to three-dimensional joint attitude and movement representation: a standardization proposal. Journal of Biomechanical Engineering 1993;115(4A):344-349.

18. Coughlin MJ, Saltzman CL, Mann RA, editors. Surgery of the Foot and Ankle. 8th ed. St. Louis: Mosby; 2006.

19. Cowan DN, Jones BH, Robinson JR. Foot morphologic characteristics and risk of exercise-related injury. Arch Fam Med 1993;2:773–777.

20. Curtis DJ, Bencke J, Stebbins JA, Stansfield B. Intra-rater repeatability of the Oxford foot model in healthy children in different stages of the foot roll over process during gait. Gait Posture 2009;30(1):118–21.

21. Davis RB, Jameson EG, Davids JR, Christopher LM, Rogozinski BR, Anderson JP. The design, development and initial evaluation of a multi-segment foot model for routine clinical gait analysis. Foot and ankle motion analysis: clinical treatment and technology. CRC Press 2007.

22. Davis RB, Saraswat P, and MacWilliams BA. Multicenter investigation of the repeatability of the foot anatomical landmark identification. In: Annual proceedings of gait and clinical motion analysis society 2008: 146–147.

23. Davis, RB, Ounpuu S, Tyburski D, Gage J. A gait analysis data collection and reduction technique. Human Movement Sciences 1991;10:575-587.

24. De Mits S, Segers V, Woodburn J, Elewaut D, De Clercq D, Roosen P, A clinically applicable six-segmented foot model. Journal of Orthopaedic Research 2012;30(4):655-61.

25. deAndrade MS, Grant C, Dixon A. Joint distension and reflex muscle inhibition in the knee. J Bone Joint Surg. 1965;47A:313-322.

26. DeHaven KE, Lintner DM. Athletic injuries: Comparison by age, sport, and gender. The American Journal of Sports Medicine 1986;14(3):218–224.

27. Dimonte P, Light H. Pathomechanics, gait deviations, and treatment for the rheumatoid foot: a clinical report. Phys Ther. 1982;62(8):1148-1156.

28. D'Andrea S, Tylkowski C, Losito J, et al. Three-dimensional kinematics of the foot. Presented at the Eighth Annual East Coast Clinical Gait Conference. Rochester (MN), May 5–8, 1993.

29. Engsberg JR. A biomechanical analysis of the talocalcaneal joint–in vitro. J Biomech 1987;20(4):429–42.

30. Gage J, Schwartz M. Dynamic deformities and lever-arm considerations. In Principles of Deformity Correction (Berlin, 2002), Springer.

31. Gage J. Gait Analysis in Cerebral Palsy. Mac Keith Press, London, 1991.

32. Giladi M, Milgrom C, Stein M. The low arch, a protective factor in stress fractures. A prospective study of 295 military recruits. Orthop Rev 1985;14:709–712.

33. Grood, E. and Suntay, W. A joint coordinate system for the clinical description of threedimensional motions: application to the knee. Journal of Biomechanical Engineering 1983;105(2):136–144.

34. Hanson R, Norris M. Analysis of measurements based on the singular value decomposition. SIAM Journal on Scientific and Statistical Computing 1981;2(3):363-373.

35. Haxton HA. Absolute muscle force in the ankle flexors of man. J Physiol. 1944; 103: 267-273.

36. Hicks JH. The mechanics of the foot. J Anat 87 (1953), 345.

37. Hunt AE, Smith RM, Torode M, et al. Inter-segment foot motion and ground reaction forces over the stance phase of walking. Clin Biomech (Bristol, Avon) 2001; 16(7):592–600.

38. Inman VT. The human foot. Med Rev 46 (1966), 513-5.

39. Jenkyn TR, Nicol AC. A multi-segment kinematic model of the foot with a novel definition of forefoot motion for use in clinical gait analysis during walking. J Biomech 2007;40(14):3271–8.

40. Kadaba MP, Ramakrishnan HK, Wootten ME, Gainey J, Gorton G, Cochran GVB. Repeatability of kinematic, kinetics and electromyographic data in normal adult gait. Journal of Orthopaedic Research 1989;7:849-860

41. Kadaba MP, Ramakrishnan HK, Wootten ME. Lower extremity kinematics during level walking. Journal of Orthopaedic Research 1990;8:849-860.

42. Kepple TM, Stanhope SJ, Lohmann KN, Roman NL. A video-based technique for measuring ankle-subtalar motion during stance. J Biomed Eng 1990;12(4): 273–80.

43. Khazzam M, Long JT, Marks RM, Harris GF. Kinematic changes of the foot and ankle in patients with systemic rheumatoid arthritis and forefoot deformity. J Orthop Res 2007;25(3):319–29.

44. Khazzam M, Long JT, Marks RM, Harris GF. Preoperative gait characterization of patients with ankle arthrosis. Gait Posture 2006;24(1):85–93.

45. Kidder SM, Abuzzahab FS Jr, Harris GF, Johnson JE. A system for the analysis of foot and ankle kinematics during gait. IEEE Trans Rehabil Eng 1996;4(1): 25–32.

46. Kitaoka HB, Crevoisier XM, Hansen D, et al. Foot and ankle kinematics and ground reaction forces during ambulation. Foot Ankle Int 2006;27(10):808–13.

47. Kite J. The classic: principles involved in the treatment of congenital clubfoot. Clin Orthop Relat Res. 1972; 84(May): 4-8.

48. Leardini A, Benedetti MG, Berti L, et al. Rear-foot, mid-foot and fore-foot motion during the stance phase of gait. Gait Posture 2007;25(3):453–62.

49. Leardini A, Benedetti MG, Catani F, Simoncini L, Giannini S. An anatomically based protocol for the description of foot segment kinematics during gait. Clin Biomech (Bristol, Avon) 1999;14(8):528–36.

50. Leitch J, (2011). The biomechanics of patellofemoral pain syndrome in distance runners. DPhil. University of Oxford.

51. Leitch J, Stebbins J, Zavatsky A. Subject-specific axes of the ankle joint complex, Journal of Biomechanics (2010) doi: 10.1016/j.jbiomech.2010.07.007.

52. List R, Stacoff A, Foresti M, Gerber H, Stüssi E. An in vivo procedure to quantify 3D kinematics of ankle arthroplasties using videofluoroscopy. J Biomech 2008;(41):S321.

53. Liu W, Siegler S, Hillstrom H, Whitney K. Three-dimensional, six-degrees-of freedom kinematics of the human hindfoot during stance phase of level walking. Human Mov Sci 1997;16:283–98.

54. Lundgren P, Nester C, Liu A, Arndt A, Jones R, Stacoff A, Wolf P, Lundberg A. Invasive, in vivo measurement of rear, mid and forefoot motion during walking. Gait Posture 2008;28(1):93–100.

55. MacWilliams BA, Cowley M, Nicholson DE. Foot kinematics and kinetics during adolescent gait. Gait Posture 2003;17(3):214–24.

56. Marks RM, Long JT, Ness ME, Khazzam M, Harris GF. Surgical reconstruction of posterior tibial tendon dysfunction: prospective comparison of flexor digitorum longus substitution combined with lateral column lengthening or medial displacement calcaneal osteotomy. Gait Posture 2009;29(1):17–22.

57. McGinley JL, Baker R, Wolfe R, Morris ME. The reliability of three-dimensional

kinematic gait measurements: a systematic review. Gait Posture 2009 Apr;29(3):360-9.

58. Morris JM. Biomechanics of the foot and ankle. Clin Orthop Rel Res 1977;122:10–17.

59. Moseley L, Smith R, Hunt A, Gant R. Three-dimensional kinematics of the rearfoot during the stance phase of walking in normal young adult males. Clin Biomech (Bristol, Avon) 1996;11(1):39–45.

60. Ness ME, Long J, Marks R, Harris G. Foot and ankle kinematics in patients with posterior tibial tendon dysfunction. Gait Posture 2008;27(2):331–9.

61. Nester C, Jones RK, Liu A, Howard D, Lundberg A, Arndt A, Lundgren P, Stacoff A, Wolf P. Foot kinematics during walking measured using bone and surface mounted markers. J Biomech 2007;(40):3412–3423.

62. Perry J. Gait Analysis: Normal and Pathological Function. Slack Inc, New Jersey, 1992.

63. Ponseti I, Campos J. Observations on pathogenesis and treatment of congenital clubfoot. Clin Orthop Relat Res. 1972;84(May):50-60.

64. Ponseti I. Current concepts review: Treatment of congenital club foot. J Bone Joint Surg Am. 1992; 74-A(3): 448-453.

65. Rang M. The Foot. The Story of Orthopaedics. Philadelphia, PA: W. B. Saunders Company; 2000: 93-114.

66. Rao S, Saltzman C, Yack HJ. Segmental foot mobility in individuals with and without diabetes and neuropathy. Clin Biomech (Bristol, Avon) 2007;22(4): 464–71.

67. Rattanaprasert U, Smith R, Sullivan M, et al. Three-dimensional kinematics of the forefoot, rearfoot, and leg without the function of tibialis posterior in comparison with normals during stance phase of walking. Clin Biomech (Bristol, Avon) 1999;14(1):14–23.

68. Recklies A, Poole A, Banerijee S. Pathophysiologic aspects of inflammation in diarthroidal joints. In: Buckwalter J, Einhorn T, Simon S, eds. Orthopaedic Basic Science: Biology and Biomechanics of the Musculoskeletal System. 2nd ed. American Academy of Orthopaedic Surgeons; 2000.

69. Reinschmidt C, Van Den Bogert AJ, Lundberg A, Nigg B, Murphy N, Stacoff A, Stano A. Tibiofemoral and tibiocalcaneal motion during walking: external vs. skeletal markers. Gait Posture 1997;6:98–109.

70. Saltzman CL, Nawoczenski DA, Talbot KD. Measurement of the medial longitudinal arch. Arch Phys Med Rehabil 1995;76(1):45-9.

71. Saraswat P, MacWilliams BA, Davis RB, D'Astous JL. A multi-segment foot model based on anatomically registered technical coordinate systems: method repeatability in pediatric feet. Gait Posture 2012;35(4):547-55.

72. Saraswat P, MacWilliams BA, Davis RB. Repeatability of virtual marker based foot model in adolescent feet. In: Annual proceedings of Gait and Clinical

Motion Analysis Society 2009:222–223.

73. Scott SH, Winter DA. Talocrural and talocalcaneal joint kinematics and kinetics during the stance phase of walking. J Biomech 1991;24(8):743–52.

74. Siegel KL, Kepple TM, O'Connell PG, Gerber LH, Stanhope SJ. A technique to evaluate foot function during the stance phase of gait. Foot Ankle Int 1995;16(12):764–70.

75. Siegler S, Chen J, Schneck CD. The three-dimensional kinematics and flexibility characteristics of the human ankle and subtalar joints–part I: kinematics. J Biomech Eng 1988;110(4):364–73.

76. Simon J, Doederlein L, McIntosh AS, Metaxiotis D, Bock HG, Wolf SI. The Heidelberg foot measurement method: development, description and assessment. Gait Posture 2006;23(4): 411–24.

77. Soderkvist I, Wedin P. Determining the movements of the skeleton using well-configured markers. Journal of Biomechanics 199;26(12):1473-1477.

78. Stebbins J, Harrington ME, Thompson N, Zavatsky A, Theologis T. Repeatability of a model for measuring multi-segment foot kinematics in children. Gait Posture 2006;23(4):401-10.

79. Stebbins J, Zavatsky A, Thompson N, Theologis TN. Repeatability of the Oxford Foot Model in hemiplegic cerebral palsy. Gait Posture 2008;28(Suppl 2):S21–2.

80. Stolze H, Kuhtz-Buschbeck JP, Mondwurf C, Jöhnk K, Friege L. Retest reliability of spatiotemporal gait parameters in children and adults. Gait Posture 1998;7(2):125–30.

81. Subotnik SI. The biomechanics of running. Sports Med 1985;2:144–153.

82. Taunton JE, Ryan MB, Clement DB, McKenzie DC, Lloyd-Smith DR, Zumbo BD. A retrospective case-control analysis of 2002 running injuries. British Journal of Sports Medicine 2002;36(2)95–101.

83. Theologis T, Stebbins J. The use of gait analysis in the treatment of pediatric foot and ankle disorders. Foot Ankle Clin 2010 Jun;15(2):365-82.

84. Theologis TN, Harrington ME, Thompson N, et al. Dynamic foot movement in children treated for congenital talipes equinovarus. J Bone Joint Surg Br 2003;85(4): 572–7.

85. Thomson S. Modified Denis Browne splint for unilateral club-foot to protect the normal foot. J Bone Joint Surg Am. 1955;37-A(6):1286-1287.

86. Tome J, Nawoczenski DA, Flemister A, et al. Comparison of foot kinematics between subjects with posterior tibialis tendon dysfunction and healthy controls. J Orthop Sports Phys Ther 2006;36(9):635–44.

87. Westblad P, Hashimoto T, Winson I, Lundberg A, Arndt A. Differences in Ankle-Joint Complex Motion during the Stance Phase of Walking as measured by Superficial or Bone anchored Markers. Foot Ankle Int. 2002;23:856–863.

88. Wiley ME, Damiano DL. Lower-extremity strength profiles in spastic cerebral palsy. Dev Med Child Neurol 1998;40:100–7.

89. Williams DS, McClay IS. Measurements used to characterize the foot and the medial longitudinal arch: reliability and validity. Phys Ther 2000;80(9):864-71.

90. Woodburn J, Helliwell PS, Barker S. Three-dimensional kinematics at the ankle joint complex in rheumatoid arthritis patients with painful valgus deformity of the rearfoot. Rheumatology (Oxford) 2002;41(12):1406–12.

91. Wright DG, Desai ME, Henderson WH. Action of the subtalar and ankle-joint complex during stance phase of walking. J Bone Jt Surg 1964;46-A(2):361–382.

92. Wu WL, Su FC, Cheng YM, Huang PJ, Chou YL, Chou CK. Gait analysis after ankle arthrodesis. Gait Posture 2000;11(1):54–61.

93. Wu, G., Siegler, S., Allard, P., Kirtley, C., Leardini, A., Rosenbaum, D., Whittle, M., D'Lima, D. D., Cristofolini, L., Witte, H., Schmid, O., and Stokes, I. ISB recommendation on definitions of joint coordinate system of various joints for the reporting of human joint motion–part I: ankle, hip, and spine. Journal of Biomechanics 2002;35(4):543–548.

94. Wu, G., van der Helm, F. C. T., Veeger, H. E. J., Makhsous, M., Van Roy, P., Anglin, C., Nagels, J., Karduna, A. R., McQuade, K.,Wang, X.,Werner, F.W., and Buchholz, B. ISB recommendation on definitions of joint coordinate systems of various joints for the reporting of human joint motion–part II: shoulder, elbow, wrist and hand. Journal of Biomechanics 2005;38(5):981–992.

95. Diagram taken from: http://www.bartleby.com/107/130.html; accessed 18-March 2015.

96. Diagram taken from: http://www.britannica.com/EBchecked/media/101314/Bones-of-the-foot-showing-the-calcaneus-talus-and-other; accessed 18-January-2015.

97. Diagram taken from: http://www.irc-web.co.jp/vicon_web/news_bn/PIGManualver1.pdf; accessed 10 April 2015.

98. Diagram taken from: http://www.physio-pedia.com/Gait_Cycle; accessed 18-January 2015.

99. Wikipedia. 2015. Anatomical terms of location - wikipedia, the free encyclopedia. Online; accessed 18-January-2015. Licensed under the Creative Commons Attribution-Share Alike 3.0 Unported License.

100. Wikipedia. 2015. Anatomical terms of motion - wikipedia, the free encyclopedia. Online; accessed 18-January-2015. Licensed under the Creative Commons Attribution-Share Alike 3.0 Unported License.

9 Appendix

Segment		Hindfoot				Tibia			
Axis		AP	HT	FPAC	FPAT	AP	APC	ANK Error	MMA Error
HF01	Right								
	Left	✔	✔	✔	✔	✔	✔	✔	✔
HF02	Right								
	Left								
HF03	Right								
	Left	✔	✔	✔	✔	✔	✔	✔	✔
HF04	Right	✔	✔	✔	✔	✔	✔	✔	✔
	Left	✔	✔	✔	✔	✔	✔	✔	✔
HF05	Right	✔	✔	✔	✔	✔	✔	✔	✔
	Left	✔	✔	✔	✔	✔	✔	✔	✔
HF06	Right	✔	✔	✔	✔	✔	✔	✔	✔
	Left	✔	✔	✔	✔	✔	✔	✔	✔
HF07	Right	✔	✔	✔	✔	✔	✔	✔	✔
	Left	✔	✔	✔	✔	✔	✔	✔	✔
HF08	Right								
	Left								
HF09	Right	✔	✔	✔	✔	✔	✔	✔	✔
	Left								
HF10	Right	✔	✔	✔	✔	✔	✔	✔	✔
	Left	✔	✔	✔	✔	✔	✔	✔	✔
HF11	Right	✔	✔	✔	✔	✔	✔	✔	✔
	Left	✔	✔	✔	✔	✔	✔	✔	✔
PF01	Right								
	Left	✔	✔	✔	✔	✔	✔	✔	✔
PF02	Right								
	Left	✔	✔	✔	✔	✔	✔	✔	✔
PF03	Right	✔	✔	✔	✔	✔	✔	✔	✔
	Left	✔	✔	✔	✔	✔	✔	✔	✔
PF04	Right	✔	✔	✔	✔	✔	✔	✔	✔
	Left	✔	✔	✔	✔	✔	✔	✔	✔
PF05	Right	✔	✔	✔	✔	✔	✔	✔	✔
	Left	✔	✔	✔	✔	✔	✔	✔	✔
PF06	Right								
	Left								
PF07	Right	✔	✔	✔	✔	✔	✔	✔	✔
	Left	✔	✔	✔	✔	✔	✔	✔	✔
PF08	Right								
	Left	✔	✔	✔	✔	✔	✔	✔	✔
PF09	Right	✔	✔	✔	✔	✔	✔	✔	✔
	Left								
PF10	Right	✔	✔	✔	✔	✔	✔	✔	✔
	Left	✔	✔	✔	✔	✔	✔	✔	✔

Figure 9.1: List of Feet Used in Chapter 4

Segment		Hindfoot									
Axis		AP	APM	APH	APC	MID Error	HEE Error	PD	PDC	PCA Error	HEE Error
HF01	Right										
	Left	✔	✔	✔	✔	✔	✔	✔	✔	✔	✔
HF02	Right										
	Left										
HF03	Right										
	Left	✔	✔	✔	✔	✔	✔	✔	✔	✔	✔
HF04	Right	✔	✔	✔	✔	✔	✔	✔	✔	✔	✔
	Left	✔	✔	✔	✔	✔	✔	✔	✔	✔	✔
HF05	Right	✔	✔	✔	✔	✔	✔	✔	✔	✔	✔
	Left	✔	✔	✔	✔	✔	✔	✔	✔	✔	✔
HF06	Right	✔	✔	✔	✔	✔	✔	✔	✔	✔	✔
	Left	✔	✔	✔	✔	✔	✔	✔	✔	✔	✔
HF07	Right	✔	✔	✔	✔	✔	✔	✔	✔	✔	✔
	Left	✔	✔	✔	✔	✔	✔	✔	✔	✔	✔
HF08	Right										
	Left										
HF09	Right	✔	✔	✔	✔	✔	✔				
	Left										
HF10	Right	✔	✔	✔	✔	✔	✔				
	Left	✔	✔	✔	✔	✔	✔				
HF11	Right	✔	✔	✔	✔	✔	✔				
	Left	✔	✔	✔	✔	✔	✔				
PF01	Right										
	Left	✔	✔	✔	✔	✔	✔	✔	✔	✔	✔
PF02	Right										
	Left	✔	✔	✔	✔	✔	✔				
PF03	Right	✔	✔	✔	✔	✔	✔	✔	✔	✔	✔
	Left	✔	✔	✔	✔	✔	✔	✔	✔	✔	✔
PF04	Right	✔	✔	✔	✔	✔	✔				
	Left	✔	✔	✔	✔	✔	✔				
PF05	Right	✔	✔	✔	✔	✔	✔				
	Left	✔	✔	✔	✔	✔	✔				
PF06	Right										
	Left										
PF07	Right	✔	✔	✔	✔	✔	✔				
	Left	✔	✔	✔	✔	✔	✔				
PF08	Right										
	Left	✔	✔	✔	✔	✔	✔				
PF09	Right	✔	✔	✔	✔	✔	✔				
	Left										
PF10	Right	✔	✔	✔	✔	✔	✔				
	Left	✔	✔	✔	✔	✔	✔				

Figure 9.2: List of Feet Used in Chapter 5

Segment		Before PCA Corrected						After PCA Corrected					
Axis		Nexus	OFM	CH	CT	COFM	FPA	Nexus	OFM	CH	FCH	COFM	FCOFM
HF01	Right												
	Left	✔	✔	✔	✔	✔	✔	✔	✔	✔	✔	✔	✔
HF02	Right												
	Left												
HF03	Right												
	Left	✔	✔	✔	✔	✔	✔	✔	✔	✔	✔	✔	✔
HF04	Right	✔	✔	✔	✔	✔	✔	✔	✔	✔	✔	✔	✔
	Left	✔	✔	✔	✔	✔	✔	✔	✔	✔	✔	✔	✔
HF05	Right	✔	✔	✔	✔	✔	✔	✔	✔	✔	✔	✔	✔
	Left	✔	✔	✔	✔	✔	✔	✔	✔	✔	✔	✔	✔
HF06	Right	✔	✔	✔	✔	✔	✔	✔	✔	✔	✔	✔	✔
	Left	✔	✔	✔	✔	✔	✔	✔	✔	✔	✔	✔	✔
HF07	Right	✔	✔	✔	✔	✔	✔	✔	✔	✔	✔	✔	✔
	Left	✔	✔	✔	✔	✔	✔	✔	✔	✔	✔	✔	✔
HF08	Right												
	Left												
HF09	Right	✔	✔	✔	✔	✔	✔						
	Left												
HF10	Right	✔	✔	✔	✔	✔	✔						
	Left	✔	✔	✔	✔	✔	✔						
HF11	Right	✔	✔	✔	✔	✔	✔						
	Left	✔	✔	✔	✔	✔	✔						
PF01	Right												
	Left	✔	✔	✔	✔	✔	✔	✔	✔	✔	✔	✔	✔
PF02	Right												
	Left	✔	✔	✔	✔	✔	✔	✔	✔				
PF03	Right	✔	✔	✔	✔	✔	✔	✔	✔	✔	✔	✔	✔
	Left	✔	✔	✔	✔	✔	✔	✔	✔	✔	✔	✔	✔
PF04	Right	✔	✔	✔	✔	✔	✔						
	Left	✔	✔	✔	✔	✔	✔						
PF05	Right	✔	✔	✔	✔	✔	✔						
	Left	✔	✔	✔	✔	✔	✔						
PF06	Right												
	Left												
PF07	Right	✔	✔	✔	✔	✔	✔						
	Left	✔	✔	✔	✔	✔	✔						
PF08	Right												
	Left	✔	✔	✔	✔	✔	✔						
PF09	Right	✔	✔	✔	✔	✔	✔						
	Left												
PF10	Right	✔	✔	✔	✔	✔	✔						
	Left	✔	✔	✔	✔	✔	✔						

Figure 9.3: List of Feet Used in Chapter 6

NHS
National Research Ethics Service
Oxfordshire REC B
2nd Floor, Astral House
Chaucer Business Park
Granville Way
Bicester
OX26 4JT

Telephone: 01869 604047
Facsimile: 01869 604055
Email: scsha.OxfordRECB@nhs.net

07 October 2009

Miss Jessica Leitch
Balliol College
Broad Street
Oxford
OX1 4BJ

Dear Miss Leitch

Study Title:	**Kinematic and morphological differences between groups of long-distance runners with and with-out a history of patellofemoral pain syndrome (PFPS): a pilot study.**
REC reference number:	**09/H0605/101**
Protocol number:	**1.0**

The Research Ethics Committee reviewed the above application at the meeting held on 06 October 2009. Thank you for attending to discuss the study.

Following the Committee's initial deliberations, you were invited into the meeting. The discussion is summarised below:

Why are only females being recruited?
It was explained that PFPS is more prevalent in females.
How long will data be stored?
It was explained that data will be stored for 10 years and then destroyed
How many members belong to the running club?
It was explained that there are approximately 150 members.

Ethical opinion

The members of the Committee present gave a favourable ethical opinion of the above research on the basis described in the application form, protocol and supporting documentation, subject to the conditions specified below.

Ethical review of research sites

The favourable opinion applies to all NHS sites taking part in the study, subject to management permission being obtained from the NHS/HSC R&D office prior to the start of the study (see "Conditions of the favourable opinion" below).

The REC has nominated the Coordinator, Miss Jo Franklin to be the point of contact should you require any further clarification upon receipt of this letter.

Conditions of the favourable opinion

The favourable opinion is subject to the following conditions being met prior to the start of the study.

Management permission or approval must be obtained from each host organisation prior to the start of the study at the site concerned.

For NHS research sites only, management permission for research ("R&D approval") should be obtained from the relevant care organisation(s) in accordance with NHS research governance arrangements. Guidance on applying for NHS permission for research is available in the Integrated Research Application System or at http://www.rdforum.nhs.uk. Where the only involvement of the NHS organisation is as a Participant Identification Centre, management permission for research is not required but the R&D office should be notified of the study. Guidance should be sought from the R&D office where necessary.

Sponsors are not required to notify the Committee of approvals from host organisations.

Conditions specified by the REC

- Please provide a copy of the MRI safety checklist for the study file

It is responsibility of the sponsor to ensure that all the conditions are complied with before the start of the study or its initiation at a particular site (as applicable).

Approved documents

The documents reviewed and approved at the meeting were:

Document	*Version*	*Date*
Covering Letter		12 August 2009
REC application		12 August 2009
Protocol	1.0	12 August 2009
Investigator CV	Amy Zavatsky	
Participant Information Sheet	1.0	12 August 2009
Participant Consent Form	1.0	12 August 2009
Letter of invitation to participant	1.0	12 August 2009
Letter from Sponsor		13 August 2009
Referees or other scientific critique report		17 June 2009
Summary/Synopsis	Flowchart V1.0	12 August 2009
Advertisement	1.0	12 August 2009
Investigator CV	Jessica Leitch	

Membership of the Committee

The members of the Ethics Committee who were present at the meeting are listed on the attached sheet.

Statement of compliance

The Committee is constituted in accordance with the Governance Arrangements for Research Ethics Committees (July 2001) and complies fully with the Standard Operating

Procedures for Research Ethics Committees in the UK.

After ethical review

Now that you have completed the application process please visit the National Research Ethics Service website > After Review

You are invited to give your view of the service that you have received from the National Research Ethics Service and the application procedure. If you wish to make your views known please use the feedback form available on the website.

The attached document "After ethical review – guidance for researchers" gives detailed guidance on reporting requirements for studies with a favourable opinion, including:

- Notifying substantial amendments
- Adding new sites and investigators
- Progress and safety reports
- Notifying the end of the study

The NRES website also provides guidance on these topics, which is updated in the light of changes in reporting requirements or procedures.

We would also like to inform you that we consult regularly with stakeholders to improve our service. If you would like to join our Reference Group please email referencegroup@nres.npsa.nhs.uk.

09/H0605/101	**Please quote this number on all correspondence**

With the Committee's best wishes for the success of this project

Yours sincerely

J Franklin

Prof Margaret Rees
Chair

Enclosures: List of names and professions of members who were present at the meeting and those who submitted written comments

"After ethical review – guidance for researchers"

Copy to: Heather House, Clinical Trials Office, John Radcliffe Hospital

Fiona Parker, R&D Dept, Nuffield Orthopaedic Centre

Amy Zavatsky, Academic Supervisor

Oxfordshire REC B

Attendance at Committee meeting on 06 October 2009

Committee Members:

Name	*Profession*	*Present*	*Notes*
Mrs Susan Dutton	Medical Statistician	No	
Ms Linda Goffey	Lay Member	Yes	
Dr Yvonne Hart	Consultant Neurologist	Yes	
Mr Robert King	Lay member	Yes	
Miss Bridget Lambert	Paediatric Dietician	No	
Dr Pamela Laurie	Consultant Anaesthetist	Yes	
Dr Jonathan Price	Qualitative Expert	Yes	
Prof Margaret Rees	Consultant Medical Gynaecologist	Yes	
Mrs Kate Thompson	In patient and day hospice manager	Yes	
Canon Jessica Turner	Lay member	No	
Mr Paul Windscheif	Pharmacist	Yes	

Also in attendance:

Name	*Position (or reason for attending)*
Miss Joanne Franklin	Committee Coordinator